THE PROCEEDINGS OF
THE PHYSICAL SOCIETY

Section A

VOL. 62, PART 6 1 June 1949 No. 354 A

The Structure and Electrical Properties of Surfaces of Semiconductors.—Part I. Silicon Carbide

BY T. K. JONES, R. A. SCOTT* AND R. W. SILLARS
Research Department, Metropolitan–Vickers Electrical Co. Ltd.

MS. received 14th January 1949; read at Science Meeting at Manchester 9th December 1948

ABSTRACT. Electrical contacts with faces of silicon carbide and of many other semiconductors do not obey Ohm's law. This property of silicon carbide has been attributed to an amorphous film known to occur on faces of the crystal. Theoretical work relating to such contacts is hampered by lack of knowledge of the essential physical features of the model. In this paper a study is made of the manner in which the surface texture of the crystal affects the electrical properties of the contact. The electrical characteristics of a contact between a rounded metal point and the demonstrably smooth face of a crystal were shown to vary only slowly across the surface. A series of observations was made of the electrical properties and of the electron diffraction patterns of a basal plane of a crystal as the overlying film of amorphous material was removed.

The results show that the presence of the amorphous film is not essential to the exhibition of the special electrical properties of the contact.

§ 1. INTRODUCTION

It is well known that the contact between the surface of some semiconductors, such as silicon carbide, and either a metal probe or a second piece of the semiconductor, has unusual electrical properties. A large fall of potential exists in the neighbourhood of the surface when current is flowing, and this potential difference rises much more slowly than in proportion to the increase of current through the contact; the resistance at the contact does not obey Ohm's law, and such a contact resistance is usually described as non-ohmic. The contact also exhibits rectification.

Various mechanisms have been postulated to give a general explanation of these phenomena. Reduced to the simplest terms, these involve assumptions on the one hand of "tunneling" of electrons through a thin insulating surface layer or, on the other hand, of thermal excitation across the potential barrier formed by a (thicker) insulating layer or formed by a space-charge region at the contact with a material of different work-function. Combinations and elaborations of these mechanisms are possible, and in order to limit the field for speculation there is a great need for direct physical evidence about the structure of the surface. It is the purpose of this paper to provide more detailed information about the physical nature of the contact in the case of contacts with silicon carbide. The work is confined primarily to contacts between a rounded metal point and the smoothest parts of naturally occurring 0001 crystal faces of hexagonal silicon carbide. Some of the theories which have been suggested involve the assumption that some layer of foreign material is present at the face, and this work was undertaken in an attempt to decide whether the peculiar electrical properties are associated with a gross detectable layer of contaminating material overlying the face.

---

* Now at Messrs. Henry Simon Ltd., Cheadle Heath, Stockport.

§2. THE HYPOTHESIS OF THE INSULATING LAYER

There is in the literature a considerable amount of evidence to suggest that an overlying layer of foreign material is commonly present at the face of silicon carbide crystals. Sand is one of the principal raw materials used in the preparation of carborundum, and the presence of films of silica on the silicon carbide crystal faces cannot be regarded as unlikely. Many of the crystal faces show interference colours. Finch and Wilman (1937) have investigated the 0001 faces by electron diffraction and have shown that layers, probably of silica and upwards of 50 A. in thickness, do exist on some crystals. Finch and Wilman showed that such layers can be removed by chemical action and by abrasion.

E. W. J. Mitchell has shown that a crystal heated to 1,800–2,000° C. for a few minutes in a bell-jar containing air at very low pressure (10^{-5} mm. Hg) possesses on cooling an ohmic contact resistance.

This experiment has been regarded as consistent with the assumption that an initial silica layer has been evaporated from the crystal plane. It has also been shown that subsequent slow heating in air to temperatures above that at which carbon rapidly combines with oxygen (800° C.) leads to a reversion to a non-linear voltage-current characteristic. This experiment has been interpreted as the removal of carbon atoms from the surface of the lattice by oxidation and the conversion of the freed silicon ions to silica.

The electron diffraction evidence of existence of contaminating layers is quite definite, but it must not be implied that such layers are always present; on the contrary, Germer (1936) has indicated that some crystals show electron diffraction patterns characteristic of a clean crystal face. It is clearly important that direct correlation be made between the known "cleanliness" of the surface as determined by electron diffraction and the electrical behaviour of the contact.

A series of experiments was therefore made to determine:

(i) whether the average electrical characteristics are consistently different between two groups of crystals, one group being formed of crystals with demonstrably obscured 0001 faces and the other with relatively uncontaminated faces;

(ii) whether crystal faces covered with amorphous layers lose their non-ohmic contact resistance when cleaned of contaminating layers so as to leave demonstrably clean single crystal patterns;

(iii) whether electron diffraction investigations of the surface of crystals which have been heated to 1,800° C. *in vacuo* show the single-crystal patterns of silicon carbide required by the hypothesis that the cause of the change in electrical properties is evaporation of silica from the crystal face;

(iv) whether the electrical properties of a face showing demonstrably clean single crystal patterns vary substantially when the face is covered with known thicknesses of evaporated silica.

Finally, a careful attempt was made to estimate the effectiveness of the electron diffraction criterion of cleanliness of surface by determining the minimum thickness of a silica layer superposed on a clean face which would be detectable in terms of perceptible obscuration of the electron diffraction pattern. This determination has made it possible to say that if the basic mechanism is to involve a surface layer physically distinct from the bulk semiconductor, the mechanism must be effective for a layer no thicker than that just perceptible by electron diffraction.

§ 3. APPARATUS

The main apparatus consists on the one hand of an electron diffraction camera and on the other of the electrical contact assembly. The electron diffraction camera is of conventional design and is of the variety supplied commercially by Metropolitan-Vickers Electrical Co. Ltd. The camera is continuously pumped by an oil-diffusion pump; the electron gun is of the thermionic type with biased Wehnelt-cylinder. The acceleration voltage is roughly 56 kv. and is stabilized electronically. An auxiliary gun is fitted and its accelerating voltage and filament current chosen so as to prevent any accumulation of charge which might otherwise collect on the crystal face because of the departure from unity of the secondary-electron coefficient of the silicon carbide face. A camera distance of 21 cm. was normally used during the experiment and the diffraction patterns were recorded on Ilford Photomechanical Plates. The apparatus is shown in cross-section in Figure 1. The contact assembly consists of a cup-shaped metal holder A supporting the crystal B and secured to the general framework of the apparatus, together with a metal electrode C held with a known pressure in contact with the crystal face by means of a tension spring. It is carefully designed to allow the complete removal and replacement of the crystal from the assembly without disturbing the fixity of location of the contact. It is considered that the location is held to within a few microns. The crystal cup is arranged so as to fit the specimen holder of the electron diffraction camera and the crystal is sufficiently rigidly attached by Wood's metal to the cup to allow the surface of the crystal to be abraded with metallurgical polishing papers.

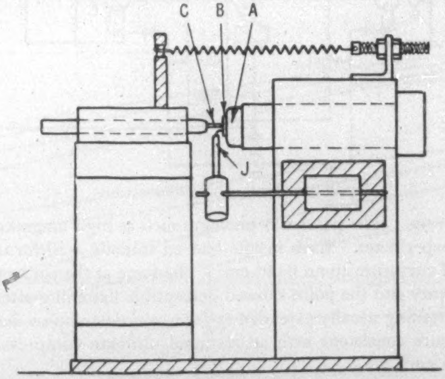

Figure 1. Contact assembly.

The electrical circuit used for determining the voltage–current characteristic is shown in Figure 2. One current-carrying electrode of the crystal is the cup itself. The cup is in electrical contact, by way of the Wood's metal, with a large area of crystal, and the drop in voltage at this contact is very small (less than 1 mv.). The principal measurements of each experiment consisted in determining with electrometer-triode circuits the voltage drop between the metal probe C which forms one current-carrying electrode, and the body of the crystal, as currents of definite magnitude flowed through the contact. The potential of the main body of the crystal was determined with the auxiliary electrode J of light phosphor-bronze wire which rested against the crystal face and was arranged in a measuring circuit of such high impedance as to involve the drawing of negligibly small current from the contact. The apparatus was electrically screened and the whole assembly hung from a type of Julius suspension to prevent disturbance of the contact by vibration. The assembly was shown not to be critically sensitive to inevitably small changes in contact pressure. The metal probe C was a gramophone needle; this form of electrode was chosen because of the relatively simple geometry of the tip. The point was photographed at high magnification before and after the experiment. Each needle had an initially well-formed spherical end of radius of curvature about 0·005 cm. The force at the contact was in each case $1{\cdot}7 \times 10^5$ dynes and the point showed perceptible flattening after the experiment. The flattening usually extended to form a circular tip of diameter about 0·008 cm. (a figure consistent with an assumed ultimate compressive stress of $4{\cdot}85 \times 10^9$ dynes/cm^2).

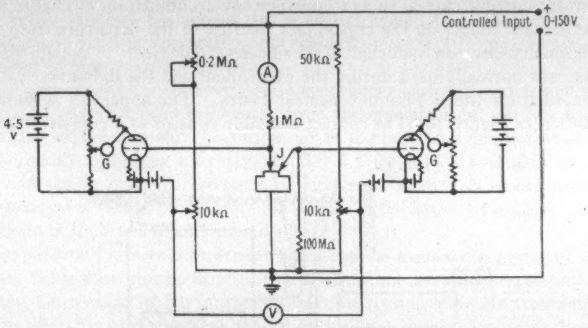

Figure 2. Electrical measuring circuit.

A selection of crystals of silicon carbide possessing well-developed crystal faces was inspected for smoothness of surface by setting up interference fringes (Fresnel) between the face and a reference surface of fire-polished glass. Crystals showing pitted surfaces or clearly-marked terraced faces were discarded; the crystals used usually possessed smooth areas of 1 or 2 mm. square in the neighbourhood of the contact. Tests made by means of multiple-beam interference (Tolansky 1948) subsequent to the set of experiments on a crystal showed the surface to be smooth on a sub-microscopic scale.

The crystals used in the course of the experiment were of the black variety unless explicitly stated otherwise. The crystals were each prised from the raw magma and therefore had not been subjected to the severe chemical cleaning which is customary in the late stages of the preparation of silicon carbide for industrial purposes. As a result of preliminary investigation it was found that the crystal faces could be effectively cleaned of grease by immersion in pure chloroform and careful drying with clean filter paper.

A typical crystal used in the experiment was crushed, and examined by x rays in a powder camera. The results showed evidence of the presence of SiC in the following hexagonal forms: I, II, III, and IV (for nomenclature see Thibault 1944).

The electrical characteristics of each particular contact were obtained by recording voltage across the crystal face for given currents for a complete cycle of increasing and decreasing current in each direction of flow of current. Preliminary tests showed a tendency for the characteristics measured immediately after forming the contact to be occasionally a little unstable (voltage high for a given current). The voltage–current curve becomes more stable after a few cycles and a standard practice was therefore adopted of completing with fair rapidity half a dozen cycles before recording the readings. When care is taken to control the location of the probe and the pressure at the contact, the voltage–current characteristics of a given smooth crystal face prove to be reasonably stable. Graphs are shown in Figure 3 of characteristics of four consecutive points spaced at 0·5 mm. along the arc of a circle in a smooth crystal face, and these curves are seen to be of very similar, but decided non-ohmic, shape and of closely similar slope at any one current.

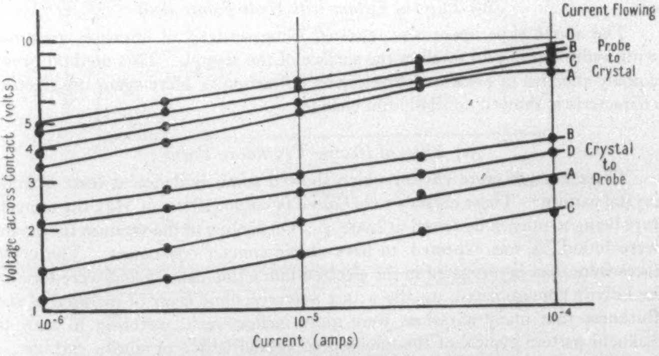

Distance between points A, B, C, D ~ 0·5 mm.

Figure 3. Change in contact characteristic with translation of probe.

§ 4. EXPERIMENTAL RESULTS

(i) *Behaviour of Untouched Crystals*

An inspection of degreased faces of crystals chosen at random showed a wide variety in the degree of obscuration of the single-crystal pattern known to be typical of 0001 faces of hexagonal silicon carbide (Germer 1936, Finch and Wilman 1937). Some faces showed clear patterns of Kikuchi lines; others showed little but the "halo-pattern" typical of a non-crystalline layer. A batch of crystals exhibiting fairly clean single crystal patterns and a second batch showing extensive halo-patterns were selected from a group of otherwise apparently similar crystals; the electrical characteristics of the contacts formed between a constant metal probe and each crystal face in turn are shown in Figure 4. The following is the order of decreasing obscurity of crystal face: 21, 11, 19; 12, 17, 14.

(ii) *Effect of Abrasion*

A second experiment of similar type was then proceeded with. A second set of six crystals showing some degree of obscuration of the single-crystal pattern was chosen. The electrical characteristics of the definitely located contact between the gramophone needle and the face were determined for the face in its initial (degreased) state. The surface was then lightly abraded with metallurgical polishing paper (Naylor & Co. Stockport No. 0), and the electron diffraction pattern redetermined. The abrasion was repeated until the surface film was so thin that the silicon carbide Kikuchi pattern appeared imperceptibly obscured. Plates 1 and 2 show the corresponding electron diffractions typical of the surface before and after abrasion. The electrical characteristics were then redetermined. The experiment was carried out carefully for each of the crystals and the typical results are shown for two such crystals in Figures 5 and 6. The electrical characteristics are little changed in slope or position after the abrasion and show the typical failure of Ohm's law for such contacts. It was found that black and green crystals behaved in similar fashion in the experiment.

(iii) *Effect of Etching with Hydrofluoric Acid*

The above experiment was repeated using, instead of abrasion, treatment with hydrofluoric acid to clean the surface of the crystal. This method proved equally effective as evidenced by electron diffraction. Here again the electrical characteristic showed no significant change.

(iv) *Effect of Heating Crystals in Vacuo*

Three crystals were chosen which showed some evidence at least of single crystal pattern. These crystals were heated *in vacuo* (10^{-5} mm. Hg), the temperature being momentarily raised to 2,000° c. On cooling in the vacuum the crystals were found, as was expected, to have ohmic contact resistances. The crystal faces were then investigated in the electron diffraction camera and were found to be heavily contaminated, usually with a polycrystalline layer of material of such thickness that many abrasions were quite ineffective in restoring to view the Kikuchi pattern typical of the unobscured crystal lattice of silicon carbide. A typical pattern taken after heating in the vacuum is shown in Plate 3.

(v) *Effect of an Artificial Layer of Silica*

Crystals were selected and cleaned by abrasion so as to yield clean single-crystal patterns. The contact characteristics were determined for this condition of the surface and for successive cases in which the crystal was covered by evaporation with increasing known thicknesses of silica. The depth of the film of silica on the crystal face was determined in the following manner. A small length (2 mm.) of fused silica rod ½ mm. in diameter is supported by means of two closely spaced parallel tungsten wires (0·4 mm. diam.). The crystal is mounted, face

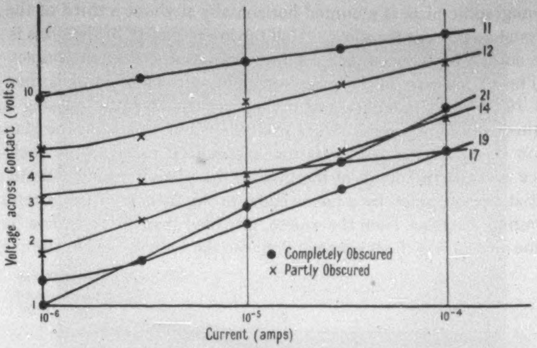

Figure 4. Voltage–current characteristics for various untreated crystals.

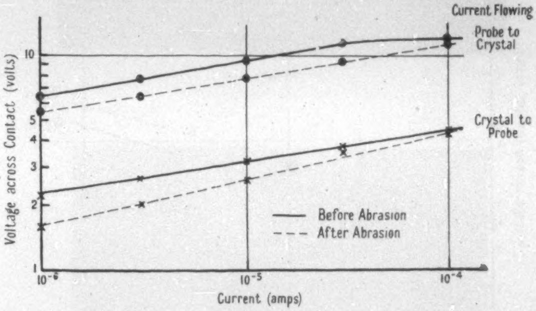

Figure 5.

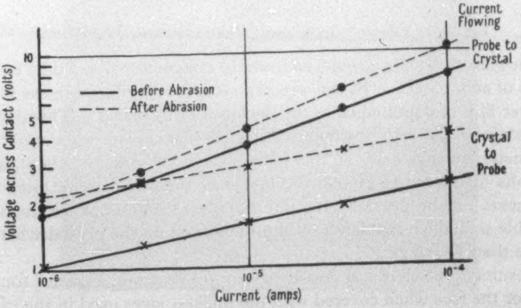

Figure 6.

downwards, on a support 15 cm. above the silica. A square piece of glass cut from photographic plate is mounted horizontally at about a third of the distance of the crystal away from the silica. Half the lower surface of the glass is screened from the source by fixing a piece of thin brass foil closely in contact with the glass. The air-pressure in the space surrounding the apparatus is then reduced to about 10^{-5} mm. of mercury and the silica evaporated by passing a suitable current through the filament. Silica from the filament falls on the glass plate as well as on the specimen and coats the unobscured parts of the plate. Since the source is small, the depth of the film on the plate is proportionately greater than that at the specimen by a factor equal to the inverse of the square of their corresponding distances from the source, provided that the test plate lies closely in the same direction as the specimen relative to the source. After the evaporation process the glass test-plate is removed from the system and silvered by evaporation to a depth of about 500 A. By this process a step is reproduced in the top surface of the silver film of depth equal to the thickness of the silica. This plate is then used in conjunction with a similarly silvered blank plate in a multiple-beam interferometer arrangement of the type used by Tolansky (1948), and from photographs of the fringe system the height of the step is determined. Since measurements can be made by the interference technique to within, say, 10 A., it is possible to deduce the depth of films deposited on the crystal when the film is no more than 1 A. thick.

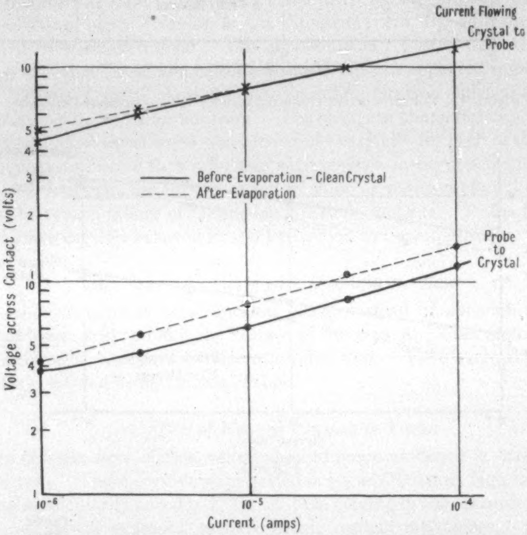

Figure 7. Effect of a thick layer (90 A.) on contact characteristic.

The results of the electrical measurements are shown in Figure 7 for the clean face and for the face when covered with the thickest layer used in the experiment (90 A.). The characteristics are very little modified by the presence of the silica film.

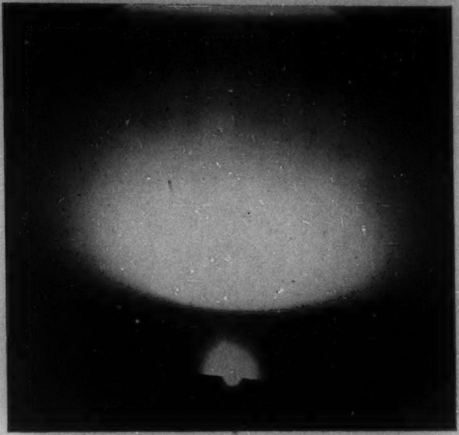

Plate 1.

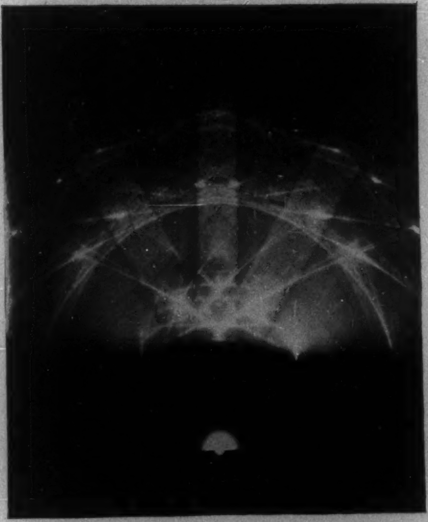

Plate 2.

To face page 340

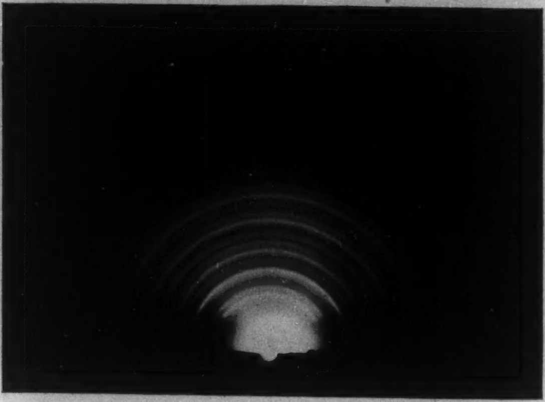

Plate 3.

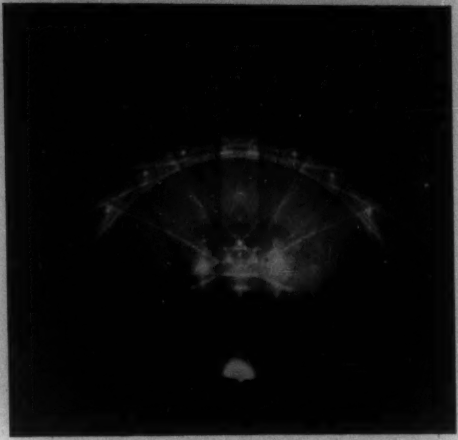

Plate 4.

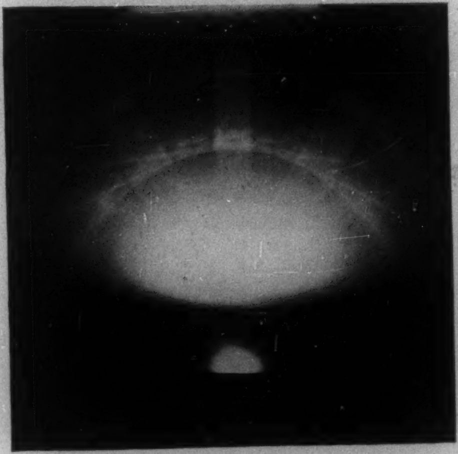

Plate 5.

(vi) *Sensitivity of the Electron Diffraction Test*

The results of the experiments described above show that the non-ohmic contact resistance of silicon carbide faces is not of necessity associated with the thick amorphous layer. In particular, a crystal face from which the amorphous material has been removed to a sufficient extent for the face to yield a clear-cut single-crystal pattern is not appreciably modified in its electrical characteristics by the process. In assessing the importance of this conclusion it is necessary to know how sensitive is the electron diffraction test for the presence of the amorphous film, for it is conceivable that the non-ohmic characteristic of the contact resistance is due to a residual film too thin to be detected by electron diffraction.

Finch and Wilman (1937) have already shown that a monolayer of a paraffin $C_{32}H_{66}$ of depth known from the geometry of the molecule to be 43 A. is just sufficient to obscure the crystal pattern. In this work it was more desirable to determine the thickness of the amorphous material that would lead to just perceptible obscuration of the single-crystal pattern. To this end a crystal which showed a sharply defined single-crystal pattern was selected and its surface lightly abraded so as to make sure that any overlying layer had been reduced to a minimum. An electron diffraction pattern of the face in this condition is shown in Plate 4. Thin amorphous films of silica of measured thickness were then evaporated on to the crystal face and after each evaporation a diffraction pattern was recorded. The diffraction patterns were taken for a fixed orientation of the crystal relative to the beam; the beam was incident on the crystal surface at an angle of about 2 degrees. The operating conditions of the camera were carefully controlled. Plates 4 and 5 show patterns taken with a clean face, and with a thickness of 10 A. of silica on the face. Control patterns were taken at various stages in the experiment to confirm that the pattern of the fully abraded crystal had not deteriorated. Clear evidence can be seen in the original negatives of increased diffuseness, particularly in the central region of the pattern, even in the case of a 3 A. layer.

§ 5. CONCLUSION

The main conclusion to be drawn from our experimental work is that the occurrence of non-ohmic contact resistances at the interface between a rounded metal probe and a smooth crystal face of silicon carbide does not depend on the presence of a detectable film of foreign material on the surface of the crystal. The principal evidence comes from the close similarity in electrical characteristics of a contact successively made under otherwise identical conditions with a naturally obscured crystal surface, and with the same surface after removal of the foreign material by abrasion. The subsidiary experiments suggest that the surface is certainly that of a lattice plane not covered by more than a few molecules of foreign material; any layer of silica-like material could not be more than 5 A. thick and is probably less than 3 A. It may well be remarked in this connection that such a surface is as clean as one might expect a surface to be in the light of the evidence that solids in general acquire layers of absorbed gas atoms when exposed to a gaseous atmosphere.

The fact that no foreign surface layer is necessary to produce non-ohmic behaviour is not surprising, and plausible explanation in terms of space-charge barrier layers is possible. It is, however, a little unexpected to find that a layer of evaporated silica 90 A. thick produces no significant change in electrical characteristics. Possible explanations of this observation are:

(1) The film is mechanically displaced or damaged by the steel probe.
(2) The film has suffered electrical breakdown before any readings of current were taken.
(3) The film offers no appreciable resistance to the passage of electrons.

Such experimental evidence on thin SiO_2 films as is available (Plessner 1948) suggests that explanations (2) and (3) are unlikely, without at least some contribution due to mechanical damage.

Little significance can be attached to the evidence that comes from the ohmic behaviour of crystal faces that have been heated *in vacuo* to 2,000° c. This evidence appeared to suggest that the ohmic behaviour might be associated with a clean lattice face exposed by evaporation of silica, or similar material, from the face of the crystal; the electron diffraction evidence clearly shows that, far from possessing a clean face, the crystal is covered with a thick tenacious film of polycrystalline material after the heat-treatment.

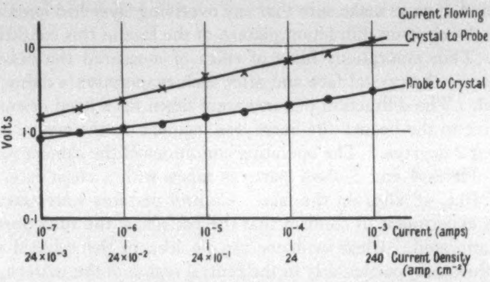

Figure 8.

The numerical value of the ohmic contact resistance in one typical case of a crystal heated to about 2,000° c. was about 10^4 ohms for a contact area which from the flattening of the contact point was estimated to be about 4×10^{-5} cm^2. This contact resistance is much too high to be accounted for by the "spreading resistance" at the contact with a material of bulk conductivity equal to that of silicon carbide, and must be attributable to contact with a contaminating layer of much lower conductivity.

The absence of an appreciable non-ohmic contribution from the silicon carbide crystal face is due to the smallness of this component consequent upon the wide distribution of current at the interface between the crystal and the contaminating layer. Moreover the wide distribution of the current at the silicon carbide face implies a low current density at the surface, and measurements on the contacts of all types indicate that the electrical characteristic of silicon carbide is essentially ohmic when the current density is small enough.

The electrical measurements of contact resistance which form one part of the evidence of the investigation are themselves interesting, since measurements refer to contacts of definable geometry for which the area of contact can be estimated with fair accuracy. The electrical characteristics are stable and repeatable to within a few tens per cent for any assigned position of the initially rounded (but necessarily flattened) steel probe when held with a definite force against a surface which is atomically smooth over the area of contact. Translation of the probe in the face of the crystal leads to relatively small changes in the shape and position of the voltage–current curve, provided care is taken to keep to smooth areas of the face. The change in characteristic from crystal to crystal is usually rather less than one order of magnitude in voltage provided that the force is held at a constant value and that the crystal surface is devoid of pits and scratches. Figure 8 shows a typical characteristic taken for a long range of current; the lower of the two abscissa scales gives the current density at the contact on the assumption that the area of contact is $4{\cdot}1 \times 10^{-5}\,\mathrm{cm}^2$. This value for area of contact is that of the visibly flattened portion of the tip and is presumably an underestimate. The area of contact calculated from Hertz's analysis of elastic deformation at the conjunction of a sphere and a plane is $1{\cdot}6 \times 10^{-6}\,\mathrm{cm}^2$, but the assumption of perfect elasticity is not acceptable for these stresses.

ACKNOWLEDGMENTS

The authors wish to acknowledge the assistance of Mr. E. W. J. Mitchell for his co-operation in many points of the work, and of Mr. A. W. Agar for his help in the early part of the investigation. We wish to express our thanks to Mr. F. R. Perry for his interest and encouragement, and to Mr. B. G. Churcher, Manager of the Research Department, and Sir Arthur P. M. Fleming, Director of Research and Education, Metropolitan-Vickers Electrical Co. Ltd. for permission to publish this paper.

REFERENCES

FINCH, G. I., and WILMAN, H., 1937, *Trans. Faraday Soc.*, **33**, 337.

GERMER, L. H., 1936, *Phys. Rev.*, **49**, 163.

HERTZ, H., 1896, *Theory of Hardness and Area of Contacts* (London : Macmillan).

MITCHELL, E. W. J., and SILLARS, R. W., 1949, *Phys. Soc. Proc.* B, **62** (in press).

PLESSNER, K. W., 1948, *Proc. Phys. Soc.*, **60**, 243.

THIBAULT, N. W., 1944, *Amer. Mineralogist*, **29**, 327.

TOLANSKY, S., 1948, *Multiple-Beam Interferometry of Surfaces and Films* (Oxford : Clarendon Press).

The Structure and Epitaxy of Lead Chloride Deposits Formed from Lead Sulphide and Sodium Chloride

By A. J. ELLEMAN and H. WILMAN
Applied Physical Chemistry Laboratories, Imperial College, London

MS. received 17*th December* 1948 ; *read at Science Meeting at Manchester* 9*th December* 1948

ABSTRACT. Electron diffraction shows that $PbCl_2$ is formed instead of PbO . $PbSO_4$ when mosaic single-crystal PbS layers a few hundred A. thick are heated on their NaCl substrates in air at 200–300° C. The structure and orientation of these $PbCl_2$ layers are described. This example of epitaxial crystal growth is particularly interesting because the $PbCl_2$ atoms adjacent to the, at least initially, atomically smooth PbS surface do not lie exactly in a single close-packed plane atomic sheet, but the atomic arrangement closely matches that of the PbS substrate in a series of parallel bands. When the composite $PbCl_2$–PbS layers were isolated from their NaCl substrate the transmission patterns showed that they must have partly broken up, leading to curvature about remarkably well-defined axes parallel to the film plane and PbS cube-face diagonals.

---

§ 1. INTRODUCTION

When lead sulphide layers on single-crystal rocksalt substrates are heated *in vacuo* there is an increase in crystal size and in certain cases a preferential growth of crystals in different orientations from those initially predominant in the layer, these changes taking place to an extent which depends on the temperature and duration of heating (Elleman and Wilman 1948). On the other hand when lead sulphide layers are heated in air at 350° to 500° C. after dissolving away the sodium chloride substrate crystal and drying, they are converted into the oxysulphate, lanarkite, PbO . $PbSO_4$ (Wilman 1948).

Experiments to determine the orientation of the PbO . $PbSO_4$ crystals relative to the PbS crystals from which they are formed have now shown that when "single-crystal" PbS layers are heated in air at 200° to 300° C. on their rocksalt substrates no PbO . $PbSO_4$ appears but a layer of lead chloride, $PbCl_2$ (cotunnite), is quickly formed on their upper surface, even when the PbS layer is 250 A. thick and is made up of crystals at least 500 A. in lateral diameter, with atomically smooth cube-face surfaces. The structure and orientation of these $PbCl_2$ layers are described below and lead to lattice constants and diffraction intensities which agree closely with previous crystallographic and X-ray data. The details of the epitaxial orientations and atomic fitting of the $PbCl_2$ with respect to the PbS crystals are particularly interesting because the substrate surface was known (Elleman and Wilman 1948) to be almost atomically smooth initially and the deposit atoms adjacent to the substrate surface do not lie in a close-packed plane atomic sheet. The atomic arrangement, however, is found to match closely that of the substrate in a series of parallel strips.

§ 2. EXPERIMENTAL

The PbS deposits on NaCl cleavage faces were prepared as already described (Elleman and Wilman 1948) so as to obtain untwinned deposits with highly smooth surface. They were heated in atmospheric air in the laboratory and were examined by electron diffraction immediately after preparation. A Finch type electron-diffraction camera was used (Finch and Wilman 1937 a) with 50–60 kv. electrons and a camera length about 50 cm. Transmission specimens were prepared by dissolving away the NaCl so as to leave the PbS film floating on the water surface, and without further washing they were lifted off and dried *in vacuo* so as to leave a trace of NaCl thus remaining on the PbS film. Eight deposits were examined by reflection after heating in air at between 200 and 300° c., and Table 3 (p. 348) shows the relation of the surface composition to the thickness and orientation of the initial PbS deposit.

§ 3. THE STRUCTURE AND ORIENTATION OF THE $PbCl_2$ DEPOSITS

(i) *Random Transmission Specimens*; *Identification as $PbCl_2$*

Figure 1 shows the ring pattern from randomly disposed crystals of the reaction product, together with the stronger arcs and some rings due to the remaining PbS, which was evidently much distorted or bent because of break-up and sagging in the meshes of the supporting nickel gauze. Table 1 gives the intensities and the net-plane spacings, calculated on a basis of $a = 5{\cdot}929$ A. for the PbS cubic axis (Wilman 1948, Elleman and Wilman 1948). The x-ray data for $PbCl_2$ powder patterns are also given in Table 1 and show that the reaction product was lead chloride with axial lengths of the rhombic lattice close to those found by x rays. Further confirmation of this identification was supplied by transmission patterns (Table 1) from $PbCl_2$ (random crystals approximately 500 A. in diameter) precipitated from hot aqueous solution and sublimed *in vacuo* on to collodion films. Table 2 gives the axial lengths and ratios previously estimated for $PbCl_2$.

The electron-diffraction spacings in Table 1 are mostly slightly higher than the recent x-ray values. A mean value of $c = 9{\cdot}035$ A. was obtained from the pairs of spacings for 101 and 103, 101 and 105, 111 and 113, 111 and 115, 020 and 023, and 031 and 032. The value of a calculated independently from 012 and 212, 002 and 202, 200 and 111 and 311, 022 and 222, and 122 and 222, was 4·530 A. For b a mean value 7·611 A. was obtained from the pairs of spacings 111 and 121, 111 and 131, 121 and 131, 011 (and 022/2) and 031, 031 and 041, 012 and 032, and from 020 and 040. By assuming the a and c values to be reliable, a slightly more representative mean value of b was obtained from the spacings of the diffractions 012, 110, 020, 111, 120, 022, 121, 122, 031, 023, 130, 032, 131, 132, 221 and 041, the mean being 7·614 A. The axial lengths are thus $a = 4{\cdot}530$, $b = 7{\cdot}614$, $c = 9{\cdot}035$ A. and $a:b:c = 0{\cdot}5950:1:1{\cdot}187$. For the sublimed $PbCl_2$ also (Table 1) $a:b:c = 0{\cdot}5950:1:1{\cdot}187$.

The electron-diffraction spacings and estimates of the axial ratios thus correspond well with those found in x-ray powder patterns, apart from a small difference in axial lengths. It may be noted that since Straumanis and Sauka (1942) did not state the wavelength they attributed to their x rays it is impossible to determine whether or not their axial lengths are in kx. units, requiring a multiplying factor of 1·00202 (Bragg 1947) to convert them to ångströms. The electron-diffraction ring intensities also show mainly a similarity with those of the x-ray patterns, and the differences are presumably partly due to different crystal shape and size, leading to different degrees of absorption in the various diffractions (cf. Wilman 1948).

No trace of any other compound was found. If Na_2S is formed in the reaction it would be attacked by moisture and oxygen in the air, forming compounds which would be easily volatilized.

Table 1. Plane Spacings, *d*, and Ring Intensities, *I*, from random $PbCl_2$ Crystals

Indices		Electron diffraction					X-ray diffraction		
		$PbCl_2$+PbS (Figure 1)			$PbCl_2$ sublimed		Powdered $PbCl_2$		
$PbCl_2$ (rings)	PbS (arcs)	d^* (A.)	I†	$d_{calc.}$‡	d	I†	$d_{calc.}$§	$d_{ASTM.}$‖	$I_{ASTM.}$‖
011	—	5·83	F	5·821	—	—	5·815	—	—
002	—	4·51	MF	4·517	4·52	MF	4·513	4·49	0·4 B
101	—	4·053	M	4·048	4·062	M	4·045	4·03	0·4 B
012 110	—	3·888	M	3·883 3·892	3·890	M	3·880 3·888	3·88	0·7
020	—	3·795	MF	3·807	3·816	M	3·802	3·79	0·6 B
111	—	3·579	MS	3·574	3·580	MS	3·571	3·57	**1·0**
—	111	3·418	M	—	—	—	—	—	—
112	200	2·964	S	2·948	2·944	MF	2·945	—	—
120 022	—	2·916	M	2·914 2·911	2·919	MF	2·911 2·907	2·91	0·6 B, 0·2 D
121	—	2·779	MS	2·773	2·779	S	2·770	2·76	**0·8**
103	—	2·508	M	2·507	2·511	MS	2·505	2·50	**0·8**
122 031	—	2·445	M	2·448 2·443	2·446	F	2·446 2·441	2·43	0·2 D
113	—	2·380	MF	2·381	2·380	F	2·379	2·37	0·3
023	—	2·362	MF	2·362	2·364	F	2·359		
200 004	—	2·268	M	2·265 2·259	2·265	S	2·262 2·256	2·26	0·7
130 032	—	2·213	M	2·214 2·212	2·213	MF	2·212 2·211	2·21	0·6
131	—	2·155	M	2·150	2·156	M	2·149	2·15	0·8
123	220	2·096	S	2·094	2·096	M	2·092	2·09	0·8
202 104	—	2·025	MF	2·024 2·021	2·025	F	2·022 2·019	—	—
132	—	1·994	F	1·988	—	—	1·987	—	—
212 114	—	1·953	M	1·956 1·953	1·951	M	1·955 1·952	1·98	0·2 B
221	—	1·901	F	1·907	1·902	VF	1·901	—	—
041	—	1·859	F	1·863	1·860	VF	1·860	—	—
222 133 124	311	1·787	MS	1·787 1·784 1·785	1·787	F	1·786 1·782 1·783	—	
213 015 140 042	—	1·760	F	1·760 1·758 1·755 1·754	1·760	F	1·759 1·756 1·753 1·752	—	—
141	222	1·711	MF	1·722	1·719	VF	1·720	—	—
105	—	1·682	F	1·678	1·682	MF	1·676	—	—
231	—	1·662	F	1·661	—	—	1·660	—	—
115 142 223 025	—	1·636	M	1·639 1·636 1·634 1·632	1·638	M	1·637 1·634 1·633 1·630	—	—
204	—	1·600	F	1·599	1·600	F	1·598	—	—
134	—	1·582	MF	1·581	1·582	MS	1·580	—	—
214	—	1·567	F	1·565	—	—	1·563	—	—
125	—	1·537	VF	1·535	—	—	1·534	—	—
143	—	1·518	VF	1·516	1·517	F	1·514	—	—

Table 1 (*cont.*)

Indices		Electron diffraction					X-ray diffraction		
$PbCl_2$ (rings)	PbS (arcs)	$PbCl_2+PbS$ (Figure 1)			$PbCl_2$ sublimed		Powdered $PbCl_2$		
		d* (A.)	I†	$d_{calc.}$†	d	I†	$d_{calc.}$§	$d_{ASTM.}$‖	$I_{ASTM.}$‖
016	400	1·482	S	1·477	1·476	F	1·476	—	—
224				1·474			1·473		
233				1·473			1·472		
035				1·472			1·471		
311	—	1·460	MF	1·461	1·460	M	1·460	—	—
240				1·457			1·455		
044				1·455			1·453		
241	—	1·442	VF	1·438	—	—	1·437	—	—
151	—	1·426	MF	1·425	1·427	MF	1·424	1·423	0·6 D
106				1·429			1·429		
116	—	1·403	M	1·404	1·402	M	1·403	1·399	0·8 D
320				1·403			1·402		
026				1·400			1·399		
321	—	1·388	M	1·386	1·387	M	1·385	1·384	0·2 D
144				1·386			1·384		
234	331	1·356	MF	1·353	1·350	MF	1·352	1·348	0·6 D
303				1·349			1·348		
—	420	1·326	MS	—	—	—	—	—	—

* Relative to $a_{PbS}=5{\cdot}929$ A. (5·917 kx.) (Wilman 1948, Elleman and Wilman 1948).

† S=strong, M=medium, F=faint, V=very.

‡ Using $a=4{\cdot}530$, $b=7{\cdot}614$, $c=9{\cdot}035$ A.

§ Using $a=4{\cdot}52476$, $b=7{\cdot}60446$, $c=9{\cdot}02666$ (Straumanis and Sauka 1942, 18° C.)

‖ Supplement File of X-ray powder-pattern data, 1945, published by the American Society for Testing Materials. B and D refer to intensity estimates by Bräkken (1932) and Döll and Klemm (1939) respectively.

Table 2. Axial Lengths and Axial Ratios of $PbCl_2$

Axial lengths			Axial ratios	Reference
a	b	c	a : b : c	
Optical Goniometer				
—	—	—	0·5951 : 1 : 1·1882	Schabus (1850) (reoriented)
			0·5952 : 1 : 1·1872	Groth (1906) from Stöber (1895)
			0·5947 : 1 : 1·1855	Zambonini (1910)
X-ray Diffraction				
4·496	7·667	9·153	0·5864 : 1 : 1·193	Bräkken and Harang (1928)
4·523	7·618	9·037	0·5938 : 1 : 1·186	Miles (1931)
4·525	7·608	9·030	0·5947 : 1 : 1·187	Bräkken (1932)
4·520	7·605	9·027	0·5947 : 1 : 1·188	Döll and Klemm (1939)
4·52476	7·60446	9·02666	0·594501 : 1 : 1·18702	Straumanis and Sauka (1942)*
4·52583	7·60648	9·02772	0·59499 : 1 : 1·18684	Straumanis and Sauka (1942)†
Present Electron Diffraction Results				
4·530‡	7·614‡	9·035‡	0·5950 : 1 : 1·187	Present results

* At 18° C. † At 25° C. ‡ Values in A. relative to PbS, $a=5{\cdot}929$ A. (5·917 kx.)

(ii) *Reflection Specimens*

Table 3 describes eight PbS specimens examined by reflection, with their thickness, orientation, duration of heating at 200° c., and whether or not the patterns contained PbS as well as $PbCl_2$ diffractions. In all cases the $PbCl_2$ was in the same two-degree orientations relative to the {001}-orientated PbS crystals, whose axes were parallel to those of the NaCl substrate crystal. The orientations shown by the patterns are of three types: (i) {010}, (ii) {012}, and (iii) {110} parallel to the {001} PbS surface plane. In (i) and (ii) *a*, and in (iii) *c*, of the $PbCl_2$ was parallel to $\langle 110 \rangle$, $\langle 1\bar{1}0 \rangle$, $\langle \bar{1}10 \rangle$ or $\langle \bar{1}\bar{1}0 \rangle$ of the PbS.

Figure 2 is the pattern obtained with the electron beam directed along the PbS cube-face diagonal in its (001) surface. The directions of the $PbCl_2$ axes as seen when looking along the cube-face diagonals of the PbS are shown in Figure 6 for the above orientations which, as just indicated, fall into three groups with four in each group corresponding to the four-fold symmetry of the (001) PbS surface plane. The composite diffraction pattern at this azimuth, resulting from $PbCl_2$ in these orientations (in the region within about 3 cm. from the undeflected beam spot), accounts for all but a few of the spots visible in Figure 2, with good agreement of the relative intensities with those recorded for the corresponding x-ray diffractions. Figure 6 is an enlarged diagram showing the spot positions in this central part of the pattern and the unit parallelograms of the spot patterns associated with the different $PbCl_2$ orientations. The spots due to the {010}-orientated $PbCl_2$ crystals are laterally sharp but are slightly elongated towards the shadow edge, indicating crystals about 500 A. in lateral diameter with (010) faces as their upper surfaces, parallel to the smooth PbS substrate. The sharp spots due to the other orientations are hardly elongated at all normal to the shadow edge but those due to the {012}-orientated $PbCl_2$ are arced by about 2° rotation about the undeflected-beam spot. This arcing is more apparent in Figure 4, obtained at an azimuth 1½° displaced from that of Figure 2. The positions and intensities of the remaining spots show that the {010}-orientated crystals were strongly twinned on {012} planes. Measurement of the spot separations in the reflection patterns gave axial ratios $c/b = 1{\cdot}186$ and $c \simeq 2a$.

Table 3. Results of Heating PbS on {001} NaCl Substrates in Air at 200–300° c.

PbS Thickness	PbS Orientation on {001} NaCl	Time of heating (min.)	Substances observed by diffraction *
50 A.	{001}	5	$PbCl_2$
	{001}+{111}	10	{001}+{111} PbS
250 A.	{001}	5	{001} PbS+$PbCl_2$
	{001}	5	$PbCl_2$
	{001}	5	{001} PbS+$PbCl_2$
	{001}	20	$PbCl_2$
	{001}+{111}	45	{001}+{111} PbS +$PbCl_2$
1000 A.	{001}	10	{001} PbS

* The $PbCl_2$ was in each case in the same orientations with respect to the {001} orientated PbS crystals. The orientations are given in the text.

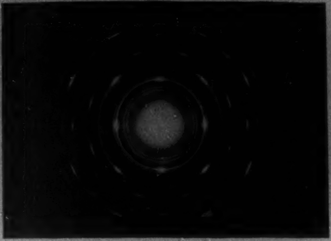

Figure 1. PbS (arcs) + $PbCl_2$ (rings); normal transmission.

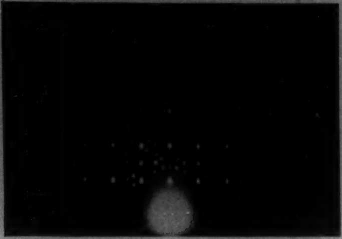

Figure 2. $PbCl_2$ on PbS; beam along [110] PbS.

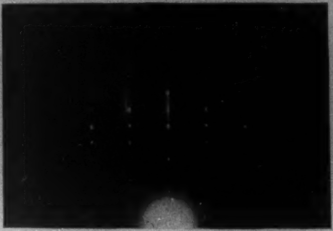

Figure 3. $PbCl_2$ (spots) + PbS (streaks); beam along [100] PbS.

Figure 4. $PbCl_2$ on PbS; azimuth 1½° from Figure 2.

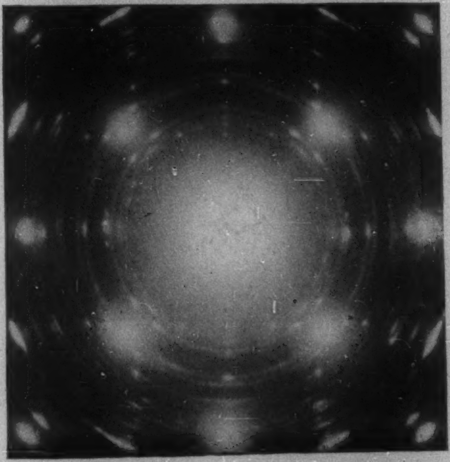

Figure 5, PbS (strong arcs) + $PbCl_2$ (short arcs and rings); normal transmission from partially broken-up film.

Figure 3 shows the pattern obtained with the beam along a PbS cube edge in the PbS substrate surface. Most of the strong spots of this pattern correspond to the {010}-orientated $PbCl_2$ which was the most preferred orientation shown in Figure 2, thus in Figure 3 the beam was along a [201] $PbCl_2$ lattice row of the (010) plane, and the [$\bar{2}$01] row was therefore practically normal to the beam (and parallel to the specimen surface).

The following diffractions (of type h, k, $2h$) were observed above the rather high shadow edge with strong or medium intensity:—020, 040, 060, 080, 0.10.0, 0.12.0, 0.14.0; 122, 142, 162; 224, 244, 264, 284.

(iii) *Transmission Patterns from the Orientated $PbCl_2$*

The patterns obtained at normal transmission from the less distorted films of the PbS partially converted to $PbCl_2$ are shown diagrammatically in Figure 7 (*a*). They contain only a few but sharp spots from the $PbCl_2$ in addition to the strong PbS ones. Figure 7 (*a*) shows the main features near the centre of the pattern, together with the typical indices assigned to the diffractions. The strongest $PbCl_2$ diffractions occurring are groups of four spots of 111 and 121 type surrounding the strong PbS 200 spots; and also the spots of 200 and 032 types close within the PbS 220 spots along the same radius, those of 204 type close within the PbS 400 spots, and the spots of 131 type.

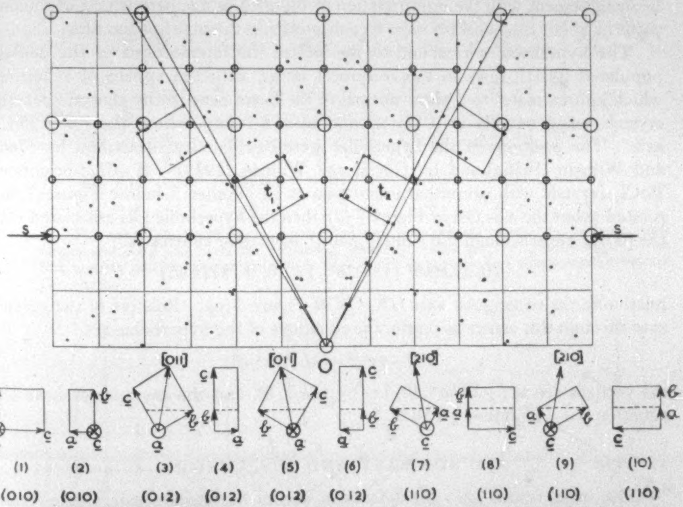

Figure 6. Spot positions in Figure 2, and their origin from the various (010), (012) and (110) orientations. The strong spots and weaker ones associated with the main orientations (010), (1) and (2), are distinguished by circles; t_1 and t_2 show the rectangular units of the spot patterns from the {012} twins of the {010} orientated crystals (orientations (3) and (5)). S–S indicates the shadow-edge region in Figure 2.

The occurrence, positions and relative intensities of the observed diffractions are consistent with the $PbCl_2$ orientations established by the reflection patterns provided it is assumed that parts of the composite PbS–$PbCl_2$ film are cylindrically curved about well-defined axes parallel to the PbS cube-face diagonals in the plane of the film. Such curvature of the remaining PbS substrate layer is shown by the occurrence and positions of PbS diffractions of *hk*1 type, for example, in Figure 5. The amounts of curvature necessary for the appearance of diffractions of types *h*11, *h*22, *h*21, and *h*32 from {012}-orientated $PbCl_2$ and 11*l*, 12*l*, 13*l* 14*l*, 22*l*, 23*l*, and 24*l* from {110}-orientated $PbCl_2$ are shown in Figures 8 (*a*), (*b*), (*c*). The *h*0*l* diffractions near the central spot can arise from the {010}-orientated $PbCl_2$ crystals without the need of assuming any curvature. Typical of the agreement of the intensities with those of the X-ray patterns are, for example, the absence of 100, 102, 122, the faintness of 002, 110, 011, 022, 101 and 103 and the relatively high intensity of 200, 204, 012, 032, 111, 121 and 131.

The patterns from more distorted films were as shown in Figure 5 and show even more clearly the curvature about the above well-defined axes. Figure 7 (*b*) shows the spot positions and intensities diagrammatically on a larger scale. The straight lines and hyperbolae represent construction lines on which the spots lie in agreement with the interpretation of Figure 5 as a superposition of rotation patterns about the two PbS cube face diagonals in the plane of the film.

The hyperbolae correspond to the loci of the intersections of the densely populated [001]* rows in the reciprocal lattice with the sphere of reflection, which approximates to a plane normal to the beam near to the central spot, the crystals being initially in (012) orientation and rotated about the $[02\bar{1}]$ $PbCl_2$ axis. The positions of the hyperbolae were calculated as described by Finch and Wilman (1936a) and by Goche and Wilman (1939). If {012}-orientated $PbCl_2$ crystals with azimuthal orientation as in number 3 below Figure 7, are rotated about the axis OA in Figure 7 (*a*), then the hyperbolic loci associated with the [001]* rows through the points [[*hk*0]]* have their centres at

$$(0,\ \lambda Lk(4b^2+c^2)^{\frac{1}{2}}/2b^2),\ \text{i.e.}\ (0,\ 0{\cdot}1511k\lambda L)$$

relative to the rectangular axes OX, OY of Figure 7 (*a*). Relative to the parallel axes through this centre as origin, the equations of the hyperbolae are

$$x^2c^2-4y^2b^2=(\lambda L)^2h^2c^2/a^2\,;$$

the vertices are at $(\pm\lambda Lha^*, 0)$, i.e. $(\pm\lambda Lh/a, 0)$, and the asymptotes have the equation $y=\pm(c/2b)x=\pm 0{\cdot}593x$.

§4. SUMMARY AND DISCUSSION

The main results are: (i) a reaction occurs between mosaic single-crystal PbS layers about 250 A. thick and their single-crystal NaCl substrates in presence of air at 200 to 300° C., to form $PbCl_2$; (ii) no other product besides $PbCl_2$ was observed, and in particular no formation of $PbO . PbSO_4$ was detected; (iii) the resulting $PbCl_2$ took up definite two-degree orientations of {010}, {012} and {110} types relative to the {001} PbS substrate surface plane; (iv) the {010}-orientated $PbCl_2$ crystals were strongly twinned on {012} planes and had relatively smooth {010} faces parallel to the substrate; (v) the $PbCl_2$ lattice constants and relative diffraction intensities agreed closely with those found previously by X-ray diffraction; (vi) parts of the initial PbS layers and of the composite PbS–$PbCl_2$ layers, when the layers were isolated from the NaCl substrates, became cylindrically curved about remarkably well-defined axes which were parallel to the film plane and to the PbS cube-face diagonals; (vii) this example illustrates the fact that reflection patterns from such deposits *in situ* on their single-crystal substrates are the most reliable for determining the types of net-plane orientated parallel to the substrate surface, and that transmission patterns, though generally affected by break-up and curvature of the film, can then provide a still more sensitive definition of the azimuthal orientations present.

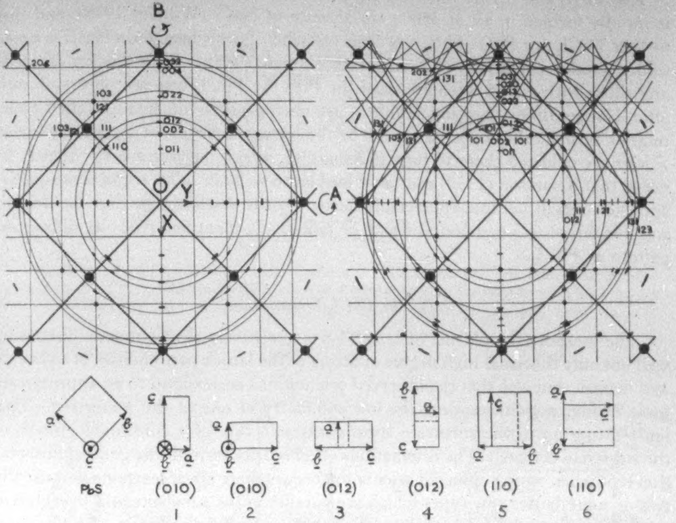
B
A
O
Y
X
204
103
121
111
110
002
004
022
012
011
131
101
123
a
b
c
PbS
(010)
(010)
(012)
(012)
(110)
(110)
1
2
3
4
5
6

Figure 7. The main features of Figure 5; the PbS spot positions are represented by large black circles and long arcs, and the remaining spots and rings are $PbCl_2$ diffractions. The $PbCl_2$ spots lie either on straight layer lines or the hyperbolic loci whose asymptotes are also shown.

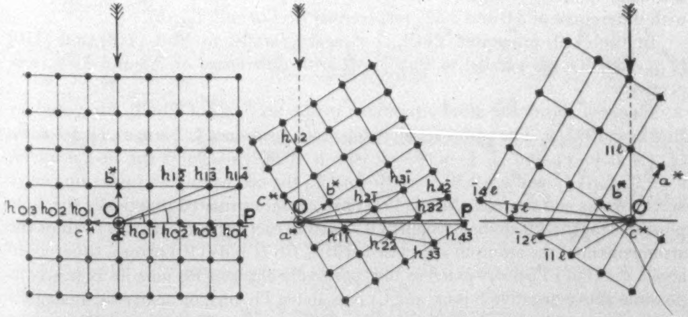
h03 h02 h01
O
P
c*
a*
b*
h0 1̄ h0 2̄ h0 3̄ h0 4̄
h1 2̄ h1 3̄ h1 4̄
h12
h2 1̄
h3 1̄
h4 2̄
h32
h11
h22
h3 3̄
h43
11ℓ
1̄4ℓ
1̄3ℓ
1̄2ℓ
1̄1ℓ
(a) (010) ORIENTATION
(b) (012) ORIENTATION
(c) (110) ORIENTATION

Figure 8. Reciprocal-lattice planes normal to the axes of curvature in the case of the (010), (012) and (1̄10) orientations, showing the angles of rotation required to cause the various diffraction spots to appear.

(i) and (ii). *The Nature of the Reaction*

Results (i) and (ii) are in strong contrast to the observation that $PbO . PbSO_4$ is rapidly formed in air at 350° c. in absence of NaCl (Wilman 1948), and that neither $PbCl_2$ nor $PbO . PbSO_4$ is observed when PbS is heated on NaCl *in vacuo* under similar conditions (Elleman and Wilman 1948). With thicker deposits and those with mixed orientations of the PbS the $PbCl_2$ was not observed until after a longer time of heating (Table 3), which appears to indicate that the Cl ions migrate through the deposit and react on the surface to form $PbCl_2$, and the excess S ions are oxidized there to form gaseous SO_2 which diffuses away. It may be noted that Thomson (1930) sputtered lead on to rocksalt in an argon atmosphere, and the rocksalt became appreciably heated by the discharge so that the deposit was converted to a compound which he tentatively identified from its diffraction pattern as $PbCl_2$.

(iii) *The $PbCl_2$ Orientations*

The present example of $PbCl_2$ on PbS is a relatively clear-cut case illustrating well not only the usual high degree of fitting of the lattice periodicities in substrate and deposit, but also that the observed orientations correspond to an approximate ionic fitting, notwithstanding the low symmetry of one of the materials. This ionic fitting on to the substrate approximates to that of a continued growth of the substrate crystal. The orientations observed conform to the general observation that when strong epitaxial orientation occurs there are at least one and usually two or more lattice row types which are parallel in the substrate and overgrowth crystals, with nearly equal lattice spacings along parallel directions. In this case, for the {010}-orientated $PbCl_2$, a (4·530 A.) or c (9·035 A.) was parallel to PbS [110] (8·385 A.) and the differences of $2a$ and c from the PbS-spacing are 8·0 and 7·7% of the PbS [110] periodicity respectively. In the {012}-orientation a is again parallel to PbS [110], and [021] ($T = 17·70$ A.) parallel to PbS $[1\bar{1}0]$, with differences of 8·0 and 5·5% respectively (for $2a$ and $T_{021}/2$).

In the {110}-orientated $PbCl_2$, c is again parallel to PbS [110] and $[1\bar{1}0]$ ($T_{110} = 8·859$ A.) is parallel to PbS $[1\bar{1}0]$, with differences of 7·7 and 5·7% respectively.

Figure 9 shows the atomic positions in the unit cell of $PbCl_2$, estimated by Bräkken (1932). The atoms are all in four-fold positions $(\frac{3}{4}, \frac{3}{4}+u, v)$, $(\frac{1}{4}, \frac{1}{4}-u, \bar{v})$, $(\frac{3}{4}, \frac{1}{4}+u, \frac{1}{2}-v)$, and $(\frac{1}{4}, \frac{3}{4}-u, \frac{1}{2}+v)$, with $u = 0·004$, $v = 0·095$ for Pb; $u = 0·40$, $v = 0·07$ for Cl_1, and $u = 0·30$, $v = 0·67$ for Cl_2, the cell having an inversion centre at its corners and centre. Miles (1931) had earlier estimated practically the same positions for the Pb atoms. Figure 10 was constructed from Figure 9 to show the arrangement of the atoms in and close to (010), (012) and (110) planes, superposed above the (001) PbS net-plane so that positively charged Pb ions lie as nearly as possible above negative S ions, and Cl ions above Pb ions, or nearly so, analogous to the continued growth of PbS on the PbS crystal. The Pb and Cl ions are joined by lines merely to show differently situated groups. It will be seen that in the {010} and {012} orientations there are chains of Cl and Pb ions parallel to the $PbCl_2$ a axis, approximating more or less closely in size and positions to the square PbS ionic arrangement, with intermediate bands where the Pb and Cl ions lie (above and) between two pairs of PbS ions in less firmly bound positions. In the {110}-orientation there are again Cl–Pb–Cl groups in similar positions of

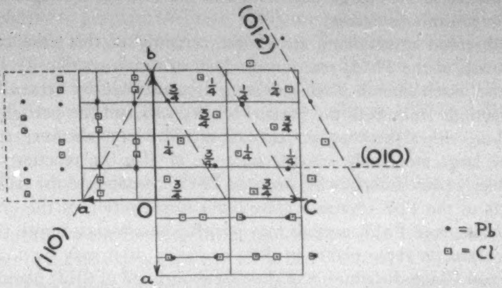

Figure 9. Projections of the atomic positions of $PbCl_2$ on the unit cell faces, according to Bräkken (1932), drawn to the same scale as Figure 10.

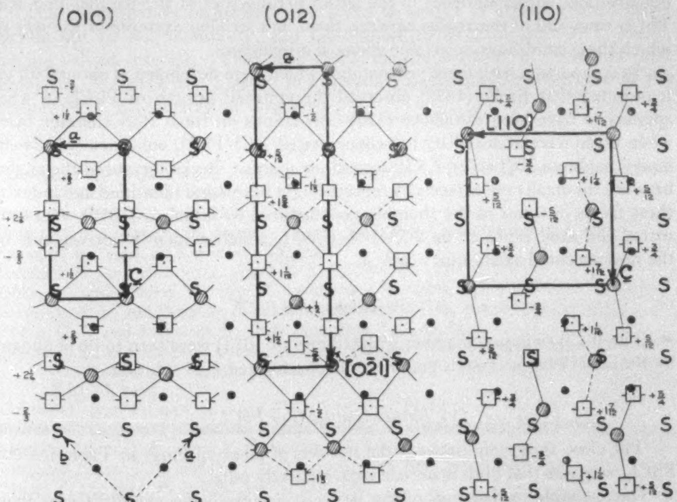

Figure 10. The epitaxial fitting of $PbCl_2$ in (010), (012) and (110) orientations on the (001) PbS surface.

● = Pb and **S** = S in PbS (001) surface.

▨ = Pb and ⊡ = Cl in adjacent $PbCl_2$.

The approximate heights of the Pb and Cl ions of the $PbCl_2$ are in A. and these heights of the ions above the (010), (012) and (110) planes shown in Figure 9 are also represented as fractions of the (002) PbS net-plane spacings by the positions of the short horizontal lines at each side of the symbol where the radius of the symbol represents the (002) PbS net-plane spacing.

correspondence to the charge distribution in the PbS ion arrangement, but this time not in continuous chains.

The observed orientations are almost certainly in this case characteristic of the growth of the $PbCl_2$ reaction product on nearly atomically smooth PbS cube-faces. Such smooth PbS faces were demonstrated by vertically elongated PbS diffractions from both the initial PbS deposits and the partially converted layers; thus, either the rougher parts of the PbS crystals were attacked first before the large atomically smooth surfaces, or else the reaction proceeds at first at a nearly plane interface between the $PbCl_2$ crystals and the still unattacked lower parts of the PbS crystals. The slight imperfection of the orientation of the {012}-orientated $PbCl_2$ crystals may possibly be associated with the twinning which occurred on these planes in these crystals; or it may be a consequence of the Pb and Cl ion distribution in the neighbourhood of (012) planes, as shown in Figures 9 and 10. It is not due to any larger difference of periodicities from those of the parallel PbS rows since the fit is as good as in the {010} and {110} orientations. Indeed, the occurrence of the three types together, with such equally close correspondence in the lattice periodicities of the parallel PbS and $PbCl_2$ rows and of the angles between them, is a striking example of the way in which these conditions determine epitaxial orientation.

In comparison with these orientations, which were developed at about 250° c., it is noted that Becke (1885) observed the epitaxial growth of $PbCl_2$ in what appears to have been the above {110} orientations on fresh PbS cleavage faces when these were attacked by hot concentrated HCl–$PbCl_2$ solutions (for 24–36 hours) or dilute HCl at 70° c. (30 seconds or more). Becke measured the angles between the small crystal facets by reflected light beams and identified and indexed these facets in terms of the rhombic axes deduced by Schabus (1850), who estimated the axial ratios to be $0{\cdot}5941:1:0{\cdot}5951$, which evidently corresponds to the now accepted axial ratios $c/2:b:a$.

(iv) *Twinning of the $PbCl_2$*

The {012}-twinning together with trillings on {012} were seen to be abundant by Stöber (1895) in crystals grown from concentrated HCl solution.

(v) *Lattice Constants of $PbCl_2$*

The close agreement between the two sets of plane spacings in Table 1, from $PbCl_2$, suggests that both materials were relatively pure.

One possible explanation of the lattice constants being slightly larger than those obtained by X-rays may be that owing to the high absorption of the electron beam in this compound the coherent diffraction pattern is mainly due to crystals which are only of the order of 100 A. thick though approximately 500 A. in lateral diameter, this severe lattice limitation being associated with a slight change of lattice dimensions. Lennard-Jones (1930) showed theoretically that such a change of lattice-dimensions was in general to be expected in the outermost two or three atomic layers of crystals, an expansion or contraction of a few per cent occurring according to the type of binding and surface-plane direction. However, no clear evidence of such a change of dimensions has yet been found in electron diffraction. The relative lattice dimensions of materials of large crystal diameter but of widely different absorbing powers, as with gold and graphite

(Finch and Fordham 1936, Finch and Wilman 1937a), and silver, AgCl, AgBr and NaCl relative to graphite (Wilman 1940), are practically identical with those of the most reliable x-ray values (for graphite see Trzebiatowski 1937, and Nelson and Riley 1945). The axial ratios of the $PbCl_2$ are effectively identical with those found by x-rays, as was the case with graphite (Finch and Wilman 1936b), MoS_2 (Finch and Wilman 1936a) and CdI_2 (Finch and Wilman 1937b). An explanation on the above lines would thus appear to be impracticable.

(vi) *The Nature of the Breaking-up and Curvature of the Composite PbS–$PbCl_2$ Layer*

The curvatures of the PbS and the composite PbS–$PbCl_2$ layers about definite axes is similar to the case described by Goche and Wilman (1939) of silver deposits on rocksalt cleavage faces, the axes of bending in both cases being mainly about the cube-face diagonals, and originating from the stepped structure of the rocksalt cleavage faces.

§ 5. ACKNOWLEDGMENTS

This investigation forms part of a series of studies of crystal growth being carried out in this laboratory, and the authors thank Professor G. I. Finch, for his valued interest. They also thank the Department of Scientific and Industrial Research for a grant to Professor Finch which enabled one of the authors (A. J. E.) to carry out this work.

REFERENCES

American Society for Testing Materials, First Supplement File of X-ray Powder-Pattern Diffraction Data, 1945.

Becke, F., 1885, *Tsch. min. Mitt.*, **6,** 240, 270.

Bragg, W. L., 1947, *J. Sci. Instrum.*, **24,** 27; 1948, *Acta Crystallographica*, **1,** 46.

Bräkken, H., 1932, *Z. Kristallogr.*, **83,** 222.

Bräkken, H., and Harang, L., 1928, *Z. Kristallogr.*, **68,** 123.

Döll, W., and Klemm, W., 1939, *Z. anorg. allg. Chem.*, **241,** 246.

Elleman, A. J., and Wilman, H., 1948, *Proc. Phys. Soc.*, **61,** 164.

Finch, G. I., and Fordham, S., 1936, *Proc. Phys. Soc.*, **48,** 85.

Finch, G. I., and Wilman, H., 1936a, *Trans. Faraday Soc.*, **32,** 1539; 1936b, *Proc. Roy. Soc.* A, **155,** 345; 1937a, *Ergebn. exakt. Naturw.*, **16,** 353; 1937b, *Trans. Faraday Soc.*, **33,** 1435.

Goche, O., and Wilman, H., 1939, *Proc. Phys. Soc.*, **51,** 625.

Groth, P., 1906-1919, *Chemische Krystallographie*, **1,** 219 (Leipzig: Engelmann).

Lennard-Jones, J. E., 1930, *Z. Kristallogr.*, **75,** 215.

Lennard-Jones, J. E., and Dent, B. M., 1928, *Proc. Roy. Soc.* A, **121,** 247.

Miles, F. D., 1931, *Proc. Roy. Soc.* A, **132,** 266.

Nelson, J. B., and Riley, D. P., 1945, *Proc. Phys. Soc.*, **57,** 477.

Schabus, C., 1850, *Sitzb. d. Akad. Wiss. Wien*, **4,** 456.

Stöber, G., 1895, *Bull. Acad. Belg.*, **30,** 345; *Groth's Zeits.*, **28,** 108.

Straumanis, M., and Sauka, J., 1942, *Z. phys. Chem.*, B, **51,** 219.

Thomson, G. P., 1930, *The Wave Mechanics of Free Electrons* (New York and London: McGraw-Hill), p. 77.

Trzebiatowski, W., 1937, *Rocz. Chem.*, **17,** 73.

Wilman, H., 1940, *Proc. Phys. Soc.*, **52,** 323; 1948, *Ibid.*, **60,** 117.

Zambonini, F., 1910, *Min. Vesuv.*, p. 45.

On the Absorption Spectrum of Cosmic Rays

By E. W. KELLERMANN and K. WESTERMAN
The Physical Laboratories, The University, Manchester

Communicated by P. M. S. Blackett; MS. received 10th November 1948

ABSTRACT. Attempts at the measurement of the absorption spectrum of cosmic rays by means of counter telescopes have been made by many authors. It is pointed out here that none of the usual methods, i.e. the determination of the number of coincidences as a function of the absorber thickness, can be satisfactory unless the influence of the geometry through scattering is known. Only then can this (integral) absorption curve be used for the determination of the momentum spectrum.

A method of determining directly the differential absorption curve is described which avoids largely the influence of scattering. This method has been used for the investigation of some specific effects which have been observed by some and denied by other authors. In particular, the region of 12 cm. Pb has been investigated, and it is found that the change of absorption observed here is due solely to the overlapping of the high momenta end of the electron spectrum and of the meson spectrum. Although the present investigation cannot confirm it, it does not exclude the possibility of a specific change of the absorption coefficient in the 22 cm. Pb region.

§1. INTRODUCTION

CLOUD chamber measurements by Blackett and others (cf. Williams 1939) of the momentum spectrum of cosmic rays confirm—within their limits of accuracy—the picture of the composition of cosmic rays at sea level generally assumed: up to a momentum of 200 MeV. electrons are preponderant in the cosmic-ray spectrum; in the low momentum region there are few mesons, as must be assumed considering their decay. The meson differential spectrum curve rises steadily to a maximum at about 700 MeV. Meson absorption, except in the low momentum region, is due to ionization loss.

Attempts have been made to interpret the integral absorption curve, i.e. coincidences per unit time plotted against varying thicknesses of absorber, as a monotonic function of the momentum spectrum. In general, the picture of the composition of the spectrum given above is confirmed. On the other hand, none of these integral absorption measurements has a claim to any great accuracy: the slopes of the absorption curves measured by various investigators differ, and the absorption coefficients show variations of up to 100%. A rough calculation shows that variations of this kind can be due to scattering conditioned by the geometry of the arrangement. This has been confirmed by Trumpy and Orlin (1943), who investigated the effect of scattering experimentally.

In addition, some authors have claimed recently to have observed specific deviations from the generally accepted course of the absorption curve. The absorption curve shows a region of relatively rapid absorption to a thickness of 10 cm. Pb, and then a lesser absorption. The first region of absorption is ascribed to the electronic component, and the second to the meson component. Now George in London and Appapillai in Ceylon (George and Appapillai 1945) consider that the integral absorption curve shows a region of zero absorption between 10 and 15 cm. Pb, and in the 23 cm. Pb region Swann and Morris (1947) find a pronounced decrease of the integral absorption at a latitude of 7° S., and they conclude that the effect in the 23 cm. Pb region is latitude dependent. It should be mentioned that in this region other authors, in particular Chandrashekhar Aiya (1944), have observed specific effects. The effect found by George and Appapillai lies just outside the limits of the single standard deviation, while Chandrashekhar Aiya's discontinuity is still within the standard deviation. None of these authors take account of the influence of scattering. Here, attention must be drawn to the work of Clay, Venema and Jonker (1940), who observe maxima of the absorption curve in the 15 and 25 cm. Pb region when lead is placed above the counters of their telescope, yet no maximum with lead placed between the counters.

Effects of this kind, if definitely established, would, of course, require a modification of the simple picture of cosmic radiation which ascribes the two regions of absorption, one to the electron component and one to the penetrating component. In particular, one would have to introduce special assumptions in order to interpret the absence of mesons of a momentum of 250 to 300 MEV., corresponding to a "plateau" between 10 and 15 cm. Pb.

Our experiment has been concerned mainly with the investigation of the 10 to 15 cm. Pb region by means of a counter telescope. We have determined not only the integral absorption curve, but simultaneously have observed the differential absorption curve. Using this latter method, the influence of scattering is greatly diminished, and we have been able to investigate the absorption under conditions when the interpretation of the measurements is less in doubt.

§ 2. EXPERIMENTAL METHOD

A diagram of the counter arrangement is given in Figure 1. The counter trays t, m and b each consisted of two counters connected in parallel, and the three pairs constituted a threefold coincidence arrangement. In addition, t, m and b were also connected in a fourfold coincidence circuit with the side counters S and the bottom counters B, all of which were in parallel.

The counters t, m, b and S were 30 cm. long, the counters B 60 cm. in length. The outside diameter of all the counters was 3·7 cm. They were pyrex Geiger–Müller counters filled with argon and alcohol. Lead could be placed between the counters t and m, and also between m and b. The counters rested on a light framework, and the lead consisted of plates about 1 cm. in thickness and 8 cm. in width. Thus the counters m and b were covered by lead, but not the anti-coincidence counters S. Between the counters b and the bottom counters B there was a space sufficient for four lead plates, each of 1 cm. thickness.

The opening angles of the telescope, 21° and 71° respectively, were large enough to give a threefold rate of about 550 counts per hour with 10 cm. Pb between the counters. The telescope gave the following information: Particles setting off t, m, b and B were recorded separately as threefold and fourfold coincidences. Particles setting off t, m and b, but unable to penetrate the additional 4 cm. of lead between b and B, were recorded as threefold coincidences only. Side showers might set off t, m, b and one of the S counters and thus give rise to simultaneously recorded threefold and fourfold coincidences. Particles penetrating t, m and b, but scattered so that they did not penetrate the 4 cm. lead, might nevertheless set off one of the counters B and thus give rise to a fourfold coincidence. Hence a separate registration of anti-coincidences, i.e. threefold coincidences unaccompanied by fourfold coincidences, gave the number of particles penetrating (say) x cm. Pb between the counters t, m and b, but not penetrating $(x+4)$ cm. Pb. This registration would then also exclude some effects due to side showers and discriminate against the influence of scattering. The recorded threefold coincidences gave the integral absorption curve when plotted against different thicknesses of lead, but did not differentiate against side showers nor any bias introduced by scattering.

The counter pairs t, m and b were each connected to the grids of pentodes in a threefold Rossi circuit triggering a thyratron which in its turn operated two telephone counters in series. The counter pairs were connected also to three other pentodes each, and the counters S and B to a seventh pentode. The latter four pentodes were again connected in a fourfold Rossi circuit triggering a thyratron which operated a telephone counter and a relay in series. The relay when operating short-circuited the second telephone counter of the threefold circuit so that this counter operated only when there was a threefold coincidence unaccompanied by a fourfold and, therefore, registered anti-coincidences.

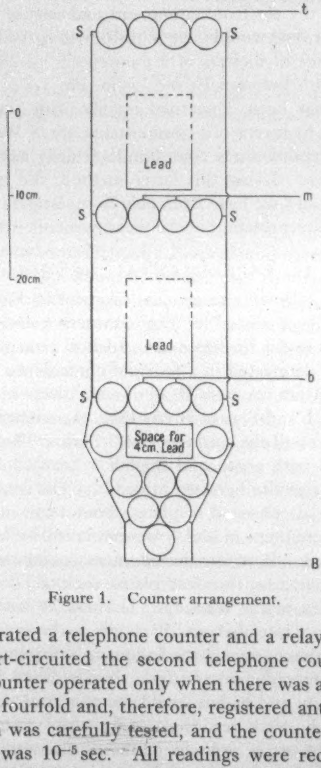

Figure 1. Counter arrangement.

The relay system was carefully tested, and the counters were checked daily. The resolving time was 10^{-5} sec. All readings were reduced to a barometric pressure of 30 in. Hg (cf. Duperier 1944). An equal number of lead plates was placed between t and m, and m and b respectively, and 4 cm. lead was placed between b and B, always after the background, i.e. the number of anti-coincidences with x cm. lead between t, m and b and no lead between b and B, had been determined. The background remained constant at $2{\cdot}5 \pm 0{\cdot}25$ counts per hour throughout the experiment.

§ 3. RESULTS

(i) *The Integral Spectrum*

Coincidence counts were taken for thicknesses x of lead varying from 0 to 26·3 cm. No point on the curve was determined with a standard deviation of less than ±0·5%. The results are tabulated in Table 1. Figure 2 shows the number of threefold coincidences per hour as a function of the thickness of the lead absorber. It is seen that there is a rapid decrease to 10 cm. Pb, and thence

Table 1

(1)	(2)		(3)	(4)	(5)
cm.	hr.	min.			
0·0	209	08	162,853	778	±2·0
1·9	190	41	115,906	608	±2·0
3·9	192	18	113,286	590	±2·0
8·0	165	30	93,764	566	±2·0
10·3	162	48	90,798	558	±2·0
12·2	230	01	128,099	558	±1·5
14·2	100	33	55,407	550	±2·5
16·2	91	30	48,969	535	±2·5
18·2	94	49	49,782	525	±2·5
20·2	140	38	70,635	503	±2·0
22·3	94	11	47,031	499	±2·5
24·3	95	06	46,760	492	±2·5
26·3	70	59	33,861	477	±2·5

(1) Total thickness of lead in layers 1 and 2. (2) Total time. (3) Total number of counts reduced to 30 in. Hg pressure. (4) Rate per hour. (5) Standard deviation.

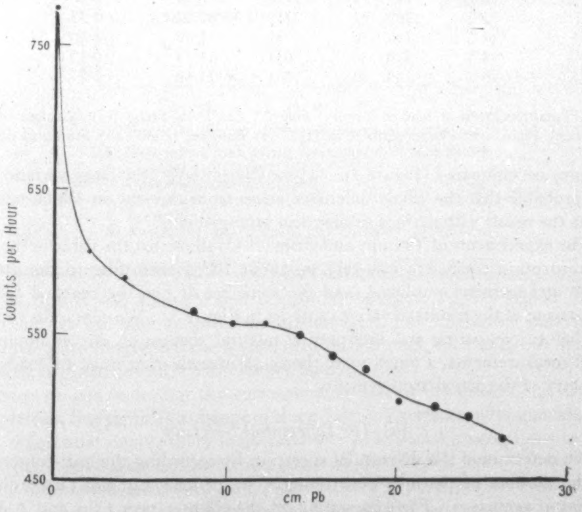

Figure. 2. Integral absorption.
Radius of circle indicates standard deviation.

a slow drop to 30 cm. Pb. From 10 to 13 cm. the graph shows distinctly an almost horizontal stretch similar to that found by George and Appapillai. Furthermore, it can be seen that there may be another change of slope at 22 cm. Pb, but the statistical error is too great for this to be certain; the change of slope suggested here, however, is of a different character from that described by Chandrashekhar Aiya.

It will be seen that, in spite of small standard deviations (cf. Table 1), our measurement of the integral spectrum alone does not contribute much to the elucidation of the information already available from the work of other authors.

As already described, the general shape of the integral curve is similar to those obtained by George and Appapillai and by other authors, in so far as they all show a region of rapid absorption up to about 9 cm. Pb, very little absorption between 9 and 13 cm. Pb, and then again more rapid absorption (though less than that up to 9 cm. Pb). There are, however, notable differences which appear if the slopes of the integral curves from say 20 cm. Pb onwards, as determined by various authors, are compared (Figure 3). These slopes show very large variations, and it is probable that the whole difference arises from the way in which scattering affects the result with various geometrical arrangements.

Table 2

(1)	(2)		(3)	(4)	(5)
cm.	hr.	min.			
3·9	46	00	603	13·10	±0·54
6·1	128	00	1480	11·58	±0·30
8·0	236	00	2520	10·69	±0·21
8·8	402	43	4235	10·51	±0·16
10·3	159	53	1716	10·74	±0·26
12·2	209	53	2355	11·22	±0·23
14·2	280	50	3281	11·68	±0·20
14·8	430	39	5051	11·74	±0·17
16·2	160	24	1861	11·60	±0·27

(1) Total thickness of lead in layers 1 and 2. (2) Total time. (3) Number of counts with 4 cm. Pb in layer 3 reduced to 30 in. Hg. (4) Rate per hour. (5) Standard deviation.

The experiments of Trumpy and Orlin (1943) show that the value of the apparent absorption coefficient can vary by about 100% according to the geometry of the arrangement employed, and the same result may be reached from our comparison of the results of various authors in Figure 3. We conclude, therefore, that before comparing and interpreting integral absorption curves obtained by direct measurements, a much more thorough investigation must be made of the geometry of the actual arrangements.

(ii) *The Differential Spectrum*

We determined the differential spectrum by recording the anti-coincidences, i.e. the number of particles penetrating x cm. of lead, but not $(x+4)$ cm., and plotting it against x. Particles setting off the counter rays t, m and b, but not penetrating the additional 4 cm. lead below the tray b, were recorded as anti-coincidences, provided no other counters were set off. It has been explained above how our arrangement discriminated against scattered particles, so that our determination of the differential spectrum is largely independent of the influence of the geometry in that respect. Hence our differential spectrum is not subject to the same criticism which must be made in the case of methods employed in measuring directly the integral absorption curve.

The differential spectrum is plotted in Figure 4. It will be seen at once that in spite of the larger standard deviation as compared with the integral curve we can extract more definite information from the differential than from the integral curve.

Consider in particular the minimum at $x=9$. This value of the abscissa corresponds to the interval of 9 to 13 cm. Pb of the abscissa of the integral curve. Whereas in the case of the integral curve we are unable to decide whether the curve in this region shows a real horizontal "plateau", i.e. a region of zero absorption, we can gain decisive information from the differential curve: here we can see quite clearly that the minimum does not touch the x axis, but that even the lowest ordinate is still 8 particles per hour.

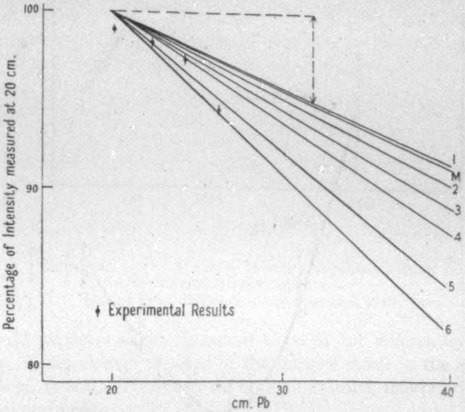

Figure 3. Slopes of integral absorption curves.

M. Determined from meson spectrum (cf. Wilson 1946).
1. Clay and van Gemert (1939).
2. Chandrashekhar Aiya (1944).
3. George and Appapillai (1945).
4. Rossi (1933).
5. Auger, Leprince-Ringuet, and Ehrenfest (1936).
6. Clay (1936).
The experimental results are those of the present authors.

Hence we conclude that the corresponding part of the integral curve is not a real plateau, but signifies a change of slope only. Therefore, after consideration of the differential curve, there is no need to make special assumptions in order to interpret the existence of particular effects of that kind.

The differential curve can be considered as a superposition of two curves, one decreasing from high values for $x=0$ to almost zero at about $x=9$, and another increasing from zero at $x=0$ to 9 at $x=14$. These two component curves, making up our differential curve, can be interpreted as due to the electron spectrum and to the meson spectrum respectively: the contribution of the electrons will decrease with increasing x, and at $x=9$ we find only the contribution of cascades containing few high momentum electrons. The meson component contains few particles of low momentum, due to the decay of slow mesons in the atmosphere.

We can compare our results with the meson spectrum determined by Wilson (1946) by means of cloud-chamber experiments. Wilson's results have been confirmed by the counter experiments of Shamos and Levy (1948). These authors have determined three points, namely, at 11·2 cm. Pb, at 31·6 cm Pb, and at 31 cm. Pb + 25·4 cm. Fe, and their points lie on Wilson's curve within the limits of error.

In the part of our differential curve due to the meson component, the interval from $x=9$ up to about $x=16$ corresponds to a range in lead from 9 cm. Pb up to 16 + 4 = 20 cm. Pb. Using the well-known Rossi–Greisen curves, this corresponds to a momentum interval ranging from 220 to 360 MEV. approximately. The momentum range investigated by us covers, therefore, only a small part of the range investigated by Wilson. However, we have sufficient data to represent our results on Wilson's curve by a point, namely the number of mesons between 220 and 320 MEV., and also to compare the slope of the meson part of our differential curve in the neighbourhood of this interval with the slope of Wilson's curve near the corresponding point.

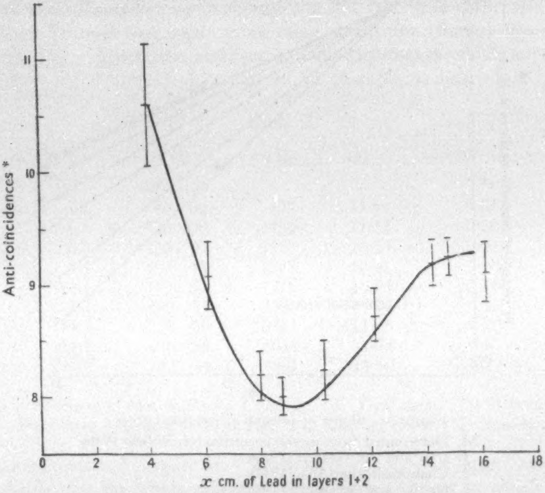

Figure 4. Differential absorption curve.
* Number of particles per hour penetrating x, but not $x+4$ cm. Pb.
(Background of 2·5 per hr. subtracted.)

Wilson gives his results as numbers per momentum interval per 1,000 mesons of a momentum > 1,000 MEV. Our telescope gives the number of particles penetrating 30 cm. Pb, i.e. of momentum ⩾ 500 MEV., as about 450 particles per hour, and we can therefore relate our results to Wilson's without difficulty. Relating both results to a total of 1,000 particles in the range ⩾ 500 MEV., we obtain from our curve in the interval 220 to 320 MEV., for example, $(16 \pm 0{\cdot}8) \times 1{,}000/450 = 36 \pm 2$ particles per hour.

Relating similarly the slopes of the two curves, we are making no allowance for the possibility that at $x=15$, i.e. in the 350 MeV. region, our curve might flatten out slightly. A small change of slope here would not show up on Wilson's curve.

In Figure 5 we have plotted Wilson's spectrum as a dotted line as well as the point and slope determined by us in the corresponding momentum region. It is seen that there is good agreement.

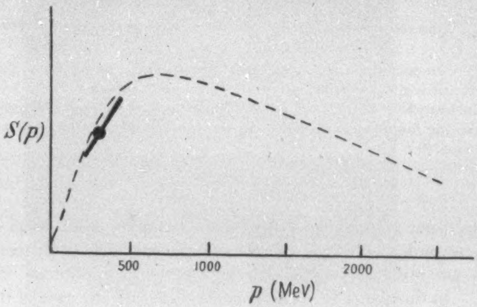

Figure 5. Point and slope of [meson spectrum determined from meson part of differential absorption curve.
Dotted line :—Wilson's meson spectrum 1946.

One should expect a slight change of slope in our differential curve in the $x=15$ region, if the change of slope of the integral curve in the corresponding region of 20 cm. is real. However, we hope to examine this point more closely in a further experiment.

ACKNOWLEDGMENTS

One of us (E. W. K.) wishes to acknowledge his indebtedness to Professor A. M. Taylor, University College, Southampton, where this work was begun. Both authors wish to thank Professor P. M. S. Blackett for his continuous interest in this investigation, Professor L. Jánossy for introducing us to these problems and for his advice, and Dr. J. G. Wilson for many helpful discussions.

REFERENCES

AUGER, P., LEPRINCE-RINGUET, L., and EHRENFEST, P., 1936, *J. Phys. Radium*, **7**, 58.
CHANDRASHEKHAR AIYA, S. V., 1944, *Nature, Lond.*, **153**, 375.
CLAY, J., 1936, *Physica*, **3**, 332.
CLAY, J., and v. GEMERT, A., cf. Clay, 1939, *Rev. Mod. Phys.*, **11**, 128.
CLAY, J., VENEMA, A., and JONKER, K. J. H., 1940, *Physica*, **7**, 673.
DUPERIER, A., 1944, *Nature, Lond.*, **153**, 529.
GEORGE, E. P., and APPAPILLAI, V., 1945, *Nature, Lond.*, **155**, 726.
ROSSI, B., 1933, *Z. Phys.*, **82**, 151.
SHAMOS, M. H., and LEVY, M. G., 1948, *Phys. Rev.*, **73**, 1396.
SWANN, W. F. G., and MORRIS, P. F., 1947, *Phys. Rev.*, **72**, 1262.
TRUMPY, B., and ORLIN, J., 1943, *Bergens Museums Årbok* (*N*), Nr. 7.
WILLIAMS, E. J., 1939, *Proc. Roy. Soc.* A, **172**, 194.
WILSON, J. G., 1946, *Nature, Lond.*, **158**, 414.

Momentum Spectrum of the Particles in Extensive Air Showers

By S. M. MITRA and W. G. V. ROSSER
The University, Manchester

Communicated by P. M. S. Blackett; MS. received 11th February 1949

ABSTRACT. An account is given of experiments on the momentum spectrum of the particles in extensive air showers at sea-level. The results are consistent with an integral spectrum of the form $N(>E) \propto (E+E_c)^{-(1 \cdot 1 \pm 0 \cdot 3)}$, where E_c is the critical energy in air. Penetrating particles are found in some of the denser showers, the ratio of penetrating particles to electrons being $(0 \cdot 8 \pm 0 \cdot 4)\%$.

---

§1. INTRODUCTION

THE electronic component of the cosmic radiation at sea-level is due partly to the secondary effects of mesons and partly to the extensive air showers which are initiated by high-energy electrons or photons in the upper atmosphere. In this paper we shall be concerned with the part of the electronic component associated with extensive air showers. The main part of the paper is an account of the determination of the momentum spectrum of the particles in extensive air showers, and of a small number of ionizing penetrating particles which were found in some of the denser showers.

If it is assumed that the electrons or photons which give rise to the extensive showers have an integral energy spectrum of the form

$$N(>E) = K_1 E^{-\gamma}, \qquad \ldots\ldots(1)$$

it is possible in principle to calculate from the cascade theory the form of the spectrum to be expected at sea-level. It has been shown by Rossi and Greisen (1941) that if ionization loss and scattering are neglected, the spectrum retains, at all depths in the atmosphere, the form given in equation (1). Bhabha and Chakrabarty (1943) have shown that if the ionization loss of the particles is taken into account the spectrum is again of the form given in equation (1), but the factor $E+E_c$ (where E_c is the critical energy in air) must be used in place of E. The best theoretical value of the exponent γ appears to be given by

$$\gamma = 1 \cdot 5. \qquad \ldots\ldots(2)$$

A possible way of testing the validity of this expression might appear to be the random operation of a cloud chamber with very thin walls. Such an experiment would, however, fail to distinguish between that part of the electronic component at sea-level which comes from knock-on and decay electrons and the part arising from extensive showers. Though it is necessary to control the cloud chamber with a counter arrangement sensitive to extensive showers, it is important that no significant bias should be imposed on the spectrum by the control system. The most important bias introduced by every counter system is the imposition of a "cut-off" for showers of less than a certain minimum density. The effect of this type of bias is twofold: (i) to cut off showers of low average density, i.e. showers initiated by low energy primaries, and (ii) to cut off the low density

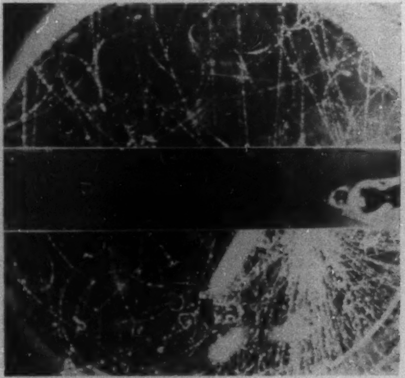

Photo 1. A dense extensive air shower in which the momenta of the particles above the lead plate range from $1{\cdot}4\times10^8$ to $4{\cdot}9\times10^9$ ev/c. This, photograph is an example of a Hoffman burst. $H=5{,}500$ gauss.

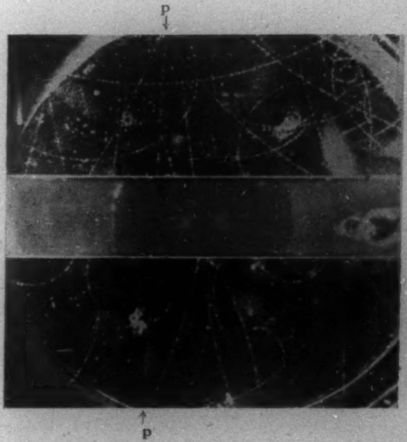

Photo 2. A dense shower containing one penetrating particle, denoted p p. The momentum of the particle above the lead plate is $2{\cdot}1\times10^9$ ev/c.; the particle is positive. $H=7{,}200$ gauss.

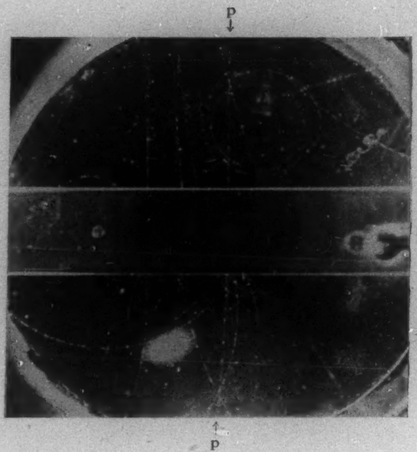

Photo 3. A dense extensive air shower with one negative penetrating particle (p, p) of momentum $1{\cdot}2\times10^9$ ev/c. above the lead plate. $H=7{,}100$ gauss.

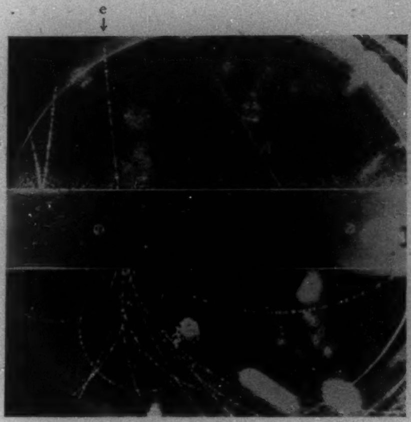

Photo 4. This photograph shows an incident electron (e) of momentum $1{\cdot}5\times10^9$ ev/c. which produces a small cascade shower in the lead plate. The penetrating track on the right-hand side of the photograph is too fine to be contemporary with the extensive air shower, and was not included in the analysis. $H=7{,}100$ gauss.

region of large showers. In each case the effect on the energy spectrum is to decrease the number of low energy electrons recorded relative to the number of high energy electrons and, therefore, to decrease the average value of γ. The minimum density of the showers recorded with the counter arrangement used in the present experiment was 50 particles per square metre.

Another important form of bias is introduced by the presence of solid material above the apparatus. Great care was taken in the present experiments to reduce this effect as much as possible. The thickness of solid material above the chamber was not more than 3 gm/cm^2 made up of light elements, and no particle in the chamber was accepted for measurement which had come through more than this thickness of matter. This criterion necessitated rejecting particles which made more than 60° with the vertical in one plane and 25° with the vertical in the other plane.

Experimental evidence that a fair sample of the particles in extensive air showers has been taken will be given in § 3, where it is shown that the observed distribution of the number of tracks in the cloud chamber agrees closely with the distribution calculated from the counter experiments of Daudin (1943) and Cocconi, Loverdo and Tongiorgi (1946 a, b).

§ 2. EXPERIMENTAL ARRANGEMENT

The general arrangement of the apparatus was essentially the same as that used by Rochester and Butler (1948) to study penetrating showers, except that no lead was placed above the chamber (see Figure 2 of their paper). It consisted of an electromagnet (Blackett 1936) and a counter-controlled cloud chamber. The chamber had an effective collecting area of 150 cm^2 and it was triggered by the five-fold coincidence of an array of counters consisting of three trays above and two trays below the chamber. Another tray of counters of area 1,700 cm^2 was placed one metre away and coincidences between this tray and the five-fold set were indicated by the flash of a small indicator lamp placed in front of the chamber, the resolving time of the control circuit being 2×10^{-6} sec.

In order to distinguish between soft and penetrating particles, a lead plate 3·4 cm. thick was placed across the chamber. The chamber, together with the small indicator lamp, was photographed through the hollow core of the electromagnet, and only the photographs taken with the indicator lamp on were considered in the present experiment. The positions of the tracks above the lead plate in the chamber were carefully determined by reprojection. The minimum track length for measurements was 6 cm.

The curvatures of the high energy tracks were measured by the null method devised by Blackett (1937), viz. by compensating the curvature with a prism; and those of the low energy tracks were measured by comparison with a family of circles of known curvatures. With a field of 7,500 gauss the maximum detectable momentum was $8{\cdot}4 \times 10^9$ ev/c. (Rochester and Butler 1948).

§ 3. DENSITY DISTRIBUTION OF THE PARTICLES IN THE SHOWERS

The work of Cocconi, Loverdo and Tongiorgi (1946 a), Daudin (1943), Clay (1943) and Chaudhuri (1948) has shown that the distribution of shower densities follows a power law of the form

$$R(>D) = \text{const. } D^{-1{\cdot}5}, \qquad \ldots\ldots(3)$$

where $R(>D)$ is the rate of showers with a density exceeding D.

Following Chaudhuri (1948) ,the density distribution obtained in the present experiment can be compared with the results of Cocconi, Loverdo and Tongiorgi by comparing the observed rate of occurrence of showers showing *n* tracks above the lead plate with the rate calculated according to the formula

$$R(n) \propto \int_0^\infty (1-e^{-S_1D})(1-e^{-S_3D})(1-e^{-S_4D})(1-e^{-S_5D}) \times (1-e^{-S_ED})e^{-S_0D} \cdot \frac{(S_0D)^n}{n\,!} \cdot \frac{dD}{D^{(\beta+1)}}, \qquad \ldots\ldots(4)$$

where $R(n)$ is the fraction of photographs with n tracks, $\beta = 1{\cdot}5$, S_0 is the collecting area of the cloud chamber and S_E is the area of the extension tray. Two of the trays of the five-fold overlapped completely, and as most of the showers at sea-level are nearly vertical, the two trays were considered as one. Only four trays of the counter set (S_1, S_3, S_4, S_5) were therefore used in the above expression.

The observed rates are shown in row 2 of Table 1, and the calculated values are shown in row 3. It is seen that the observed and calculated values are in good agreement. The lead plate introduced a slight bias towards particles which multiplied in the plate. However, since the rate of occurrence of particles of sufficient energy to multiply in the plate was comparatively low, and since the area of the lead plate was small compared with the areas of the bottom counter trays, the bias towards events penetrating the lead plate was small.

Table 1. Density Distribution of Particles in Extensive Air Showers

No. of particles*		0	1	2	3	>3
No. of showers	Observed	697	245	75	11	20
	Calculated	726	220	64	20	18

* Number of particles above the plate in the photograph.

The Momentum Spectrum of the Particles

A total of 474 tracks were selected from 1,048 photographs of extensive air showers taken with high and low magnetic fields. While the chamber was run with a high field (7,500 gauss) there was a stray field of several hundred gauss above the chamber which caused an appreciable loss of low energy particles. In order to find what proportion of these particles was lost, an equal number of photographs was taken at a lower magnetic field (1,500 gauss) when the stray field was negligible. The results are shown in Table 2. It was found that for 62 particles obtained in the range 1×10^7 to 5×10^7 ev/c. with the high field 109 were obtained with the low field, the numbers above $p = 5 \times 10^7$ ev/c. being approximately equal (147 and 156 respectively).

The corrected momentum distribution of the particles in the extensive air showers is shown in Table 2, row 4, where the results with low field and high field are added together, the number below $p = 5 \times 10^7$ ev/c. being calculated, however, from the low field results only.

Of the 60 particles with momenta greater than 8×10^8 ev/c., 22 particles were in the range 8 to 10×10^8 ev/c., and 38 particles had momenta greater than 10^9 ev/c.

The momentum spectrum has been plotted on a log–log scale in Figure 1. The results are consistent with an integral spectrum of the form $N(>E) \propto (E+E_c)^{-\gamma}$ with $\gamma = 1{\cdot}1 \pm 0{\cdot}3$, if E_c is assumed to have the value $1{\cdot}14 \times 10^8$ ev., which is the theoretical critical energy in air. This result is consistent with the predictions of cascade theory. The observed value of γ was less than the value of 1·5 given in equation (2), due probably to the effects of the angular scattering of the particles and the selection of high density showers by the counter arrangement.

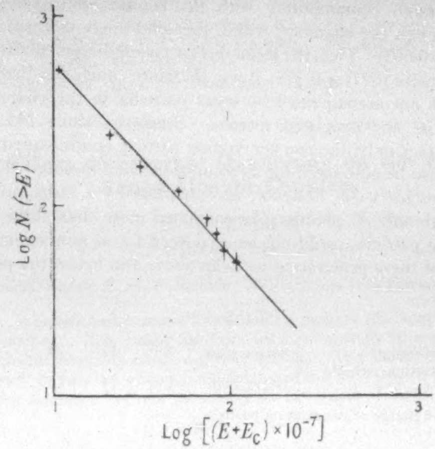

Figure 1.

Table 2. Momentum Distribution of the Particles in Extensive Air Showers

Momentum (10^8 ev/c.)	0–5	5–10	10–15	15–20	20–30	30–40	40–50	50–60	60–70	70–80	>80
Distribution with high field	62	38	21	9	10	12	10	7	7	7	26
Distribution with low field	109	34	20	17	12	6	8	10	8	7	34
Corrected distribution	285		67		22	18	18	17	15	14	60

Ratio of the Penetrating Component to the Soft Component in Extensive Air Showers

It is known that there are penetrating particles associated with extensive air showers (e.g. Rogozinski 1944, Cocconi, Loverdo and Tongiorgi 1946 b, Broadbent and Jánossy 1948, Cocconi and Greisen 1948, Fretter 1948).

During the present experiment, eight penetrating particles were obtained, and of these, three were single, one was accompanied by a single particle in the chamber, and the other four were accompanied by a number of electrons. Some of these penetrating particles were probably non-associated mesons, since all tracks entering the chamber over a time interval of approximately 0·02 second after the expansion appeared contemporary with the counter-controlled tracks. The meson flux through the chamber, within the solid angle defined in §1, during 0·02 second was 0·005. Thus the mean flux corresponding to all the photographs containing no tracks (697) was 3·5; it was therefore concluded that all the penetrating particles not accompanied by other particles in the chamber could be accounted for as non-associated mesons. Similarly, since 245 photographs contained one track only, the one penetrating particle accompanied by one other particle could also be accounted for as a non-associated meson. The other four penetrating particles were, however, accompanied by a large number of soft particles. Since only 20 photographs contained more than three tracks, these four penetrating particles could not be accounted for as non-associated mesons. The momenta of these penetrating particles above and below the plate are given in Table 3.

Table 3

Momentum of penetrating particle ($\times 10^8$ ev/c.)	Above plate	8·0	12	19	21
	Below plate	7·4	11	17	19
Sign of charge of penetrating particle		+	−	+	+

It is seen that the loss of energy of each of the particles whilst traversing the plate is less than 10%. If the particles were electrons they would have been unlikely to have emerged from the plate unaccompanied by secondaries. Moreover, even if they did so, the probability of the energy loss being less than 10% was negligible (Heitler 1944). Furthermore, the penetrating particles all travelled in the same direction as the shower.

It was therefore concluded that non-electronic particles were present in the showers, the number observed being $(0{\cdot}8 \pm 0{\cdot}4)\%$ of the total number of particles. This value is consistent with the estimates of other workers. On no occasion was more than one penetrating particle observed on a photograph. The fact that one of the penetrating particles was negative indicates that some at least of the penetrating particles were not protons. This conclusion is consistent with the suggestion of Cocconi, Cocconi and Greisen (1949) that there are μ-mesons present in extensive air showers in air.

ACKNOWLEDGMENTS

In conclusion, the authors wish to record their sincere thanks to Professor P. M. S. Blackett, Dr. C. C. Butler, Dr. J. G. Wilson and Professor L. Jánossy for their encouragement and great help in all possible ways, and to Dr. G. D. Rochester for his kind guidance.

REFERENCES

Bhabha, H. J., and Chakrabarty, S. K., 1943, *Proc. Roy. Soc.* A, **181,** 267.
Blackett, P. M. S., 1936, *Proc. Roy. Soc.* A, **154,** 504; 1937, *Ibid.*, **159,** 1.
Broadbent, D., and Jánossy, L., 1948, *Proc. Roy. Soc.* A, **191,** 517; **192,** 364.
Chaudhuri, B., 1948, *Nature, Lond.*, **161,** 680.

Clay, J., 1943, *Physica*, **9**, 897.
Cocconi, G., Cocconi, V. O., and Greisen, K., 1949, *Phys. Rev.*, **75**, 1063.
Cocconi, G., and Greisen, K., 1948, *Phys. Rev.*, **74**, 62.
Cocconi, G., Loverdo, A., and Tongiorgi, V., 1946 a, *Phys. Rev.*, **70**, 841; 1946 b, *Ibid.*, **70**, 852.
Daudin, J., 1943, *Ann. Phys., Paris*, **18**, 145, 217.
Fretter, W. B., 1948, *Phys. Rev.*, **73**, 41.
Heitler, W., 1944, *Quantum Theory of Radiation* (Oxford: University Press), p. 226.
Rochester, G. D., and Butler, C. C., 1948, *Proc. Phys. Soc.*, **61**, 307.
Rogozinski, A., 1944, *Phys. Rev.*, **65**, 291.
Rossi, B., and Greisen, K., 1941, *Rev. Mod. Phys.*, **13**, 276.

The Effect of External Quenching on the Life of Argon-Alcohol Counters

By H. ELLIOT
The University, Manchester

Communicated by P. M. S. Blackett; MS. received 18*th February* 1949

ABSTRACT. A simple multivibrator for eliminating multiple discharges in argon–alcohol counters is described. This circuit has been used successfully in cosmic-ray intensity recording equipment requiring a high degree of stability. It is shown that the increase in counter life which is observed when a multivibrator of this kind is used is probably due to quenching of the discharge before it has spread the full length of the counter wire.

§1. INTRODUCTION

In the course of experiments using large numbers of commercially produced argon–alcohol counters, difficulty was experienced because of the large percentage of multiple discharges and a tendency towards instability which developed after a few months of continuous operation. In addition, the life of the counters was very short, amounting on the average to about six months' operation, after which it was necessary to refill them with fresh argon and alcohol.

These counters had an effective length of 60 cm. and a diameter of 4 cm.; the cathodes were of copper foil and the anodes of tungsten wire. They were filled with a mixture of argon (11 cm. Hg) and alcohol (1·5 cm. Hg). The background counting rate was about 15 per second.

In an effort to improve the performance of these counters a single-stroke multivibrator was used for suppressing the multiple discharges. A multivibrator has also been used by Putman (1948) for this purpose. In addition to an improvement in plateau slope and stability, it soon became evident that there was an appreciable increase in counter life, and it therefore seemed worth while to investigate the action of the multivibrator more thoroughly.

§2. EXPERIMENTAL PROCEDURE

Multivibrator circuits of varying degrees of complexity have been used by many workers for quenching the discharge in non-self-quenching counters and are described in the literature (Getting 1938, Lewis 1942, Maier Leibnitz 1948).

The circuit of the multivibrator used here is shown in Figure 1. When an ionizing particle produces a discharge in the counter a negative voltage pulse appears across the 220 kΩ resistance which initiates the usual trigger action

This operation drops the voltage across the counter by about 200 volts. This fall in potential reduces the field below threshold and the discharge ceases. The time constants of the circuit are such that the potential of the counter anode is held below threshold for 1·5 milliseconds, which allows the positive ions to reach the cathode before the anode potential rises again. Any secondary electrons which may be produced cannot therefore cause any further discharge.

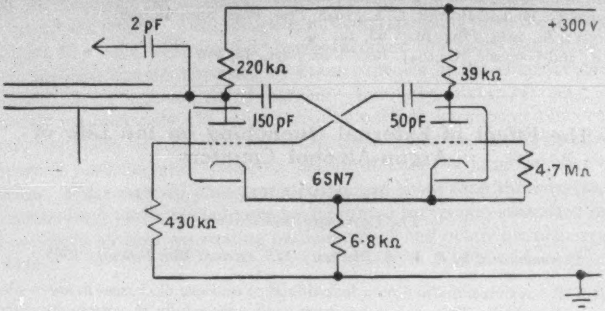

Figure 1.

Since it seemed likely that the increase in life was connected with a decrease in the extent of the discharge, due to the quenching action of the multivibrator, measurements were made of the quantity of electricity Q passing through the counter during a discharge. These measurements were made by partially discharging a 0·96 μF. condenser through the counter and recording the number of pulses for a given fall in potential across the condenser, correction being made for the finite leakage resistance of the condenser itself.

§ 3. EXPERIMENTAL RESULTS

Measurements of Q were made for two counters of the same type (60 cm. × 4 cm.). Figure 2 (A) shows Q plotted against counter voltage for one of these counters, which was operated with a 200,000-ohm series resistance but no multivibrator. Figure 2 (B) shows Q as a function of voltage for the same counter but operated with a multivibrator.

The multivibrator shown in Figure 1 was developed for use in a cosmic-ray intensity recorder which incorporated trays of ten counters connected in parallel, each counter being connected to its own multivibrator. In order to prevent mutual interaction, the multivibrators were not adjusted for maximum sensitivity. Figure 2 (C) shows the effect of increasing the sensitivity of the multivibrator (by reducing the cathode bias resistance from 6·8 kΩ to 4·0 kΩ). Similar results were obtained for the second counter.

It is clear from the results of these measurements that Q is reduced when the counter is externally quenched, the reduction being greater for the more sensitive multivibrator.

§ 4. DISCUSSION OF RESULTS

Hodson (1948) has used a multivibrator for decreasing the dead time of a counter by reversing the anode potential. At the time, this decrease in dead time was interpreted as being due to positive ion collection at the anode, but later measurements showed that a reduction in effective dead time was still observed if a 250-volt negative pulse of 10 microsecond duration was applied to the counter wire. Positive ion collection could not occur under these conditions, and it was suggested by Sherwin that the application of a negative pulse prevented the discharge from spreading the full length of the counter. Further measurements by Hodson (unpublished) and by Smith (1948) have confirmed this interpretation.

The reduction in Q when the counter is used with a multivibrator is a further indication that the discharge is being limited in this way. The reduction in Q as shown in Figure 2 indicates that the discharge is limited to roughly a quarter of the total length of the counter, depending on the sensitivity of the multivibrator and the counter voltage. It should be possible to reduce the extent of the discharge still further by quenching with a more sensitive multivibrator, using two pentodes. A double triode valve has been used here in order to economize in valves and components.

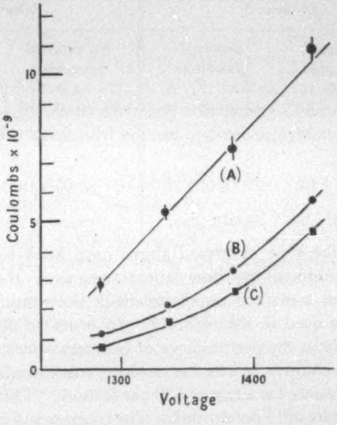

Figure 2.

It is not clear what factors determine the life of a counter, but whether it be dissociation of the alcohol molecules or some surface effect on the cathode or anode it is clear that, if the discharge is confined to part of the counter only, there should be an increase in counter life. Measurements of the velocity of spread of the discharge along counter wires (Hill and Dunworth 1946) give values of the order of 10 cm. per microsecond. If, for example, the anode potential of a 60-cm. counter is reduced to threshold in 1 microsecond, then the discharge will have spread some distance which will be less than 20 cm. (10 cm. in each direction) before being extinguished. Under these conditions it seems reasonable to expect the counter life to be increased by a factor of at least three.

As a further check on this interpretation Q was measured when the counter was stimulated by γ-rays passing through (*a*) the middle of the counter, (*b*) the end of the counter. Under conditions (*a*) the discharge can spread along the wire in both directions, whereas in (*b*) it can spread in one direction only. When the counter operates without a quenching pulse the discharge will spread to the full length of the counter for both (*a*) and (*b*) and Q should be the same for both conditions. When a quenching pulse is applied, however, the discharge will spread further under condition (*a*) than under condition (*b*), and consequently Q should be greater when γ-rays pass through the middle than when they pass through the end.

Measurements were made on two counters with quenching pulses applied to their anodes, and in each case a significant decrease in Q was observed when the γ-rays passed through the end of the counter. Measurements were also made on the counters when operated without quenching and, as expected, there was no significant difference in Q as measured under conditions (*a*) and (*b*). The results of these measurements are given in the Table.

Values of Q for Different Operating Conditions

	Counter 1		Counter 2	
	No external quenching	External quenching	No external quenching	External quenching
γ-rays through middle	$3{\cdot}17 \pm 0{\cdot}06 \times 10^{-9}$	$1{\cdot}47 \pm 0{\cdot}01 \times 10^{-9}$	$4{\cdot}51 \pm 0{\cdot}03 \times 10^{-9}$	$1{\cdot}04 \pm 0{\cdot}02 \times 10^{-9}$
γ-rays through end	$3{\cdot}22 \pm 0{\cdot}04 \times 10^{-9}$	$0{\cdot}87 \pm 0{\cdot}02 \times 10^{-9}$	$4{\cdot}51 \pm 0{\cdot}03 \times 10^{-9}$	$0{\cdot}63 \pm 0{\cdot}01 \times 10^{-9}$

Multivibrators of the type described above have been used in cosmic-ray intensity recording equipment in these laboratories since the middle of 1947 and have brought about a marked improvement in the stability and life of the argon–alcohol counters used in the recorder. In order to obtain information, in a reasonable time, about the performance of counters operated in this way for prolonged periods, one counter, selected at random, was stimulated by means of a γ-ray source so that it counted at a rate of 520 per second. This is about 35 times its normal background rate of 15 per second. The counter was operated at 75 volts above threshold. Initially the plateau slope of this counter was 0·02% per volt, but this gradually increased to 0·10% per volt after approximately 3×10^9 counts.

The length of the plateau remained very nearly the same (200 v.) during this period, but the background rate rose sharply after $2{\cdot}7 \times 10^9$ counts, and the useful life of this counter was therefore approximately $2{\cdot}7 \times 10^9$ counts, which corresponds to approximately 6 years' operation at the normal background rate. Assuming that the life of a counter depends on the total number of particles counted, we might expect a counter of this type to last for approximately 6 years without suffering any serious deterioration when used for counting cosmic rays.

This increase in life appears to be greater than might be expected from the measurements of Q, but it must be remembered that the elimination of multiple discharges alone will increase the life since each ionizing particle passing through the counter produces one discharge only. In addition, a counter which is unusable without external quenching because of multiple discharges will often operate quite satisfactorily with a multivibrator. Because of this a counter which would normally be supposed to have reached the end of its life can continue to perform satisfactorily if used with a quenching multivibrator. The observed increase in life must be due to a combination of these three effects.

§ 5. CONCLUSION

The increase in life of argon–alcohol counters which has been observed when these counters have been used with a single-stroke multivibrator appears to be due to the extinction of the discharge before it has spread the full length of the counter and to the suppression of multiple discharges. Under the most favourable conditions described the discharge appears to be limited to about one-quarter of the total length. Measurements made on a counter of length 60 cm. and diameter 4 cm. indicate that such a counter has a life of about $2{\cdot}7 \times 10^9$ counts.

In addition to this increase in lifetime, further advantages in using a simple multivibrator of this kind are: (*a*) the slope of the counter plateau is reduced because of the suppression of multiple discharges; (*b*) the counter dead time is determined by the time constants of the multivibrator and is, therefore, virtually independent of counter voltage.

ACKNOWLEDGMENTS

The writer is indebted to Mr. D. W. N. Dolbear for much valuable help and advice, to Mr. A. L. Hodson for many stimulating discussions and to Professor P. M. S. Blackett for continued interest and encouragement.

REFERENCES

Getting, I. A., 1938, *Phys. Rev.*, **53**, 103.
Hill, J. M., and Dunworth, J. V., 1946, *Nature, Lond.*, **158**, 833.
Hodson, A. L., 1948, *J. Sci. Instrum.*, **25**, 11.
Lewis, W. B., 1942, *Electrical Counting* (Cambridge: University Press), p. 111.
Maier Leibnitz, H., 1948, *Rev. Sci. Instrum.*, **19**, 500.
Putman, J. L., 1948, *Proc. Phys. Soc.*, **61**, 312.
Smith, P. B., 1948, *Rev. Sci. Instrum.*, **19**, 453.

On the Absorption of Meson-producing Nucleons

By W. HEITLER and L. JÁNOSSY
Dublin Institute for Advanced Studies

MS. received 23rd January 1949

ABSTRACT. The absorption of nucleons passing through any number of nuclei is calculated with due consideration of all fluctuations of energy loss. For the probability $w(\epsilon, E)\, d\epsilon$ for an energy loss ϵ by a nucleon with energy E hitting a nucleon at rest, a law of the form $w\, d\epsilon = w(\epsilon/E)\, d\epsilon/E$ is assumed, a law suggested by meson theory and Bremsstrahlung. It is shown that, with a primary spectrum, following a power law, the absorption is strictly exponential for any thickness of the absorber and for all energies of the nucleons, apart from small deviations at low energies due to the latitude cut-off. This agrees well with recent experimental results. The experiments also permit some conclusions about the shape of the function w, and it is shown that w must be a fairly broad distribution extending up to $\epsilon/E=1$, possibly favouring, but not to a very large extent, low values of ϵ/E. The average energy loss of a fast nucleon hitting a nucleon at rest is determined by the experiments within very narrow limits. The conclusions that can be drawn about w, the total cross-section for meson production and the average energy loss are all compatible with the theory of Hamilton, Heitler and Peng, in its later version.

---

§ 1. INTRODUCTION

THE absorption of the fast cosmic ray nucleons which are capable of producing small or large penetrating showers has recently been measured throughout the whole atmosphere by various authors using various experimental arrangements for recording different sized showers. It has been found (Braddick and Hodson (private communication), Wataghin 1947, George and Jason 1947, 1948, Tatel and Van Allen 1948, Tinlot 1948 a, b, Rossi 1948, Bernardini, Cortini and Manfredini 1948), that the absorption is exponential with the same absorption coefficient of about 100 gm/cm^2, independent of the thickness of the absorber (up to a thickness of 1,000 gm/cm^2 = whole atmosphere) and of the arrangement. The effective mean free path of 100 gm/cm^2 in air is twice that to be expected if the cross-section for absorption per nucleus is the geometrical one.

At first sight one is tempted to interpret these findings as follows: (i) the absorption is catastrophic: the nucleons lose so much energy in a single nuclear hit that they are no longer capable of producing further mesons; (ii) the cross-section for such a hit is half the geometrical cross-section; one might, indeed, expect exponential absorption only, if the nucleons are absorbed in a single hit.

However, the comparatively small cross-section of only half the geometrical one is not very likely to be true. The transition curve of penetrating showers favours a larger cross-section, and cases have been observed where one nucleon creates two penetrating showers in succession. So we conclude that the primary nucleons are capable of penetrating on the average through two air nuclei, and the question arises whether we can then account for the purely exponential absorption.

We shall consider the problem here in a fairly general way, taking into consideration all the fluctuations of energy loss. These are due to the following causes: (i) In passing through a nucleus the length of path (and therefore the number of nucleons hit) can range from 0 to d_A, where d_A is the diameter of the nuclei, and there will be a certain probability for a length of path between these two limits. (ii) The nucleon may pass through any number of nuclei and there will be a probability for hitting a specified number of nuclei. (iii) In hitting a single nucleon the primary nucleon with energy E may lose any energy $\epsilon = 0 \ldots E$ through meson production, and there will be a certain probability $w(\epsilon, E)\,d\epsilon$ for a specified energy loss.

While the fluctuations (i) and (ii) are due to statistical and geometrical causes, $w(\epsilon, E)$ should be taken from a theory of meson production. Since, however, any such theory suffers from many uncertainties, we investigate the problem here in a more phenomenological way: in the present paper we shall assume a simple model for w and assume that w depends on ϵ/E only:

$$w(\epsilon, E) = w\left(\frac{\epsilon}{E}\right)\frac{d\epsilon}{E}. \qquad \ldots\ldots(1)$$

A consequence of (1) is that the total cross-section for meson production is independent of E and the average energy loss proportional to E:

$$\int_0^E w\left(\frac{\epsilon}{E}\right)\frac{d\epsilon}{E} = \text{const.}; \qquad \int_0^E \epsilon w\left(\frac{\epsilon}{E}\right)\frac{d\epsilon}{E} \sim \text{const.}\, E. \qquad \ldots\ldots(1')$$

In a later paper we hope to investigate also other cases, for instance $w = w(\epsilon)$, independent of E, etc.

A theory of meson production has been put forward by Hamilton, Heitler and Peng (1943) and improved by Jánossy (1943) and Heitler and Walsh (1945). The result is that the most essential parts of the cross-section fall into the class (1), (1′), and the constants in (1′) could be determined within certain limits, the uncertainty being a factor 4 or so (see §4). We shall be able to determine the constants from experiment to some extent, and it will be seen that they are compatible with the predictions of the theory. Moreover, something can also be concluded about the shape of $w(\epsilon/E)$; further, this conclusion agrees qualitatively with the theory.

The original theory was developed before the discovery of the π-meson. It is now clear that the theory should be applied to π-mesons, but not to μ-mesons, and also probably to τ-mesons (mass 700–1,000). Furthermore, it has been assumed that there occur "transverse" mesons with a short life whose decay is responsible for the soft component. The rôle of this type of meson may be taken over by any short-lived meson that decays into photons or electrons. ϵ in (1), (1′) includes, of course, all types of meson produced, charged and neutral, whether long- or short-lived.

Furthermore, we shall assume a power law for the primary spectrum of nucleons. This is well justified on many experimental grounds. We shall then show that this spectrum is reproduced after passage through any thickness of material while the total intensity decreases exponentially. This is true for all energies above the latitude cut-off, while for smaller energies certain deviations from the power spectrum and the exponential absorption arise. These deviations are of no importance for European or American latitudes because nucleons which are capable of producing mesons in appreciable numbers must anyhow possess energies close to or larger than the European cut-off energy.

§ 2. THE FLUCTUATIONS OF THE LENGTH OF NUCLEAR PATH

We assume the nuclei to be spheres of diameter

$$d_A = 3 \times 10^{-13} A^{\frac{1}{3}} \text{ cm.} \qquad \ldots\ldots(2)$$

For oxygen $d_O = 7{\cdot}5 \times 10^{-13}$ cm., and the geometrical cross-section is

$$\Phi_O = 4{\cdot}4 \times 10^{-25} \text{ cm}^2. \qquad \ldots\ldots(2')$$

This corresponds to a mean free path of 50 gm/cm². The average number of collisions with nuclei when passing through a thickness θ gm/cm² is

$$\bar{p} = \theta n \Phi_A, \qquad \ldots\ldots(2'')$$

where n is the number of nuclei per gram.

We denote by $X d_A$ the total length of path which the fast nucleon passes through *nuclear* matter. X is thus the length of path in units of the nuclear diameter. We require the probability $P(\theta, X)\,dX$ for X to lie in the interval dX when the nucleon traverses θ gm/cm² of material.

The probability for hitting altogether p nuclei is $\{\exp(-\bar{p})\}\bar{p}^p/p!$ Thus, writing $P_p(\theta, X)$ for the probability of a length of path X when it is known that actually p nuclei are hit, we have

$$P(\theta, X) = \sum_{p=0}^{\infty} \{\exp(-\bar{p})\} \frac{\bar{p}^p}{p!} P_p(X). \qquad \ldots\ldots(3)$$

Consider now the kth collision with a nucleus. The probability that the length of path through the nucleus is x_k is evidently, on purely geometrical grounds, $2x_k\,dx_k$. Thus,

$$\left.\begin{aligned} &P_p(X)\,dX = \int \ldots \int 2^p x_1 x_2 \ldots x_p \, dx_1\, dx_2 \ldots dx_p, \\ &0 \leqslant x_k \leqslant 1, \qquad X \leqslant x_1 + x_2 + \ldots x_p \leqslant X + dX. \end{aligned}\right\} \qquad \ldots\ldots(4)$$

The integral can be worked out in terms of polynomials, but this is very cumbersome, and the result appears in different analytical forms according to the intervals in which X lies. Instead we introduce the Laplace-transform of P_p:

$$L_\lambda(P_p) = \int_0^\infty e^{-\lambda X} P_p(X)\,dX = 2^p \left(\int_0^1 x e^{-\lambda x}\,dx \right)^p. \qquad \ldots\ldots(5)$$

Actually only values $X \leqslant p$ contribute to the integral. Introducing (5) into (3), we obtain for the Laplace-transform of $P(\theta, X)$:

$$L_\lambda(P) \equiv \int_0^\infty e^{-\lambda X} P(\theta, X)\,dX = \exp\{-\bar{p} f(\lambda)\}. \qquad \ldots\ldots(6)$$

$$f(\lambda) = 1 - 2\int_0^1 x e^{-\lambda x}\,dx = 1 - 2\,\frac{1-(1+\lambda)e^{-\lambda}}{\lambda^2}. \qquad \ldots\ldots(6')$$

$f(\lambda)$ has no singularity at $\lambda = 0$; the expansion is

$$f(\lambda) = \frac{2}{3}\lambda - \frac{\lambda^2}{4} + \ldots \qquad \ldots\ldots(6'')$$

Thus $f(0) = 0$ and $\int_0^\infty P(\theta, X)\,dX = 1$. $P(\theta, X)$ is therefore properly normalized.

$f(\lambda)$, together with its first and second derivatives, is given in the Table.

λ	$f(\lambda)$	$f'(\lambda)$	$f''(\lambda)$	λ	$f(\lambda)$	$f'(\lambda)$	$f''(\lambda)$
−1·0	−1·00000	1·43656	−1·1269	−0·5	−0·40511	0·97443	−0·7483
−0·9	−0·86183	1·32839	−1·0378	−0·4	−0·31131	0·90255	−0·6900
−0·8	−0·73404	1·22876	−0·9560	−0·3	−0·22442	0·83627	−0·6364
−0·7	−0·61581	1·13697	−0·8809	−0·2	−0·14389	0·77518	−0·5866
−0·6	−0·50640	1·05239	−0·8118	−0·1	−0·06924	0·71880	$-0{\cdot}54_{00}$
0·0	0·00000	0·66667	−0·5000	0·5	0·27837	0·46041	−0·3363
0·1	0·06424	0·61860	$-0{\cdot}46_{00}$	0·6	0·32277	0·42806	−0·3109
0·2	0·12385	0·57425	−0·4265	0·7	0·36406	0·39815	−0·2876
0·3	0·17919	0·53326	−0·3938	0·8	0·40248	0·37049	−0·2660
0·4	0·23060	0·49540	−0·3639	0·9	0·43823	0·34489	−0·2462
1·0	0·47152	0·32121	−0·2279	1·6	0·62885	0·21156	−0·1443
1·1	0·50253	0·29927	−0·2110	1·7	0·64930	0·19766	−0·1339
1·2	0·53143	0·27897	−0·1954	1·8	0·66842	0·18476	−0·1219
1·3	0·55837	0·26015	−0·1811	1·9	0·68629	0·17278	−0·1154
1·4	0·58350	0·24271	−0·1678	2·0	0·70300	0·16166	−0·1072
1·5	0·60696	0·22655	−0·1556				

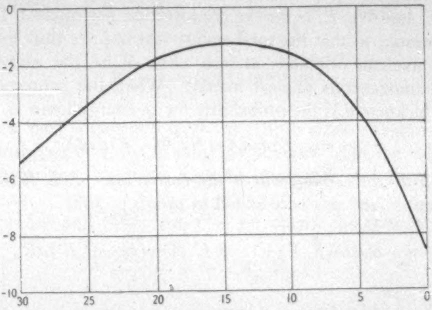

Figure 1. The probability $P(\theta, X)$ for a path length X in nuclear matter. $\bar{p}=20$ (sea level).

Although, for the actual calculation of the absorption, we shall only require the Laplace-transform $L_\lambda(P)$, the distribution $P(\theta, X)$ is also of some interest. We have, according to the theory of Laplace transformations,

$$P(\theta, X)=\frac{1}{2\pi i}\int_{\lambda'-i\infty}^{\lambda'+i\infty}\exp\{\lambda X-\bar{p}f(\lambda)\}\,d\lambda. \qquad \ldots\ldots(7)$$

Since $f(\lambda)$ has no singularity except at infinity, λ' can be chosen arbitrarily. Equation (7) can be worked out approximately by the saddle-point method. The position of the saddle-point λ_0 is given by

$$\frac{\partial}{\partial\lambda}\{\lambda X-\bar{p}f(\lambda)\}=0 \quad \text{or} \quad X=\bar{p}f'(\lambda_0). \qquad \ldots\ldots(8a)$$

Expanding the exponent in (7) up to the order of $(\lambda-\lambda_0)^2$ and using (8*a*) we may identify λ' with λ_0 and obtain

$$P(\theta, X)=\frac{1}{[2\pi\bar{p}f''(\lambda_0)]^{\frac{1}{2}}}\exp[\bar{p}\{\lambda_0 f'(\lambda_0)-f(\lambda_0)\}]. \qquad \ldots\ldots(8b)$$

(8a) and (8b) are a parameter representation for $P(\theta, X)$ in terms of λ_0. In Figure 1 we have plotted $P(\theta, X)$ for $\bar{p}=20$, i.e. the distribution to be expected near sea level.

From (6) we can also obtain directly the average of X and X^2. We find

$$\langle X\rangle \equiv \int_0^\infty XP(\theta, X)\,dX = \left\{-\frac{\partial}{\partial\lambda}\ln L_\lambda(P)\right\}_{\lambda=0} = \tfrac{2}{3}\bar{p}. \qquad \ldots\ldots(9a)$$

$$\langle X^2\rangle - \langle X\rangle^2 = \left\{\frac{\partial^2}{\partial\lambda^2}\ln L_\lambda(P)\right\}_{\lambda=0} = \tfrac{1}{2}\bar{p}, \qquad \ldots\ldots(9b)$$

(Note that X and $\bar{p}$ are dimensionless.)

§ 3. THE DIFFUSION IN HOMOGENEOUS NUCLEAR MATTER

Having obtained the probability distribution for the length of path in nuclear matter, we now consider the diffusion of nucleons through homogeneous nuclear matter. Let $S(E, X)\,dE$ be the number of nucleons with energy E after having traversed a thickness X of nuclear matter. $S(E, 0)$ is the primary spectrum and is given. Let $\Phi(\epsilon, E)\,d\epsilon$ be the cross-section per nucleon for production of any type of meson, so that the total energy lost is ϵ. ϵ thus includes the recoil energy of the nucleon originally at rest. Let N be the number of nucleons per cm^3 in homogeneous nuclear matter. When the primary nucleon passes through the thickness dX, the probability for an energy loss ϵ is, therefore,

$$w(\epsilon, E)\,d\epsilon\,dX = Nd_\Lambda\Phi(\epsilon, E)\,d\epsilon\,dX\,; \qquad \ldots\ldots(10)$$

X is measured in units of d_Λ, $w\,d\epsilon$ is dimensionless. $S(E, X)$ follows now the diffusion equation (see also note added in proof, p. 385)

$$\left.\begin{aligned} \frac{\partial S(E, X)}{\partial X} &= -a(E)S(E, X) + \int_E^\infty S(E', X)\,w(E'-E, E')\,dE', \\ a(E) &= \int_0^E w(\epsilon, E)\,d\epsilon. \end{aligned}\right\} \qquad \ldots\ldots(11)$$

The first term of (11) describes the decrease of intensity of nucleons with energy E losing any amount of energy, the second term the increase of intensity through nucleons having originally the higher energy E' and losing the amount $E'-E$.

If the solution of (11) is found, the energy spectrum of nucleons after having traversed a thickness θ of the absorber is evidently

$$S(E, \theta) = \int_0^\infty S(E, X)P(\theta, X)\,dX, \qquad \ldots\ldots(12)$$

where P is the function determined in § 2.

In order to solve (11) we now make the more specific assumption: $w(\epsilon, E)$ shall be of the form

$$w(\epsilon, E)\,d\epsilon = w\left(\frac{\epsilon}{E}\right)\frac{d\epsilon}{E}, \qquad \ldots\ldots(13)$$

and thus the cross-section shall depend on the ratio ϵ/E only. This is a law similar to that for Bremsstrahlung by electrons but is very different from the law for ionization loss. It follows from (13) that $a(E)=a=$ const. and that the average energy loss $\bar{\epsilon}$ is given by (1′). It is very likely that, for meson production, some law similar to (13) will hold, and, indeed, theory (Hamilton, Heitler and Peng 1943, Heitler 1945, Heitler and Walsh 1945) also suggests to it.* We discuss the particular form of $w(\epsilon/E)$ derived from that theory in §4.

Accepting (13), the diffusion equation (11) can be written

$$\frac{\partial S(E,X)}{\partial X} = -aS(E,X) + \int_0^\infty S(E+\epsilon, X)\, w\left(\frac{\epsilon}{E+\epsilon}\right)\frac{d\epsilon}{E+\epsilon}. \qquad \ldots\ldots(14)$$

(14) can be solved generally by a Mellin transformation. We put

$$\int_0^\infty E^{s-1} S(E,X)\, dE = M_s(X). \qquad \ldots\ldots(15)$$

Multiplying (14) by E^{s-1} and integrating over E, we have

$$\int_0^\infty E^{s-1}\frac{\partial S(E,X)}{\partial X}\, dE = \frac{\partial M_s(X)}{\partial X} \qquad \ldots\ldots(15\,a)$$

and

$$\int_0^\infty E^{s-1}\int_0^\infty S(E+\epsilon, X)\, w\left(\frac{\epsilon}{E+\epsilon}\right)\frac{d\epsilon}{E+\epsilon} = M_s(X) W_s, \qquad \ldots\ldots(15\,b)$$

with

$$W_s = \int_0^1 w(z)(1-z)^{s-1}\, dz. \qquad \ldots\ldots(16)$$

s must have a real part sufficiently large for (16) to exist. If $w(z)$ is regular for $z \to 1$, then the real part of s, Re(s), must be positive. On the other hand $w(z)$ may have a singularity at $z=1$ but must be integrable, and, therefore, Re(s)>1 is always sufficient.

Introducing (15 *a*) and (15 *b*) into (14) we obtain the transformed equation

$$-\frac{\partial M_s(X)}{\partial X} = (a - W_s) M_s(X). \qquad \ldots\ldots(17)$$

The transformed equation for $s=1$ has direct physical meaning: $W_1 = a$, thus

$$\frac{\partial M_1(X)}{\partial X} = 0 \quad \text{as} \quad M_1(X) = \int_0^\infty S(E,X)\, dE;$$

this equation expresses the conservation of the total number of particles.

The solution of the transformed equation is given by

$$M_s(X) = M_s(0)\exp\{-(a-W_s)X\}. \qquad \ldots\ldots(18)$$

$M_s(0)$ can be obtained from the initial condition

$$M_s(0) = \int_0^\infty E^{s-1} S(E,0)\, dE. \qquad \ldots\ldots(19)$$

For $S(E, 0)$ we may now well assume a power law (normalized to 1):

$$S(E,0) = \begin{cases} \dfrac{E\gamma_0{}^\gamma}{E^{\gamma+1}} & E > E_0 \\ 0 & E < E_0. \end{cases} \qquad \ldots\ldots(20)$$

---

* Compare in particular the formulae in Heitler (1945).

E_0 is the latitude cut-off energy. The value of γ, derived from the latitude effect of energy flow, is about 1·5. This gives, by (18),

$$M_s(0) = \frac{\gamma}{\gamma - s + 1} E_0^{s-1} \qquad \mathrm{Re}(s) < \gamma + 1. \qquad \ldots\ldots(21)$$

The condition $\mathrm{Re}(s) < \gamma + 1$ is required to make (19) convergent and is compatible with $\mathrm{Re}(s) > 1$. Applying the inverse Mellin transformation to (17), we find

$$S(E, X) = \frac{1}{2\pi i E_0} \int_{s_0 - i\infty}^{s_0 + i\infty} \frac{\gamma}{\gamma - s + 1} \left(\frac{E_0}{E}\right)^s \exp\{-(a - W_s)X\}\, ds. \qquad \ldots\ldots(22)$$
$$1 < s_0 < \gamma + 1.$$

The limits for s_0 are taken so as to conform with the above conditions for $\mathrm{Re}(s)$.

We first consider the case $E > E_0$, i.e. energies larger than the cut-off energy. The quantity $a - W_s$ has now always a positive real part. Hence, for $E > E_0$, the integrand of (21) vanishes sufficiently rapidly for $s \to \infty$ and the path of integration can be completed and deformed into a circle round the pole $s = \gamma + 1$. Then

$$S(E, X) = \frac{E\gamma_0{}^{\gamma}}{E^{\gamma+1}} \exp\{-(a - W_{\gamma+1})X\} = S(E, 0) \exp\{-(a - W_{\gamma+1})X\}. \qquad \ldots\ldots(23)$$
$$E > E_0.$$

That (23) is the solution of (14) can also be checked directly, by insertion. We see that (i) the primary spectrum is reproduced at any depth, and (ii) the absorption is exponential.

So far (23) refers to a passage through homogeneous nuclear matter. To find $S(E, \theta)$ for a given thickness of the absorber we have to apply (12), using for P the results of §2. Since $S(E, X)$ varies exponentially, it is just the Laplace-transform of $P(\theta, X)$ which occurs. From (6), (6′), (12) we get

$$S(E, \theta) = S(E, 0) L_\lambda(P) \qquad \ldots\ldots(23a)$$

or

$$S(E, \theta) = S(E, 0) \exp\{-\theta n \Phi_A f(\lambda)\}, \qquad \lambda = a - W_{\gamma+1}, \qquad \ldots\ldots(23b)$$

$$W_{\gamma+1} = \int_0^1 w(z)(1 - z)^{\gamma}\, dz, \qquad a = \int_0^1 w(z)\, dz. \qquad \ldots\ldots(23c)$$

$f(\lambda)$ is given by (6′). For $E > E_0$ the problem is now completely solved, as soon as $S(E, 0)$, i.e. γ and $w(\epsilon/E)$ are given. We see that also $S(E, \theta)$ *decreases exponentially with an effective absorption coefficient* $n\Phi_A f(\lambda)$ *and that the power spectrum* $\sim E^{-(\gamma+1)}\, dE$ *is reproduced at any depth.*

The physical meaning of $f(\lambda)$ is now also clear: it is the reciprocal of the effective number of nuclear collisions, before the nucleon disappears (i.e. becomes ineffective for meson production).

§4. COMPARISON WITH EXPERIMENTS AND THE THEORY OF MESON PRODUCTION

According to the experimental findings the effective mean free path is ~ 100 gm/cm² in air and, since $n\Phi_A \sim 50$ gm/cm², the experimental value of $f(\lambda)$ is $f(\lambda)_{\mathrm{exp}} = 0{\cdot}5$.

From the Table we find that

$$\lambda_{\mathrm{exp}} = (a - W_{\gamma+1})_{\mathrm{exp}} = 1{\cdot}1. \qquad \ldots\ldots(24)$$

To interpret this result we express the cross-section in natural meson units $(\hbar/\mu\mathbf{c})^2$. For a meson mass $\mu=286\boldsymbol{m}$, which corresponds to the mass of the π-meson $(\hbar/\mu\mathbf{c})^2=1\cdot8\times10^{-26}\,\mathrm{cm}^2$, thus:

$$\Phi(\epsilon, E)\,d\epsilon=\left(\frac{\hbar}{\mu\mathbf{c}}\right)^2\phi\left(\frac{\epsilon}{E}\right)d\left(\frac{\epsilon}{E}\right).$$

In a and $W_{\gamma+1}$ we can then split off the factor

$$Nd_{\mathrm{A}}\left(\frac{\hbar}{\mu\mathbf{c}}\right)^2=0\cdot95 \text{ for oxygen.} \qquad \ldots\ldots(25)$$

(24) is therefore equivalent to

$$\int_0^1\phi(z)[1-(1-z)^\gamma]\,dz=1\cdot15 \qquad (z=\epsilon/E). \qquad \ldots\ldots(26)$$

From this relation we can now draw some conclusions about the shape of $\phi(\epsilon/E)$. We can best do that by considering a variety of shapes of the type

$$\phi(z)=\alpha(1-z)^\beta. \qquad \ldots\ldots(27)$$

Varying α and β, all sorts of possible, and reasonable, curves are obtained, favouring either small (large β) or large (small β) energy losses, and the true law, if it can be at all represented by a function of ϵ/E only, can probably well be approximated by (27). The case $\beta\leqslant-1$ must be excluded, otherwise the total cross-section would diverge. Even the case $\beta<0$ is unlikely, because so far no known law of energy loss favours high energy losses so strongly. The total cross-section (in units $(\hbar/\mu\mathbf{c})^2$) is

$$\int_0^1\phi(z)\,dz=\frac{\alpha}{\beta+1}\equiv k \quad\text{and}\quad \int_0^1\phi(z)(1-z)^\gamma\,dz=\frac{\alpha}{\beta+\gamma+1}. \qquad \ldots\ldots(28)$$

Now it is inconceivable, on physical grounds, that k is much larger than the cross-section corresponding to the range of nuclear forces, i.e. $\pi(\hbar/\mu\mathbf{c})^2$. We can therefore say that $\alpha/(\beta+1)<4$, approximately. Now the experimental relation (26) gives

$$\frac{\alpha\gamma}{(\beta+1)(\beta+\gamma+1)}=1\cdot15, \qquad \ldots\ldots(29)$$

or, inserting $\gamma=1\cdot5$,

$$\frac{1\cdot5}{\beta+2\cdot5}>\frac{1\cdot15}{4} \quad\text{or}\quad \beta<2\cdot7. \qquad \ldots\ldots(29')$$

Thus β cannot be too large, and this means that although small energy losses are favoured (as they are in all cases where the law of energy loss is known), *high energy losses are comparatively frequent*, roughly as in the case of Bremsstrahlung. The numerical figures in (29′) must, of course, not be taken too literally, but it is safe to say that β cannot be larger than 3, and is probably less.

The average energy loss follows also from (28):

$$\bar{\epsilon}=\left(\frac{\hbar}{\mu\mathbf{c}}\right)^2E\int_0^1\phi(z)\,z\,dz=\left(\frac{\hbar}{\mu\mathbf{c}}\right)^2E\sigma, \qquad \ldots\ldots(30)$$

$$\sigma=\frac{\alpha}{(\beta+1)(\beta+2)}.$$

Comparing this with (29), we see that

$$\sigma=\frac{1\cdot15}{1\cdot5}\,\frac{\beta+2\cdot5}{\beta+2}=0\cdot96-0\cdot77,$$

as β ranges from 0 to ∞. Thus the *mean energy loss is practically determined within narrow limits from the experiments alone.* This can be seen also directly from (26), because $1-(1-z)^{\gamma}$ is not very different from z.

The unit $(\hbar/\mu\mathbf{c})^2$ was introduced for dimensional reasons only; what follows from the experiment is, of course, the numerical value of the energy loss. This, as derived from the experiment, can be stated as being (per collision with one nucleon)

$$\bar{\epsilon} = \int_0^E \Phi(\epsilon, E)\,\epsilon\, d\epsilon = E(1{\cdot}6 \pm 0{\cdot}3)10^{-26}\,\text{cm}^2. \qquad \ldots\ldots(30')$$

This result, of course, holds only if the assumed law $w = w(\epsilon/E)$ is valid.

Finally we compare our more phenomenological results with the theory of meson production (Heitler 1945, Heitler and Walsh 1945). The main contribution to meson production follows indeed a cross-section of the form $\phi(\epsilon/E)d(\epsilon/E)$, with less important contributions of the form $\phi(\epsilon)\,d\epsilon$ independent of E. When the more complicated formulae (Heitler 1945) are plotted, it is seen that they agree fairly well with a form (27) with $\beta \sim 2$. (Indeed, the most important terms of ϕ are $(1-\epsilon/E)^2$.) This agrees with the condition (30). The total cross-section and the average energy loss are given by Heitler (1949) for a meson mass 315 :*

$$\left.\begin{aligned} \int_0^E \phi(\epsilon, E)\,d\epsilon &\sim \left(\frac{\hbar}{\mu\mathbf{c}}\right)^2 k, &\quad k &= 4-18,\\ \int_0^E \epsilon\phi(\epsilon, E)\,d\epsilon &= \left(\frac{\hbar}{\mu\mathbf{c}}\right)^2 E\sigma, &\quad \sigma &= 0{\cdot}9-4. \end{aligned}\right\} \qquad \ldots\ldots(31)$$

The rather wide range for the constants is due to an uncertainty of the lower limit of the impact parameter, but obviously, from what was said above, the lower, rather than the upper, figure must be accepted if the total cross-section is not to be unphysically large. It is clear that all this is well compatible with the conclusions derived from experiment, and in particular the value for σ, which could be determined from experiments directly, agrees well with the theoretical prediction. The value of k, however, does not follow from the experiments alone but requires a knowledge of β. If we accept for instance $\beta = 2$, it is clear that we should also get the theoretical value for k, because the theoretical formulae are close to $\beta = 2$. In fact (29) gives $k \sim 3{\cdot}5$.

All the above conclusions hold only with the provision that a law $\phi(\epsilon/E)d(\epsilon/E)$ is valid. The validity of such a law can hardly be deduced yet from the experiments, and it remains to be seen whether different laws for the energy loss can also account for the experiments.

§ 5. EFFECTS FROM THE LATITUDE CUT-OFF

The results of the previous sections (§§ 3 and 4) hold only for $E > E_0$. For European latitudes $E_0 = 3 \cdot 10^9$ ev., and energies less than this limit are probably of little importance for meson production. This will not be so for the equator, and we therefore investigate now the solution (21) for $E < E_0$. We assume, as before,

---

* The constant k refers to charged mesons only, whereas σ includes, of course, neutrettos. k should therefore be multiplied by 3/2. On the other hand, for the total cross-section some contribution from low energy mesons is included which does not follow the $w(\epsilon/E)\,d(\epsilon/E)$ law, and which contributes to the energy loss only in a lower order in E, but makes k bigger by a factor 2. For a fair comparison with the assumed $a(1-\epsilon/E)^{\beta}$ law we should therefore multiply k by a factor 3/4, which is evidently of no importance.

$w(z)=\alpha(1-z)^\beta$, $W_s=\alpha/(\beta+s)$, $k=\alpha/(\beta+1)$. $S(E,X)$ is thus given by (22) and s_0 can be chosen in the interval $-\beta<s_0<\gamma+1$. As $E<E_0$, the integrand vanishes for $s\to-\infty$ and, therefore, the path of integration can be completed to the left and deformed to a small circle round $s=-\beta$. This procedure gives for $S(E,X)$ a series in terms of Bessel functions of imaginary argument. However, the series converges only slowly, and as we are primarily interested in $S(E,\theta)$ rather than in $S(E,X)$, we do not give the explicit expression.

We obtain $S(E\,\theta)$ by introducing (22) into (12), thus

$$S(E,\theta)=\frac{1}{2\pi i E_0}\int_0^\infty P(\theta,X)\,dX\int_{s_0-i\infty}^{s_0+i\infty}\left(\frac{E_0}{E}\right)^s\frac{\gamma}{\gamma-s+1}\exp\{-(a-W_s)X\}\,ds. \qquad\ldots\ldots(32)$$

Reversing the order of integration in (32) we obtain with the help of (6),

$$S(E,\theta)=\frac{1}{2\pi i E_0}\int_{s_0-i\infty}^{s_0+i\infty}\left(\frac{E_0}{E}\right)^s\exp\{-\bar{p}f(a-W_s)\}\frac{\gamma}{\gamma-s+1}\,ds, \qquad\ldots\ldots(33)$$

$$-\beta<s_0<\gamma+1;\qquad \bar{p}=n\Phi_0\theta.$$

The integrand of (37) tends towards ∞ when s approaches either $-\beta$ or $\gamma+1$ from the inside of this interval. Therefore the integrand must have a minimum on the real axis in the interval $-\beta<s<\gamma+1$, and thus the integral can be approximated by the saddle-point method. To do this, we write in the usual way

$$\Xi(s)\equiv s\ln\frac{E_0}{E}-\bar{p}f(a-W_s)-\ln(\gamma+1-s)$$

and

$$S(E,\theta)=\frac{\gamma}{2\pi i E_0}\int_{s_0-i\infty}^{s_0+i\infty}\exp\{\Xi(s)\}\,ds.$$

We choose s_0 so as to make $\Xi(s_0)$ a minimum on the real axis; this gives

$$\ln\frac{E_0}{E}=-\bar{p}\frac{dW_s}{ds}f'(a-W_s)-\frac{1}{\gamma+1-s},\qquad s=s_0 \qquad\ldots\ldots(34)$$

$$-\beta<s_0<\gamma+1$$

and

$$S(E,\theta)\simeq\frac{\gamma}{E_0}\,\frac{\exp\{\Xi(s_0)\}}{\{-2\pi\Xi''(s_0)\}^{\frac{1}{2}}}. \qquad\ldots\ldots(34')$$

The equations (34) and (35) give a parametric representation of $S(E,\theta)$.

We note that for a given ratio $E_0/E>1$, for sufficiently large $\bar{p}$ $(dW_s/ds<0)$

$$\ln\frac{E_0}{E}\ll-\bar{p}\frac{dW_s}{ds}f'(a-W_s). \qquad\ldots\ldots(35)$$

For such large values of $\bar{p}$ (34) can only be satisfied by values of s_0 approaching $\gamma+1$. Introducing $\gamma+1-s_0=s'$, we see that s' will be small for sufficiently large $\bar{p}$. Developing in powers of s', we find as the result of a short calculation

$$S(E,\theta)=\gamma\left(\frac{E_0}{E}\right)^{\gamma+1}\frac{e}{\sqrt{(2\pi)}}(1+\text{terms of order } s'^3). \qquad\ldots\ldots(36)$$

The factor $e/\sqrt{(2\pi)}=1{\cdot}08$ is nearly unity, and thus we see that for values of E and $\bar{p}$ such that (35) with $s=\gamma+1$ is satisfied, the spectrum is simply a continuation of the power spectrum which is exactly valid above E_0.

For $\beta=2$, $\gamma=1{\cdot}5$ the condition for (36) to be valid is $\ln(E_0/E) \ll 0{\cdot}15\bar{p}$. Thus at $\bar{p}=20$ (sea level), the power spectrum just starts to extend below E_0.

That the power spectrum should extend below E_0 for very large values of $\bar{p}$ is obvious, as the primaries below the cut-off E_0 must cease to be effective at sufficiently large depth. Thus (36) can be regarded as a test for the accuracy of the saddle-point method. It appears thus that the error of this method for large $\bar{p}$ amounts to the deviation of $e/\sqrt{(2\pi)}$ from unity, i.e. to about 8%.

We have evaluated the integral spectrum

$$T(E,\theta)=\int_E^\infty S(E,\theta)\,dE$$

by the saddle-point method for $\beta=1, 2$ and $\bar{p}=10, 20, 30$. The results for $\beta=2$ are shown in a double logarithmic plot in Figure 2.

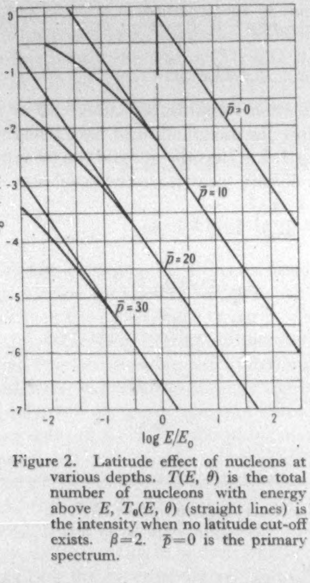

Figure 2. Latitude effect of nucleons at various depths. $T(E,\theta)$ is the total number of nucleons with energy above E, $T_0(E,\theta)$ (straight lines) is the intensity when no latitude cut-off exists. $\beta=2$. $\bar{p}=0$ is the primary spectrum.

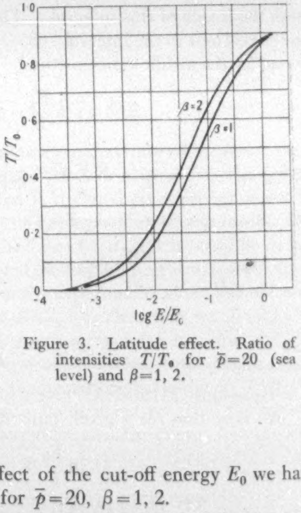

Figure 3. Latitude effect. Ratio of intensities T/T_0 for $\bar{p}=20$ (sea level) and $\beta=1, 2$.

In order to show more clearly the effect of the cut-off energy E_0 we have also plotted $T(E,\theta)/T_0(E,\theta)$ in Figure 3 for $\bar{p}=20$, $\beta=1, 2$.

$$T_0(E,\theta)=(E_0/E)^\gamma \exp\{-\bar{p}f(\lambda)\}$$

is the extended integral power spectrum.

We see from the graphs that $T(E,\theta)/T_0(E,\theta)=0{\cdot}9$ if evaluated by the saddle-point method for $E=E_0$. Thus the method involves an error of about 10%, just as in the case considered above. For $E=\frac{1}{5}E_0$ (e.g. $E_0=15\times10^9$, $E=3\times10^9$), we find

$$T(E,\theta)/T_0(E,\theta)=\begin{cases}0{\cdot}76 & \beta=2\\ 0{\cdot}69 & \beta=1\end{cases}$$

Allowing for the error of the method, we conclude that the decrease of intensity should be about 15% for $\beta=2$ and 23% for $\beta=1$.

The effect is expected to increase with height quite considerably, as seen from Figure 2.

The only experimental data so far available on the latitude effect of penetrating showers are those of Appapillai and Mailvaganam (1948). These workers do not find an effect, but their observations are not incompatible with an effect of the order of magnitude predicted by the theory.

Note added in proof. In the above treatment, contributions to the nucleon intensity arising from the possible production of secondary (recoil) nucleons in the process of meson emission have been neglected. If the production of secondary nucleons also follows a law of the form (1) this contribution can easily be taken into account by adding a further term to the diffusion equation (11). Nothing changes then, except the numerical value of $W_{\gamma+1}$. If, for instance, the probability of an energy loss ϵ, accompanied by the production of a secondary nucleon of energy ϵ' is of the form

$$\propto \left(1-\frac{\epsilon}{E}\right)^{\beta}\left(1-\frac{\epsilon'}{E}\right)^{\beta_1},$$

then
$$W_{\gamma+1} \rightarrow W_{\gamma+1}\left(1-\frac{\gamma}{\beta+\beta_1+\gamma+2}\right)+W_1\,\frac{\gamma!\,(\beta+\beta_1+1)!}{(\beta+\beta_1+\gamma+1)!}.$$

For reasonable values of β and β_1 the change is quite small, certainly smaller than the uncertainty of the constants β, γ, etc. At any rate, whatever change occurs, it will make the determination of $\bar{\epsilon}$ in § 4 change slightly in favour of a higher value, because the effective absorption coefficient is fixed by experiment.

REFERENCES

Appapillai, V., and Mailvaganam, A. W., 1948, *Nature, Lond.*, **162,** 887.

Bernardini, G., Cortini, G., and Manfredini, M., 1948, *Phys. Rev.*, **74,** 1878.

George, E. P., and Jason, A. C., 1947, *Nature, Lond.*, **160,** 327; 1948, *Ibid.*, **161,** 248.

Hamilton, J., Heitler, W., and Peng, H. W., 1943, *Phys. Rev.*, **64,** 78.

Heitler, W., 1945, *Proc. Roy. Irish Acad.*, **50,** 155; 1949, *Rev. Mod. Phys.*, in the press.

Heitler, W., and Walsh, P., 1945, *Rev. Mod. Phys.*, **17,** 252.

Jánossy, L., 1943, *Phys. Rev.*, **64,** 345.

Rossi, B., 1948, *Rev. Mod. Phys.*, **20,** 537.

Tatel, H. E., and Van Allen, J. A., 1948, *Phys. Rev.*, **73,** 87.

Tinlot, J., 1948, *Phys. Rev.*, **73,** 1476; 1948, *Ibid.*, **74,** 1197.

Wataghin, G., 1947, Cracow Conference (communication by Gross).

Some Cut-off Methods for the Electron Self-Energy

By J. RZEWUSKI
Department of Mathematical Physics, University of Birmingham

Communicated by R. E. Peierls; MS. received 4th February 1949

ABSTRACT. Some Lorentz-invariant cut-off procedures for the electron self-energy are investigated. Expressions for the self-energy are obtained as expansions in inverse powers of the cut-off constant K. The first term, logarithmic in K, has the correct transformation properties for all the cut-offs. The second term, independent of K, is covariant only for one of the procedures. The remaining terms have not the correct properties in any of the procedures, but contain negative powers of K and, therefore, vanish for $K \to \infty$. The one cut-off procedure which gives a covariant constant term can therefore be used for an unambiguous subtraction of the electron self-energy provided that in the final results one proceeds to the limit $K \to \infty$.

The electron self-energy in hole theory was first calculated by Weisskopf (1934, 1939). He showed that while the self-energy is still infinitely large, the divergence is only logarithmic owing to the partial cancellation of terms referring to "holes" and real electrons. If the integrations are cut off at some finite wave vector **K** the self-energy is, of course, finite and quite small unless K is chosen extremely large. In Weisskopf's result even the leading term, logarithmic in K, is not Lorentz invariant, so that the self-mass would appear to depend on the velocity.

Lamb (1947) corrected some numerical errors in Weisskopf's paper and found that the sum of the static and dynamic self-energies (which Weisskopf had given separately), the total self-energy, has the form

$$W = \frac{3}{2}\frac{e^2}{\pi}\frac{m_0^2}{E_0}\ln\frac{K}{m_0} + \text{finite terms}. \qquad \ldots\ldots(1)$$

Here E_0, m_0 are energy and mechanical rest mass of the electron, K is the upper limit in the integrals over the energy k of the virtual photon which can be emitted by the electron. We have chosen units in which $\hbar = c = 1$. The first term of (1) diverges logarithmically as $K \to \infty$. One would, of course, obtain finite answers if one could keep the upper limit K of integration finite instead of making it tend to infinity.

For physically consistent results the total rest mass of the particle must be constant, so that the energy for a given momentum is $E_{\text{total}} = \sqrt{(m^2 + p^2)}$, and if, as perturbation theory implies, the electromagnetic self-mass Δm is small compared to the mechanical mass m_0,

$$E_{\text{total}} = E_0 + m_0 \Delta m / E_0. \qquad \ldots\ldots(2)$$

This shows that for Lorentz invariance the self-energy W should be inversely proportional to E_0.

This is true of the first term in (1). However, the next term in the expansion, which is independent of K, has a different behaviour. This was pointed out by Lennox (1948), who obtains the following expression for these terms:

$$W = \frac{e^2}{2\pi}\frac{m_0^2}{E_0}\left\{3\ln\frac{2K}{m_0} - \frac{1}{2} + \frac{4}{9}\left(\frac{p_0}{m_0}\right)^2\right\}. \qquad \ldots\ldots(3)$$

The lack of covariance can be due to two circumstances. First of all, putting a constant upper limit for k in the momentum integrals means that the domain of integration is a sphere of radius K in momentum space. Such a sphere is obviously not invariant. The second case might be in the foundations of quantum mechanical perturbation theory. The concept of a virtual state is certainly not invariant. To see this it is only necessary to consider the four-vector $\Delta\mathbf{p}$, ΔE corresponding to the change of total momentum and energy in a transition from a real to a virtual state. Conservation of momentum requires $\Delta\mathbf{p}=0$, but ΔE is arbitrary since in transitions to virtual states the unperturbed energy is not conserved. Transformation to another Lorentz-frame gives $\Delta\mathbf{p}\neq 0$. Conservation of momentum is therefore satisfied only in one particular frame of reference.

It is easy to remove the first cause of non-invariance by introducing an invariant cut-off function. The second cause cannot be removed in general without abandoning altogether the perturbation method.

It is, however, interesting to know what improvements can be achieved by retaining the usual perturbation method and eliminating only the first source of non-invariance.

In the case of one electron in interaction with the radiation field, the four-vector $\Delta\mathbf{p}$, ΔE is a sum of two four-vectors corresponding to the change of momentum and energy of the particle $\Delta\mathbf{p}_{\text{el}}$, ΔE_{el} and the field $\Delta\mathbf{p}_{\text{f}}$, ΔE_{f}. There are two independent invariants which can be constructed out of these four-vectors:

$$\Delta\mathbf{p}_{\text{el}}^2-\Delta E_{\text{el}}^2 \qquad \ldots\ldots(4)$$

and

$$\Delta\mathbf{p}_{\text{el}}\Delta\mathbf{p}_{\text{f}}-\Delta E_{\text{el}}\Delta E_{\text{f}}. \qquad \ldots\ldots(5)$$

The other obvious combination, $\Delta\mathbf{p}_{\text{f}}^2-\Delta E_{\text{f}}^2$, vanishes for the processes we are considering, and all other invariants can be expressed in terms of (4) and (5).

Wataghin (1934) has suggested cutting off the integrals by means of a weight factor depending on the first invariant (4). Professor Peierls suggested using a function of (5) instead. Both procedures are investigated in this paper. In the limiting case $K\rightarrow\infty$ the second procedure will be shown to give invariant results whereas the first one does not.

As cut-off function any scalar function $f(x)$ of the invariants (4) or (5) can be used. The most convenient way is to take a rectangular function: $f(x)=1$ for $|x|<C$, $f(x)=0$ for $|x|>C$. (The symbol x stands here for the expressions (4) or (5)). This means that we allow only such virtual states which satisfy the restriction $|x|<C$. This is, as we shall see later, essentially a restriction on the energy k of the virtual quantum. For the cut-off constant C we choose $2Km$ in the case of the invariant (4) and $2K^2$ in case (5). The reasons for this definition will be apparent when we consider the behaviour of the invariants for large k (see below).

There are two kinds of transitions which contribute to the electron self-energy:

1. Transitions between two states with positive energy ((+ +) transitions) in which the electron in a state of momentum $\mathbf{p}_0$ energy E_0 goes over to a state $\mathbf{p}$, E emitting a light quantum $-\mathbf{k}$, k, or the reverse process. In both cases $E_0>0$, $E>0$, $\mathbf{p}=\mathbf{p}_0+\mathbf{k}$, $\Delta\mathbf{p}_{\text{el}}=+\mathbf{k}$, $\Delta E_{\text{el}}=E-E_0$, $\Delta\mathbf{p}_{\text{f}}=-\mathbf{k}$, $\Delta E_{\text{f}}=k$. Energy and momentum of the free electron satisfy, of course, the relation $E^2=p^2+m^2$ (we use energy units for momentum). In this case the invariants (4) and (5) become

$$k^2-(E-E_0)^2, \qquad \ldots\ldots(6)$$

$$k(k+E-E_0), \qquad \ldots\ldots(7)$$

where $E=+\sqrt{(E_0^2+k^2+2p_0k\cos\theta)}$. With this choice of sign they are both positive. θ is the angle between $\mathbf{p}_0$ and $\mathbf{k}$.

2. Transitions from negative to positive energy states ((− +) transitions) in which the electron in a negative energy state $\mathbf{p}$, $E<0$ emits a quantum $\mathbf{k}$, k and goes over to a state of positive energy $\mathbf{p}_0$, $E_0>0$. In this case $\mathbf{p}=\mathbf{p}_0+\mathbf{k}$, $\Delta\mathbf{p}_{\text{el}}=-\mathbf{k}$, $\Delta E_{\text{el}}=E_0-E$, $\Delta\mathbf{p}_{\text{f}}=\mathbf{k}$, $\Delta E_{\text{f}}=k$. The invariants (4) and (5) become now

$$-k^2+(E_0-E)^2, \qquad \ldots\ldots(6')$$

$$k(k-E+E_0), \qquad \ldots\ldots(7')$$

where $E=-\sqrt{(E_0^2+k^2+2p_0k\cos\theta)}$. Here again the sign is chosen in such a way as to make both invariants positive.

To obtain the invariant upper limits for the momentum integrals we have therefore to solve the following equations:

$$k^2-(\sqrt{(E_0^2+k^2+2p_0k\cos\theta)}\mp E_0)^2=\pm 2Km_0, \qquad \ldots\ldots(6'')$$

$$k(k+\sqrt{(E_0^2+k^2+2p_0k\cos\theta)}\mp E_0)=2K^2, \qquad \ldots\ldots(7'')$$

where the upper sign corresponds to (+ +), the lower to (− +) transitions. The exact solution of (6″) is

$$\left.\begin{aligned} k^+(x)&=Km_0\frac{p_0x+E_0\sqrt{(1+\epsilon)}}{E_0^2-p_0^2x^2}, \qquad & k^-(x)&=Km_0\frac{-p_0x+E_0\sqrt{(1-\epsilon)}}{E_0^2-p_0^2x^2},\\ \epsilon&=2\frac{E_0^2-p_0^2x^2}{Km_0}, & x&=\cos\theta. \end{aligned}\right\} \quad \ldots\ldots(8)$$

$k^+(x)$ is the upper limit for (+ +), $k^-(x)$ for (− +) transitions. Equation (7″) is cubic in k, but it is sufficient for our purpose to solve it approximately for large K. The solution is

$$\left.\begin{aligned} k^+(x)&=\frac{1}{4}(E_0-p_0x)+K\sqrt{(1-\epsilon_1)}, \qquad & k^-(x)&=\frac{-1}{4}(E_0+p_0x)+K\sqrt{(1-\epsilon_2)},\\ \epsilon_1&=\frac{1}{16K^2}(E_0-p_0x)(3E_0+5p_0x), & \epsilon_2&=\frac{1}{16K^2}(E_0+p_0x)(3E_0-5p_0x). \end{aligned}\right\} \quad \ldots\ldots(9)$$

To calculate the self-energy we use Weisskopf's (1934, 1939) method for the static part and the usual perturbation method for the dynamic part. The results are

$$W_{\text{static}}=\frac{e^2}{4\pi}\int_{-1}^{+1}dx\int_0^\infty dk\sum_{\sigma_0}^{1,2}\left\{\sum_{\sigma}^{1,2}-\sum_{\sigma}^{3,4}\right\}(u_0^*u)(u^*u_0), \qquad \ldots\ldots(10)$$

$$W_{\text{dyn}}=\frac{e^2}{4\pi}\int_{-1}^{+1}dx\int_0^\infty k\,dk\sum_{\pi}\sum_{\sigma_0}^{1,2}\left\{\frac{\sum\limits_{\sigma}^{1,2}(u_0^*\alpha_e u)(u^*\alpha_e u_0)}{E_0-|E(\mathbf{k})|-k}-\frac{\sum\limits_{\sigma}^{3,4}(u_0^*\alpha_e u)(u^*\alpha_e u_0)}{-E_0-|E(\mathbf{k})|-k}\right\}. \qquad \ldots\ldots(11)$$

Here u_0 and u are the Dirac spinors for free electrons with energy E_0 and E respectively. α_e is the component of the Dirac matrix-vector $\boldsymbol{\alpha}$ in the direction of polarization of the emitted quantum. $\sum\limits_{\sigma}^{1,2}$ and $\sum\limits_{\sigma}^{3,4}$ denote summations over the two spin states with positive or negative energy respectively. σ_0 corresponds to energy E_0; $\sum_{\pi}$ is the summation over both directions of polarization of the emitted quantum. Carrying out the summations in the usual way, taking $k^+(x)$ or $k^-(x)$ as upper limit in the integrals over k according to the kind of transitions they concern, and adding the two results (10) and (11) together, we get for the total self-energy the following expression:

$$\begin{aligned} W &= W_{\text{static}} + W_{\text{dynamic}} \\ &= \frac{e^2}{2\pi}\int_{-1}^{+1} dx \left\{ \int_0^{k^+(x)} dk \left[\frac{1}{2}\frac{E_0^2 + E_0|E| + p_0kx}{E_0|E|} + \frac{k}{E_0|E|} \cdot \frac{E_0|E| - m_0^2 - p_0kx - p_0^2x^2}{E_0 - |E| - k} \right] \right. \\ &\quad \left. + \int_0^{k^-(x)} dk \left[\frac{1}{2}\frac{E_0^2 - E_0|E| + p_0kx}{E_0|E|} + \frac{k}{E_0|E|} \cdot \frac{E_0|E| + m_0^2 + p_0kx + p_0^2x^2}{E_0 + |E| + k} \right] \right\}. \qquad \ldots\ldots(12) \end{aligned}$$

Here the first terms are the contributions to the static and dynamic self-energy from the $(++)$ transitions and the second two terms are the corresponding contributions from the $(-+)$ transitions.

It is difficult to carry out the integrations in (12) exactly. We shall, therefore, use an approximate method which, as we shall see, will yield the most important features of the procedure.

We split up the integrals over k in the following way:

$$\int_0^{k(x)} = \int_0^{\kappa} + \int_{\kappa}^{k(x)}, \qquad \ldots\ldots\ldots(13)$$

where κ is an arbitrary constant, equal for both kinds of transitions, which we can choose so large as to ensure convergence of an expansion of the integrand in the second integral in powers of $1/k$. Both integrals on the right-hand side of (13) have one non-invariant limit, viz. κ. We may, however, hope that in the sum, which has invariant limits, the non-invariant terms will cancel. The first of the two integrals must, of course, be calculated exactly. Its value for $k=\kappa$ can then eventually be expanded in powers of $1/\kappa$.

The calculation of (12) for $k^+(x)=k^-(x)=\kappa$ is straightforward. The result is

$$\begin{aligned} W_0^{\kappa} &= \frac{e^2}{2\pi p_0 E_0}\left[\tfrac{3}{2}p_0 m_0^2 \ln\left(k + p_0 + \sqrt{(+)}\right)\left(k - p_0 + \sqrt{(-)}\right) + m_0^2 k \ln\frac{\sqrt{(+)} + k + p_0}{\sqrt{(-)} + k - p_0} \right. \\ &\quad \left. + p_0k^2 - \tfrac{1}{6}(2E_0^2 + 2k^2 - 3p_0^2 + 6m_0^2)\left(\sqrt{(+)} - \sqrt{(-)}\right) - \tfrac{1}{6}p_0k\left(\sqrt{(+)} + \sqrt{(-)}\right) \right]_0^{\kappa}, \qquad \ldots\ldots(14) \end{aligned}$$

where $\quad \sqrt{(+)} = \sqrt{(E_0^2 + k^2 + p_0k)}, \qquad \sqrt{(-)} = \sqrt{(E_0^2 + k^2 - p_0k)}.$

Expanding the value of the bracket for $k=\kappa$ in powers of $1/\kappa$, and using the exact value for $k=0$, we get, up to terms of the order $1/\kappa$,

$$W_0^{\kappa} = \frac{e^2}{2\pi}\frac{m_0^2}{E_0}\left\{ 3\ln\frac{2\kappa}{m_0} - \frac{1}{2} + \frac{1}{3}\left(\frac{p_0}{m_0}\right)^2 \right\}. \qquad \ldots\ldots\ldots(15)$$

This is, with $\kappa=K$, the result of a constant cut-off. It confirms the result (3) of Lennox * that, in this case, even the constant term has wrong transformation properties.

---

* The numerical factor in the term dependent on p_0 appears to differ from that of Lennox as quoted by Bethe (1948).

Now we proceed to the calculation of the contribution of the second integral in (13). Here we first expand the integrand in powers of $1/k$ and then integrate the series over k between the limits κ and $k^+(x)$ or $k^-(x)$. The result is, up to terms of the order $1/k(x)$ or $1/\kappa$,

$$W_\kappa^K = \frac{e^2}{4\pi E_0}\int_{-1}^{+1} dx \left\{ 2p_0x(k^+(x)+k^-(x)-2\kappa) \right.$$
$$\left. +\tfrac{1}{2}(E_0+2m_0^2-3p_0^2x^2)\ln\frac{k^+(x)k^-(x)}{\kappa^2}+E_0p_0x\ln\frac{k^+(x)}{k^-(x)}\right\}. \quad \ldots\ldots(16)$$

Before further integration we must put in (16) the explicit expressions for $k^+(x)$ and $k^-(x)$. Expanding these functions also in powers of $1/K$, we get the following results for the logarithmic and constant terms:

(1) For the Wataghin cut-off (4, 6, 8)

$$W_\kappa^K = \frac{e^2}{2\pi}\frac{m_0^2}{E_0}\left\{3\ln\frac{K}{\kappa}+3+\frac{2}{3}\left(\frac{p_0}{m_0}\right)^2-\frac{3}{2}\frac{E_0}{p_0}\ln\frac{E_0+p_0}{E_0-p_0}\right\}. \quad \ldots\ldots(17)$$

(2) For the scalar product cut-off (5, 7, 9)

$$W_\kappa^K = \frac{e^2}{2\pi}\frac{m_0^2}{E_0}\left\{3\ln\frac{K}{\kappa}-\frac{1}{3}\left(\frac{p_0}{m_0}\right)^2\right\}. \quad \ldots\ldots(18)$$

To obtain the self-energy corresponding to the invariant cut-off we must add the expression (15) to either (17) or (18). In the case of the Wataghin cut-off (4) the constant term is still not invariant. In the case of the scalar product cut-off, however, the non-invariant terms cancel:

$$W = W_0^\kappa + W_\kappa^K = \frac{e^2}{2\pi}\frac{m_0^2}{E_0}\left\{3\ln\frac{2K}{m_0}-\frac{1}{2}\right\}. \quad \ldots\ldots(19)$$

Of the simple cut-off expressions the scalar product seems to be the only one with this property. For example, if we take the expression

$$(\Delta E)^2 \equiv (\Delta E_{\mathrm{el}}+\Delta E_{\mathrm{f}})^2 \equiv (\Delta E_{\mathrm{el}}+\Delta E_{\mathrm{f}})^2-(\Delta \mathbf{p}_{\mathrm{el}}+\Delta\mathbf{p}_{\mathrm{f}})^2, \quad \ldots\ldots(20)$$

which is a linear combination of the two invariants (4) and (5), we obtain

$$W = \frac{e^2}{2\pi}\frac{m_0^2}{E_0}\left\{3\ln\frac{2K}{m_0}-\frac{1}{2}-\frac{1}{3}\left(\frac{p_0}{m_0}\right)^2\right\}, \quad \ldots\ldots(21)$$

which is not invariant.

Obviously the next step is to calculate (12) exactly using the scalar product (5), which gives the only promising cut-off. This has been carried out, reversing in (12) the order of integrations. The result is

$$W = \frac{e^2}{2\pi E_0}\left\{F_1(E_0,k)\Big|_{k=k^+(1)}^{k=k^+(-1)}+F_1(-E_0,k)\Big|_{k=k^-(1)}^{k=k^-(-1)}+F_2(E_0,k^+(1))\right.$$
$$\left.+F_2(-E_0,k^-(1))+F_3(E_0,k^+(-1)+F_3(-E_0,k^-(-1))-3m_0^2\ln m_0\right\}, \quad \ldots\ldots(22)$$

where the $F_i (i=1, 2, 3)$ are rather complicated functions of k which we shall not write down explicitly, and where $k^+(1)$, $k^+(-1)$, $k^-(1)$, $k^-(-1)$ are the roots of the two cubics (7″) for $\cos\theta=1$ and $\cos\theta=-1$ respectively.

If (22) is to transform like $1/E_0$, the expression in the braces must be invariant (independent of p_0). This, however, is not the case. To see this we note that the quantities F_i contain logarithmic terms, the remainder being rational. Since the solutions $k^{\pm}(\pm 1)$ of the cubic equations are algebraic functions of the parameters K, E_0, m_0, the whole expression cannot be constant unless the logarithmic terms by themselves are constant. These can be shown to be

$$\frac{e^2}{2\pi}\frac{m_0^2}{E_0}\left\{\frac{3}{4}\left(1-\frac{E_0}{p_0}\right)\ln\left|\left(\frac{2K^2}{k^+(1)}+E_0+p_0\right)\left(\frac{2K^2}{k^-(-1)}-E_0-p_0\right)\right|\right.$$
$$+\frac{3}{4}\left(1+\frac{E_0}{p_0}\right)\ln\left|\left(\frac{2K^2}{k^+(-1)}+E_0-p_0\right)\left(\frac{2K^2}{k^-(1)}-E_0+p_0\right)\right|$$
$$\left.+2\frac{E_0}{p_0}\frac{K^2}{m_0^2}\ln\frac{k^+(-1)k^-(1)}{k^+(1)k^-(-1)}-3\ln m_0\right\}. \qquad \ldots\ldots(23)$$

In order to obtain some information about the dependence of (23) on p_0 we consider the limiting case of large energies: $E_0 \gg m_0$, and expand (23) in a series in powers of m_0/E_0, expanding also the roots $k^{\pm}(\pm 1)$ of the cubic equations as series in m_0/E_0. The coefficient of every power of m_0/E_0 in (23) is a sum of a logarithmic term and a rational function of K, E_0, $\sqrt{(K^2+\frac{1}{4}E_0^2)}$. Since E_0/K is arbitrary it is necessary for constancy of every coefficient that each of these terms separately be constant. However, the logarithmic part of the series is

$$\frac{e^2}{2\pi}\frac{m_0^2}{E_0}\left\{3\ln\frac{2K}{m_0}+\frac{3}{8}\frac{m_0^2}{E_0^2}\ln\left|\frac{K^2}{K^2-E_0^2}\right|+\ldots.\right\}. \qquad \ldots\ldots(24)$$

The expansion used here converges certainly for sufficiently large E_0. In (24) the second term is not constant, which proves the non-covariance of (23) and, therefore, also of (22). This result is not in contradiction with (19) since if we assume that K is large, the leading non-covariant terms are of the order E_0^2/K^2.

It is therefore impossible by use of the scalar product cut-off to make the electron self-energy finite and covariant. The important property of this cut-off, however, is that for any subtraction procedure of the kind used in the calculation of the energy level shift (Bethe 1948) in which the diverging terms cancel and it is possible in the result to go over to the limit $K \to \infty$, the scalar product cut-off must yield unambiguous results because in this case only the first two terms (19) matter. It could be used, therefore, as a basis for any calculation of this type, and may sometimes be more convenient than the equivalent devices of Weisskopf (Bethe 1948) and Feynman (1948), or the more elaborate theory of Schwinger (Bethe 1948, Schwinger 1948).

ACKNOWLEDGMENTS

It is a pleasure to thank Professor R. E. Peierls for suggesting this problem and for helpful advice, and Dr. E. E. Salpeter for useful discussions. I should also like to thank the Polish Central Planning Institute for the award of a research scholarship.

REFERENCES

BETHE, H. A., 1948, *Report to the Solvay Conference*, Sept. 1948.

FEYNMAN, R. P., 1948, *Phys. Rev.*, **74,** 1430.

LAMB, W. E., 1947, Paper given at the Cosmic Ray Conference at the Brookhaven National Laboratory, September 1947, as quoted by Bethe (1948).

LENNOX, E., 1948, Cornell University *Thesis*, as quoted by Bethe (1948).

SCHWINGER, J., 1948, *Phys. Rev.*, **74,** 1439.

WATAGHIN, G., 1934, *Z. Phys.*, **88,** 92, and **92,** 547.

WEISSKOPF, V., 1934, *Z. Phys.*, **89,** 27, and **90,** 817; 1939, *Phys. Rev.*, **56,** 72.

LETTERS TO THE EDITOR

The Use of Liquid Helium in Magnetic Cooling Experiments *

It is well known that vessels containing liquid helium and cooled below the lambda point are subject to a large heat influx due to the helium film in the connecting tube between the vessel and the warmer parts of the apparatus (Rollin and Simon 1939). It seemed to us that, in order to make use of liquid helium in experiments involving the magnetic method of cooling, it was important to devise means of minimizing this effect, for in such experiments it is frequently desired to cool down such a vessel to a very low temperature and to maintain the temperature in that region for a period of time sufficiently long to permit one to make a series of measurements. For example, the properties of liquid helium II have hitherto mainly been investigated down to 1° K. only and, as has already been emphasized (Kurti and Simon 1938), it is desirable to extend these measurements—especially those on the anomalous transport phenomena—to temperatures where the vapour pressure of helium is negligibly small. Again, liquid helium might be used as an agent for heat transfer at very low temperatures; whilst it is true that its heat conductivity is very small at such temperatures (Kurti and Simon 1938, de Klerk 1946), it can be estimated that the heat transmittance of thin layers of liquid helium would be sufficiently good to be of practical value; e.g. at 0·05° K. a layer 0·1 mm. thick would transmit 100 ergs per minute per cm^2 for a temperature difference of 0·001° K., the contact resistance on the liquid–solid boundary (Kapitza 1941) being probably comparatively small. Liquid helium could be used, therefore, to improve heat transfer between solid surfaces, and " make-and-break " thermal contacts at very low temperatures would thus become feasible.

To eliminate the large heat influx sealed capsules have been used successfully in the past (Kurti, Rollin and Simon 1936, Shire and Allen 1938). This technique, in doing away with the connecting tube and thus eliminating " creep ", makes good thermal insulation possible, but it has obvious drawbacks from the practical point of view.

The ideal solution would be to insert a valve at the low temperature end of the filling tube, but a valve that is tight to liquid helium II is hard to make. Experiments in Leyden (de Klerk 1946) with such a valve resulted in a heat influx of several thousand ergs per minute. A simpler solution seemed to us to be offered by the use of a long capillary as filling tube. In such an arrangement the rate of film flow, which is roughly proportional to the circumference of the tube (Rollin and Simon 1939) would be reduced. As, moreover, the capillary offers considerable flow resistance to the re-descending helium vapour, one could hope to prevent most of it from re-condensing by connecting the top of the capillary to a pumping system.

Figure 1 shows the experimental arrangement. The thin-walled German silver vessel A containing about 4 gm. of iron ammonium alum was suspended by means of the German silver capillary C (0·2 mm. inside diameter, 0·5 mm. outside diameter, 7 cm. long) the upper end of which was at the temperature of the helium in the surrounding cryostat (about 0·9° K.) and was connected to a diffusion pump of a speed of a few litres per second. About 1 cm^3 of liquid helium was introduced into A by condensation below the lambda point. The demagnetization procedure was as for a salt specimen except that it was found necessary to have a reasonably good vacuum—10^{-5} mm. Hg—round A, which is probably explained by a less efficient " clean-up " of the residual gas by the metallic container than by a salt specimen.

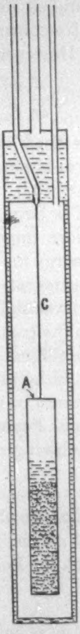

Figure 1.

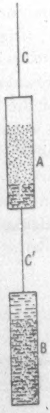

Figure 1(*a*).

---

* A brief account of some of this work was given at the Langevin–Perrin Colloquium, Paris, November 1948.

Figure 2 shows the heating-up curve after demagnetization from 12 kG. and 1·0° K (In order to improve the vacuum the temperature of the cryostat was reduced to 0·9° immediately before demagnetization.) From the specific heat of iron alum (that of liquid helium being negligible below 0·5° K.) the initial heat influx was calculated as 300 ergs/min., increasing to about 1000 ergs/min. at higher temperatures. The time of heating-up to 0·9° was about 1½ hours and this could easily be increased by the use of larger quantities of salt.

For experiments requiring higher thermal insulation or better temperature constancy a double container assembly as shown in Figure 1 (*a*) may be used with advantage. In our experimental arrangement the thin walled German silver vessels A and B, each containing 2·5 gm. of iron alum, were connected by the 3 cm. long capillary C′ (0·2 mm. inside diameter), A being connected to the pumping line through another 3·5 cm. long capillary C. The assembly could be filled with liquid helium to any desired level. One would then expect that owing to the small heat transfer through helium, whether bulk or film, below 0·5° K. (Kurti and Simon 1938) container B would receive only a small heat influx from A as long as the latter's temperature was less than 0·5° K. (Heat conduction along the German silver capillary C′ was estimated to be negligible at these temperatures.)

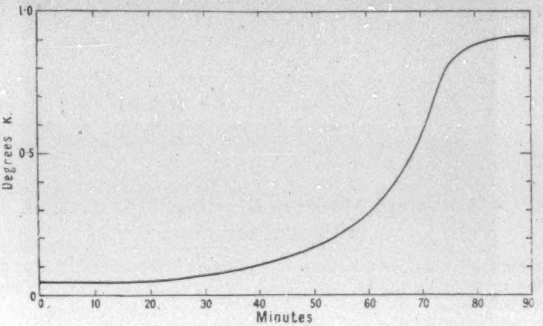

Figure 2.

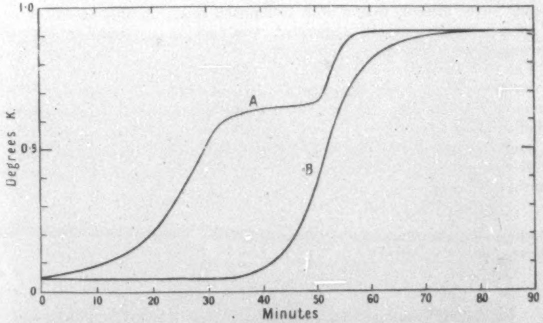

Figure 3.

Figure 3 gives the heating-up curves of A and B, with B and the capillary C′ filled with helium. The heating-up rate of A was higher than in the single container experiment, partly because of the smaller heat capacity and partly because of the shorter length of capillary C. The heating-up rate of the lower vessel B on the other hand was very small indeed until A reached about 0·5° K. (The same general characteristics were found by de Klerk (1946) in his experiments where a column of liquid helium was used to provide thermal contact between two salt specimens.) The temperature of B increased by less than 0·001° K. in half an hour and the heat influx was found to be 50 ergs/min. By increasing the heat capacity of A and thus delaying its rise of temperature to 0·5° K. it would be possible to prolong the time during which the temperature of B remained sensibly constant.

This arrangement seems to offer a relatively simple means of realizing constant temperature baths below 0·5° K. and it can be easily adapted for measurements of heat conductivity, specific heats, etc. and for two-stage demagnetization experiments.

Clarendon Laboratory,
Oxford.
2nd May 1949.

R. P. Hudson,
B. Hunt,
N. Kurti.

Kapitza, P. L., 1941, *J. Phys. U.S.S.R.*, **4,** 181.
de Klerk, D., 1946, *Physica*, **12,** 513.
Kurti, N., Rollin, B. V., and Simon, F. E., 1936, *Physica*, **3,** 266.
Kurti, N., and Simon, F. E., 1938, *Nature*, Lond., **142,** 207.
Rollin, B. V., and Simon, F. E., 1939, *Physica*, **6,** 219.
Shire E. S., and Allen, J. F., 1938, *Proc. Camb. Phil. Soc.*, **34,** 301.

A Lantern Model to Illustrate Dislocations in Crystal Structure

For some years I have been accustomed to illustrate roughly the nature of dislocations in a perfect crystal lattice by means of a lantern slide in which a single layer of small spheres is retained between two glass plates. Having been asked from time to time how the slide is made, I think that interest may be sufficient to warrant the following brief description.

As spheres I use carbon shot of about 1 mm. diameter, as supplied for telephone microphones by Messrs. Le Carbone, Ltd. These are enclosed between two ordinary lantern-slide cover glasses, bound with cellophane tape. If this assembly is shaken or tapped, spheres settle down into regions of close packing, separated by lines along which the fit is imperfect, which show white in projection. Occasional holes also appear in the lattice. Figure 1 illustrates a typical appearance (see Plate opposite).

The carbon spheres show variations of diameter up to ±0·05 mm. This variation seems favourable for the production of the desired appearance. I have also tried a layer of steel ball-bearing spheres, of 1/16 inch diameter, which are very uniform. These tend to show larger regions of close packing, but also exhibit dislocations and holes. Figure 2 is a typical appearance. On the whole, the steel spheres seem to be less satisfactory and are certainly more expensive.

University College,
London, W.C. 1.
30th March 1949.

E. N. da C. Andrade.

Viscosity and Superfluidity in Liquid Helium

The anomalous transport phenomena exhibited by liquid helium below 2·19° K. are clearly manifestations of a new physical state into which the liquid passes at this temperature. While as yet there exists no generally accepted theory of this state, it is evident that its establishment is accompanied by a rapid decrease in entropy. The shape of the specific heat curve (Keesom and Keesom 1935) shows, however, that the anomalous drop in the entropy of the liquid begins at a considerably higher temperature (~2·6° K.) and that at 2·19° K. about 8% of the total entropy has already disappeared.

The question therefore arises whether this initial drop in entropy will show itself in the transport properties of liquid helium I below 2·6° K. The available data show little indication of such a behaviour. Super-flow, the thermo-mechanical effect and the film transfer all seem to approach the value zero as, on warming, the temperature of 2·19° K. is reached. The viscosity has been measured by the oscillation method (Wilhelm *et al.*

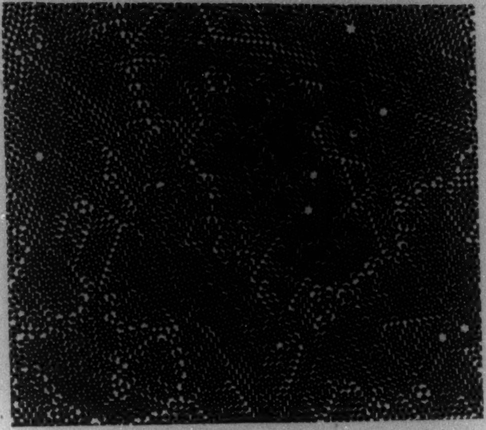

Figure 1.

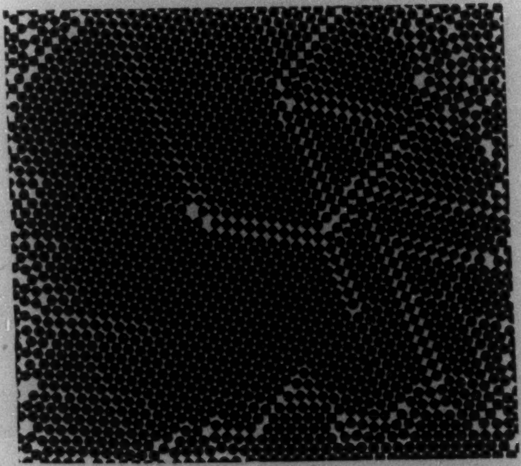

Figure 2.

(R. BOWERS AND K. MENDELSSOHN)

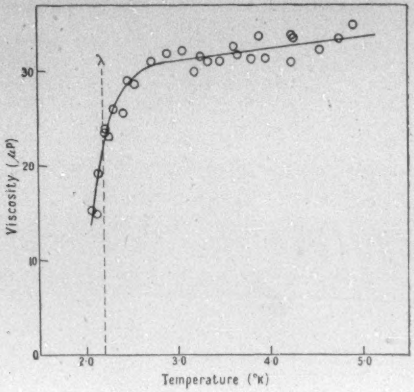

Viscosity of liquid helium.

(L. E. BEGHIAN AND H. H. HALBAN)

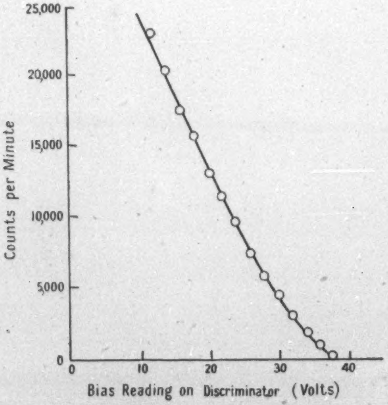

Pulse height distribution for methane chamber filled to 35 atmospheres using D+D neutrons.

1935, Keesom and MacWood 1938, Keesom and Keesom 1941). The results are not very consistent, but the most recent of these measurements indicate that the viscosity drops gradually in the helium I region and then shows a sharp decrease at 2·19° K. The one existing determination of the viscosity of helium I by a flow method (Johns *et al.* 1939) also indicates a drop, but there is, unfortunately, only one point measured (at 3·4° K.) between the boiling point and the lambda point. It was therefore decided to determine the viscosity of helium I by means of a flow method in some detail.

The apparatus used consisted of a glass capillary of 4×10^{-3} cm. radius and 2·5 cm. length, one end of which was attached to a glass reservoir while the other opened into the helium bath. The results given in the accompanying figure* show that between 5° K. and 2·7° K. the viscosity falls slightly, from about 33 μP. to 30 μP. This is followed by a sharp drop to about 23 μP. at 2·19° K. Although below the lambda point the flow becomes increasingly non-classical, our value at 2·14° K. does not indicate a sharp break in the curve such as was observed with the oscillation methods. One may be inclined to ascribe this anomalous decrease in the viscosity of helium I to the first appearance of superfluidity. However, the observation of flow in this region gave no indication of a non-classical term. In order to decide the question by a more sensitive method, the glass capillary was replaced by a metal tube containing 900 wires of 46 S.W.G. This tube was drawn down until its Poisseulle constant was of the same order as that of the glass capillary. In the helium I region, between 3° K. and 2·19° K., the flow rate in this tube did not increase more than in the glass capillary. On the other hand, just below the lambda point, at 2·13° K., the flow through this tube was increased more than six times.

Comparison between the results with the capillary and the wire tube thus shows that the rapid fall in viscosity observed by us above 2·19° K. cannot be interpreted as the appearance of superflow similar to that in helium II. We are, therefore, clearly faced with a decrease in the true viscosity of helium I accompanying the decrease in entropy in a temperature interval of about half a degree above the lambda point. The size of this interval, amounting to about one-fifth of the absolute temperature, also makes it unlikely that the viscosity change is due to fluctuations, i.e. the appearance of small regions of helium II. Phenomenologically, the anomaly above the lambda point corresponds to the appearance of short range order in an order–disorder transformation which at 2·19° K. is followed by the establishment of long range order. All evidence so far indicates that in the case of helium the increase of order with falling temperature occurs in momentum space and not with regard to positions. Consequently we are inclined to ascribe the sharp drop in viscosity above the lambda point to a re-distribution in the velocity spectrum of the liquid preceding the actual condensation phenomenon. It is to be hoped that further investigation of this gradual transition to the state of velocity condensation will lead to a clearer understanding of the latter, and experiments on other physical properties (heat conduction, diffusion etc.) are now in progress. A more detailed account of the present experiments will be given at a later date.

* See opposite page.

Clarendon Laboratory,
Oxford.
6th April 1949.

R. Bowers.
K. Mendelssohn.

Johns, H. E., Wilhelm, J. O., and Grayson Smith, H., 1939, *Canad. J. Res.*, **17A,** 149.
Keesom, W. H., and Keesom, A. P., 1935, *Physica*, **2,** 557.
Keesom, W. H., and Keesom, P. H., 1941, *Physica*, **8,** 65.
Keesom, W. H., and MacWood, G. E., 1938, *Physica*, **5,** 737.
Wilhelm, J. O., Misener, A. D., and Clark, A. R., 1935, *Proc. Roy. Soc.* A., **151,** 342.

Electron Collection in High Pressure Methane Ionization Chambers

It was pointed out by Klema and Barschall (1943) that to achieve electron collection in an ionization chamber filled to high pressure with gases such as hydrogen, nitrogen and argon, it is necessary to remove the last traces of electronegative impurities, principally oxygen.

Where an ionization chamber is used for single-particle counting instead of continuous current operation, it is important for many purposes to keep the pulse-rise time as short as possible, and consequently it is desirable to use electron collection. Recently, by filtering hydrogen through a palladium leak, Stafford (1948) has obtained electron collection up to 90 atmospheres pressure; Wilson, Collie and Halban (1948) have employed electrolytically made deuterium up to 30 atmospheres pressure for photodisintegration experiments.

Hydrogen by itself, however, has comparatively small stopping power, and is, therefore, unsuitable for the measurement of proton recoils caused by high energy neutrons; in such cases it has been customary to use hydrogen argon mixtures (Staub and Nicodemus 1946). Alternatively, we have found that carefully purified methane will also give electron collection at high pressure. The high hydrogen content of methane makes it especially useful for proton recoil work, and its stopping power is only slightly less than that of argon.

Investigations were made using a cylindrical chamber of phosphor bronze, 4 cm. diameter, 12 cm. long, with a wall thickness of 2 mm. The collecting electrode consists of a length of Kovar wire 1 mm. in diameter, and is fitted with a guard ring.

The purification of the methane was carried out in a packed fractionating column consisting of thirty equivalent plates. The column was immersed in liquid oxygen and the methane distilled off at this temperature. This was done by Drs. Kronberger and London at A.E.R.E., Harwell.

To avoid contamination of the pure gas, both the storage cylinder and chamber were thoroughly outgassed.

Measurements of proton recoil from neutrons from a D+D source (see Figure*) show that not more than 15% loss of pulse height occurs up to 35 atmospheres, the highest pressure used. At this pressure, the saturation voltage is 15,000 volts, and the collection time as measured on a triggered oscilloscope is 1 μsec.

According to Snyder (1946), the collection time in a cylindrical chamber is given by the formula

$$t=\frac{b-a}{\alpha}-\frac{\beta V}{\alpha^2 p \ln(b/a)}\ln\left\{\left[b+\frac{\beta V}{\alpha p \ln(b/a)}\right]\bigg/\left[a+\frac{\beta V}{\alpha p \ln(b/a)}\right]\right\},$$

where a and b are the wire and outer cylinder radii, V the applied voltage, and p the pressure. For methane Snyder quotes $\alpha=15\times10^5$ cm/sec. and $\beta=7{\cdot}5\times10^5$ cm^2 cm. Hg/sec. Using these constants, $t=0{\cdot}7$ μsec., which is in fair agreement with our result.

The efficiency of counting 2·3 MEV. neutrons from a D+D source which pass through the whole length of the chamber is 12% at 35 atmospheres pressure, and the maximum range of a proton recoil at this energy is 2·5 mm.

We are very grateful to Drs. Kronberger and London, of A.E.R.E., Harwell, for purifying the methane, to Messrs. R. Wilson and G. Bishop for their helpful advice, and to Lord Cherwell for his interest in this work.

* Opposite p. 395.

Clarendon Laboratory,
Oxford.
5th April 1949.

L. E. BEGHIAN.
H. H. HALBAN.

KLEMA, E. D., and BARSCHALL, H. H., 1943, *Phys. Rev.*, **63,** 18.
STAFFORD, G. H., 1948, *Nature, Lond.*, **162,** 771.
STAUB, H., and NICODEMUS, D., 1946, Report on an investigation of the behaviour of Argon-Hydrogen Mixtures and Isobutane in a Spherical chamber, *Manhattan District Publication*, P.B. 49, 577.
SNYDER, T., 1946, "High Efficiency Neutron Counter for Fast Coincidence Measurement", *Manhattan District Publication*, P.B. 52,800.
WILSON, R., COLLIE, C. H., and HALBAN, H., 1948, *Nature, Lond.*, **162,** 771.

REVIEWS OF BOOKS

Theoretical Structural Metallurgy, by A. H. COTTRELL. Pp. viii+256. (E. Arnold & Co., 1948.) 21*s*.

The rapid progress of the physics and mechanics of solids in recent years has placed the majority of metallurgists in a difficult position: with the slender fundamental knowledge dispensed in most University metallurgy degree courses (Dr. Cottrell's University, Birmingham, is a praiseworthy exception) they can hardly follow recent scientific developments in their own field, let alone take an active part in them. Most of the pioneers in the science of metals have been physicists, chemists, or engineers by training; the activity of the professional metallurgist is usually confined to the application of available scientific results to particular metals and alloys, unless he is capable of acquiring the necessary fundamental knowledge by home study. In this difficult situation the appearance of Hume-Rothery's brilliant non-mathematical *Atomic Theory for Students of Metallurgy* in 1946 was an event of great importance, and Dr. Cottrell's new book represents a further welcome addition to the means by which the metallurgist can get acquainted with the modern aspects of the science of metals.

Dr. Cottrell's book falls into two parts of rather different character. The first six chapters give a good elementary account of the electron theory of metals, with a brief sketch of the Bohr theory and of the basic conceptions of wave mechanics; the remaining eight chapters deal with statistical thermodynamics, heterogeneous equilibria, thermodynamical properties of metals and alloy systems, order–disorder transformations, diffusion, and the kinetics of phase changes. These eight chapters treat their subject on a University science standard; in fact, the amount of mathematics used is sometimes above the minimum necessary for the purpose.

Physicists may question whether a useful purpose is served by a mainly descriptive treatment of a mathematical subject such as is the electron theory of metals. In the reviewer's opinion the answer is definitely in the affirmative. A recent text-book entitled *Modern Metallurgy for Engineers* (New York: Pitman, 1941) gives a list of references to literature on metals, with brief commentaries on each item, and here Mott and Jones' book receives the following remark: " For enthusiasts on quantum mechanics. A few engineers may be interested in the mental calisthenics ". Since the author of this revealing utterance is an influential metallurgist, and since the future of metallurgical education depends very much on influential metallurgists, little progress can be expected before these are convinced, by means of clear elementary reviews, that the physics of metals is no more mental calisthenics unworthy of a he-metallurgist.

No doubt many metallurgists will take advantage of Dr. Cottrell's excellent book, and a new edition may have to be printed in due course. This would give an opportunity to increase the accuracy of expression in many passages which, although usually correct from a legalistic point of view, appear likely to be misunderstood by a beginner. One of the first examples of this is found on page 5, where the uncertainty principle might seem to have preceded quantum mechanics, in which " it has become necessary, however, to specify four quantum numbers instead of the single one used in the original formulation of the Bohr theory ".

On page 34 the law of rational intercepts is thought to govern the positions, not of the natural crystal faces, but of lattice planes (for which the statement of the law would be partly trivial, partly—in its emphasis on *small* integers—wrong).

On page 43 we read: " There is some evidence, particularly from the study of crystals by x-ray diffraction, suggesting that a real crystal is not of perfectly uniform orientation, but is composed of a mosaic of small crystals, or crystallites." This seemed a possibility until 1934, when Renninger, using the double-crystal spectrometer, found that a synthetic NaCl crystal was ideally perfect in the sense of the Darwin-Ewald theory; recently Guinier, by means of another x-ray method, came to a substantially identical conclusion for recrystallized aluminium. Thus, a " mosaic " imperfection is characteristic of a *bad* crystal, not of a *real* crystal; the early x-ray workers found most crystals imperfect because they did not know how to obtain perfect ones.

It is a pity that the last chapter, " Phase precipitation by nucleation and growth ", does not include strain transformations (martensitic transformations), which are of the very greatest fundamental and practical importance in metallurgy. In this chapter Widmanstätten structures are attributed to oriented nucleation and growth governed by the condition of minimum interface energy. That the typical Widmanstätten pattern does not arise by such a process can be recognized from the very frequent occurrence of lamellae penetrating one another; the absence of isothermal growth, the reversibility of some strain transformations (e.g. the transformation of metastable β-brass by cooling), and many other phenomena show sufficiently that there can be no question of an explanation on the basis of oriented growth. Readers of this chapter will do well to follow it up by consulting Chapter XXII in Barrett's *Structure of Metals*, where a balanced view of the subject is given.

These remarks, however, should not obscure the fact that Dr. Cottrell's book is a most useful contribution to metallurgical literature; it deserves to be present in the library of every metallurgist, and it would certainly have deserved a more attractive paper and binding.

E. OROWAN.

CORRIGENDUM

" Experiments with the Delayed Coincidence Method, including a Search for Short-lived Nuclear Isomers ", by D. E. BUNYAN, A. LUNDBY and D. WALKER (*Proc. Phys. Soc.* A, 1949, **62**, 253).

It has been pointed out that pp. 261–263 are difficult to follow. The whole of p. 262 constitutes a table which follows the second paragraph of p. 263. The actual text runs from the bottom of p. 261 to the top of p. 263.

P. 256, line 8. " $T_{\frac{1}{2}} \geqslant 10^{-8}$ sec." *should read* " $T_{\frac{1}{2}} \gtrsim 10^{-8}$ sec."

CONTENTS FOR SECTION B

PAGE

Mr. W. H. Walton and Mr. W. C. Prewett. The Production of Sprays and Mists of Uniform Drop Size by Means of Spinning Disc Type Sprayers . . . 341
Mr. P. B. Fellgett. Dynamic Impedance and Sensitivity of Radiation Thermocouples . . . 351
Mr. F. W. Cuckow and Mr. J. Trotter. Some Experiences in the Application of the Electron Microscope to the Study of Steels . . . 360
Prof. F. Llewellyn Jones. Electrode Ionization Processes and Spark Initiation . 366
Dr. G. F. Hodsman, Dr. G. Eichholz and Mr. R. Millership. Magnetic Dispersion at Microwave Frequencies . . . 377
Dr. J. W. Leech. The Measurement of the Specific Heats of some Organic Liquids using the Cooling Method . . . 390
Letters to the Editor:
    Mr. D. A. Wright. D.C. and Pulsed Emission from Oxide Cathodes . . 398
Reviews of Books . . . 400
Corrigendum . . . 402
Contents for Section A . . . 403
Abstracts for Section A . . . 403

ABSTRACTS FOR SECTION B

The Production of Sprays and Mists of Uniform Drop Size by Means of Spinning Disc Type Sprayers, by W. H. Walton and W. C. Prewett.

ABSTRACT. Spray of almost uniform drop size is formed when liquid is fed under suitable conditions on to the centre of a rotating disc and centrifuged off the edge. This method of spraying has been studied over a wide range of variables and homogeneous clouds have been produced in the drop-size range from 3 mm. to 15 μ diameter. The size of the spray drops is given approximately by the equation $d=3{\cdot}8\ (T/D\rho)^{\frac{1}{2}}/\omega$ where d=drop diameter, D=disc diameter, ω=angular velocity of disc, T=surface tension of liquid, ρ=density of liquid. The spray thus formed also contains a proportion of fine satellite drops, but their smaller distance of projection from the disc enables them to be removed from the cloud when their presence is undesirable. Relatively coarse sprays are easily produced by means of a simple electric motor-driven disc. The finer spray sizes require rotor speeds up to several thousands of revolutions per second and high speed air driven "tops" have been used for this purpose. Suitable designs of apparatus are described.

Dynamic Impedance and Sensitivity of Radiation Thermocouples, by P. B. Fellgett.

ABSTRACT. The concept of dynamic impedance is applied to radiation thermocouples. An equivalent circuit is derived, in terms of which the working of a thermocouple and the factors leading to high sensitivity can be visualized. Methods are given for measuring the dynamic impedance and it is shown that these measurements lead to values for thermoelectric power, heat loss from the receiver, and time constant of the thermocouple. Expressions are given, in terms of the dynamic impedance, for the important properties of radiation thermocouples, namely the signal-to-noise sensitivity, ultimate sensitivity, noise factor and power efficiency. These properties are thus obtained in terms of parameters that can be predicted from the design, or measured in the finished instrument. The

sensitivity is found without recourse to micro-measurements and therefore independent of limitations set by the thermocouple amplifier. The expression for sensitivity differs from those previously published, and the discrepancy is discussed. The way in which the ultimate sensitivity might be approached in practice is indicated. The efficiency is shown to depend on the amount of radiation falling on the receiver of the thermocouple, but to be a constant fraction of the thermodynamic limit $\Delta T/T$. For an ideal thermocouple the fraction is one-half, for an actual thermocouple it is less by a factor which we call the relative efficiency.

Some Experiences in the Application of the Electron Microscope to the Study of Steels, by F. W. CUCKOW and J. TROTTER.

ABSTRACT. Steel specimens have been examined in the light and electron microscopes. The replica technique has been used for the electron microscope work, and all the specimens have been studied with both "Formvar" plastic and polystyrene-silica replicas. The micrographs are critically examined and compared.

There is an obvious gain in picture sharpness in the electron micrographs, particularly in those from silica replicas. It is found, however, that interpretation of the micrographs from plastic replicas in terms of the geometry of the specimen surfaces is more straightforward.

Electrode Ionization Processes and Spark Initiation, by F. LLEWELLYN JONES.

ABSTRACT. Spark time lags in short gaps with tungsten electrodes were measured for different degrees of oxidation and activation, and the distributions of lags examined and compared. The results, which showed a reduction of mean lag and a narrowing of distribution following oxidation and activation, are discussed in relation to the mechanism of electron emission from oxidized cathodes for impulse and static conditions, and also for the Geiger counter.

Magnetic Dispersion at Microwave Frequencies, by G. F. HODSMAN, G. EICHHOLZ and R. MILLERSHIP.

ABSTRACT. A method is described which has been developed for the measurement of initial permeabilities of ferromagnetic wires in the microwave region and successfully applied over the range from 3 to 13 cm. wavelength to a variety of materials. The measurements are carried out by comparing the attenuations of coaxial transmission lines with the ferromagnetic specimen and with a non-ferromagnetic reference material as inner conductors. The attenuation constants are derived from observations on the input impedance of the line for different terminations as embodied in a circle diagram of impedance. The results are interpreted in the light of modern theories of magnetic dispersion and an estimate of domain sizes is made. The limitations of the theoretical treatments are indicated.

The Measurement of the Specific Heats of some Organic Liquids using the Cooling Method, by J. W. LEECH.

ABSTRACT. The cooling method for the determination of the specific heats of liquids is further developed. The power law of cooling $d\theta/dt=k\theta^n$, is shown to hold only approximately, and a new method for deducing values of $d\theta/dt$ is described. The specific heats of a number of liquid carbinols are measured over the approximate range 40–70° c.